Chapter 4

Multi-scale modelling of dry granular flows

4.1 Introduction

In nature, instabilities of slopes or cliffs are dramatic events involving sudden release of a large mass of soil. The prediction of these catastrophic events represents several challenges, one difficulty being our incomplete understanding of the granular flow dynamics (Rondon et al., 2011). Understanding the mechanics is of particular importance for risk assessment. Small scale laboratory experiments are usually unable to properly capture the dynamics of geophysical events. However, they can be useful to precisely study the physical mechanisms, which may play a crucial role in real flows (Iverson, 1997).

Conventionally, granular materials such as soils are modelled as a continuum. On a macroscopic scale, granular materials exhibit many collective phenomena and the use of continuum mechanics to describe the macroscopic behaviour can be justified. However on a grain scale, the granular materials exhibit complex solid-like and/or fluid-like behaviour depending on how the grains interact with each other. Numerical studies at grain scale allow a precise understanding of the internal flow structure. However, even in simplified geometries such as those investigated in the laboratory-scale experiments, DEM suffers from a serious short-coming in the number of grains that can be simulated in a reasonable time. This is a critical issue when more complex geometries or long-time granular processes are considered, or when particle size distributions are broad. For this reason, most numerical studies are performed in 2D or simple particles shapes and size distributions are considered.

Classical modelling strategies based on the finite element method (FEM) cannot be used for the simulation of very large deformations due to mesh distortion effects. In various application of FEM, this problem is treated by means of technical tools such as re-meshing. These methods are, however, not robust and lead to round-off errors and are sensitive to the mesh characteristics. Recent works on granular materials suggest that a continuum law may be incapable of revealing in-homogeneities at the grain-scale level, such as orientation of force chains, collapse of local voids and grain rearrangements, which are purely micro-structural effects (Rycroft et al., 2009). Discrete element approaches are capable of simulating the granular material as a discontinuous system allowing one to probe into local variables such as position, velocities, contact forces, etc. The fundamental question is how to model granular materials which exhibit complex phenomenon. It is important to understand the mechanics of granular flows and the ability and limitations of continuum methods in modelling the granular flow dynamics.

4.2 Granular column collapse

The collapse of a granular column, which mimics the collapse of a cliff, has been extensively studied in the case of dry granular material (Hogg, 2007; Kerswell, 2005; Lajeunesse et al., 2004; Lo et al., 2009; Lube et al., 2005; Staron and Hinch, 2007; Zenit, 2005). The granular column collapse experiment involves filling a rectangular channel of height H_0 and width L_0 with a granular material of mass 'm' (see figure 4.1). The granular column is then released *en masse* by quickly removing the gate, thus allowing the granular material to collapse onto the horizontal surface, forming a deposit having a final height H_f and length L_f. Despite the complexity of the intermediate flow dynamics, experimental investigations have shown that the flow evolution, the spreading velocity, the final extent of the deposit, and the energy dissipation can be scaled in a quantitative way independent of the substrate properties, grain size, density, the shape of the granular material and the released mass (Lajeunesse et al., 2005; Lube et al., 2005; Staron and Hinch, 2007). The granular collapse has also been studied using discrete element method, which allows precise measurement of the internal flow structure (Lo et al., 2009; Staron and Hinch, 2007; Staron et al., 2005; Utili et al., 2014). Power laws relating the final run-out and height to the initial aspect ratio ($a = H_0/L_0$) of the column were observed. These findings immediately pose a question: are these simple scaling fortuitous, an oversimplification, or in fact indicative of a simple dynamical balance?

Granular flows are conventionally modelled as a frictional dissipation process in continuum mechanics but the lack of influence of inter-particle friction on the energy dissipation and spreading dynamics (Lube et al., 2005) is surprising. However, Kerswell (2005) showed the run-out behaviour has a clear material dependence. Although, the collapse of a granular column on a horizontal surface is a simple case of granular flow, a proper model that describes the flow dynamics is still lacking. Simple mathematical models based on conservation of horizontal momentum capture the scaling laws of the final deposit, but fail to describe the initial transition regime. From a theoretical point of view, the spreading has been described using depth averaged equations (Kerswell, 2005; Larrieu et al., 2006). The depth-averaged and Saint-Venant equations, however, struggle to recover the precise dynamic behaviour of the system (Warnett et al., 2013) and only succeeds in predicting the scaling observed for aspect ratio less than one. Describing the behaviour of larger aspect ratio and capturing the initial stage of the collapse, when the grains experience a rapid change of direction from vertical to horizontal, remain an open challenge.

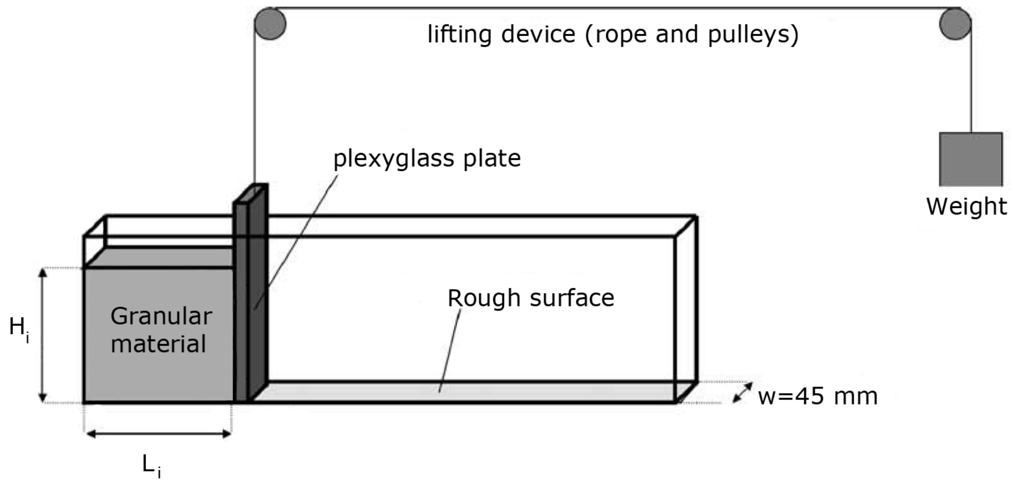

Figure 4.1 Schematic of experimental configuration for 2-D collapse in a rectangular channel, (Lajeunesse et al., 2004)

In the present study, multi-scale numerical modelling, i.e. grain-scale modelling and continuum analyses, of quasi-two dimensional collapse of granular columns are performed using two-dimensional Discrete Element Method (DEM) and Generalised Interpolation Material Point Method (GIMPM). GIMPM, a hybrid Eulerian – Lagrangian approach, with Mohr-Coloumb failure criterion is used to describe the continuum behaviour of the granular column collapse. Whereas, the micro-mechanics of the flow is captured using DEM simulations. Comparing the grain scale behaviour with the continuum simulations highlights the limitations of the continuum approach in modelling dense granular flows and their ability in capturing the complex flow kinematics which are due to micro-scale rheology.

4.2.1 Numerical set-up

In this study, the numerical set-up of granular columns are analogous to the experimental investigation performed by Lajeunesse et al. (2004). The experimental configuration of Lajeunesse et al. (2004) is shown in figure 4.1. Granular material of mass '*m*' is poured into a container to form a rectangular heap of length 'L_0', height 'H_0' and thickness 'W'. The internal friction angle and the wall friction between the wall and the glass beads measured by Lajeunesse et al. (2004) are listed in table 4.1. The gate is then quickly removed to release the granular mass that spreads in the horizontal channel until it comes to rest. The final run-out distance 'L_f' and the collapsed height 'H_f' are measured. The run-out distance and collapse height exhibit a power law relation with the initial aspect ratio 'a' $(= H_0/L_0)$ of the column.

Table 4.1 Material properties of glass ballotini (Lajeunesse et al., 2004)

Parameter	**Value**
Mean grain diameter	1.15 mm
Repose angle	22±0.5°
Avalanche angle	27.4±0.5°
Wall friction angle	24.8±0.2°

Granular materials when released suddenly on a horizontal surface exhibit transient flow. In this study, the mechanism of flow initiation, spreading dynamics and energy dissipation are studied for varying initial aspect ratios of the granular column. The soil grain characteristics of the DEM sample match that of the experiment. The particle size distribution (PSD) is one of the most important factors controlling landslide initiation and soil permeability (Utili et al., 2014). Cumulative β distribution (described in **??**) is used to generate a graded sample with a mean grain diameter of 1.15mm (see figure 4.2b). The DEM sample is composed of $\sim$ 3000 disks with a uniform distribution of diameters by volume fractions in the range $[d_{min}, d_{max}] = 0.92 - 1.38$ mm with polydispersity $r = \frac{d_{max}}{d_{min}} = 1.5$. The granular column is prepared by allowing randomly placed grains to undergo ballistic deposition with a constant potential head between layers of soil grains. A snapshot of the sample generated is shown in figure 4.2a. A DEM sample with soil grains arranged in a regular hexagonal lattice is also used to study the influence of crystallisation and jamming on the run-out behaviour.

The overlap between grains are determined by the stiffness k_n of the spring in the normal direction. Typically, an average overlap in the range 0.1 to 1.0% is desirable (Zenit, 2005) and the spring constant is chosen to produce grain overlaps in this range. The stiffness is determined as

$$k_n = \frac{2\pi G}{(1-\nu)[2\ln(\frac{2r}{A}) - 1]} \tag{4.1}$$

$$A = [\frac{2r(1-\nu)f_n}{\pi G}]^{\frac{1}{2}}, \tag{4.2}$$

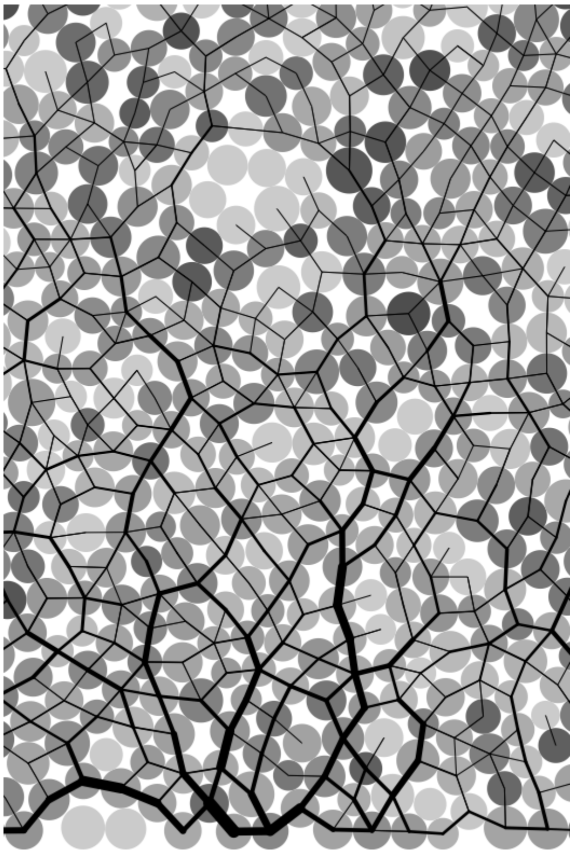

(a) DEM sample prepared using ballistic deposition

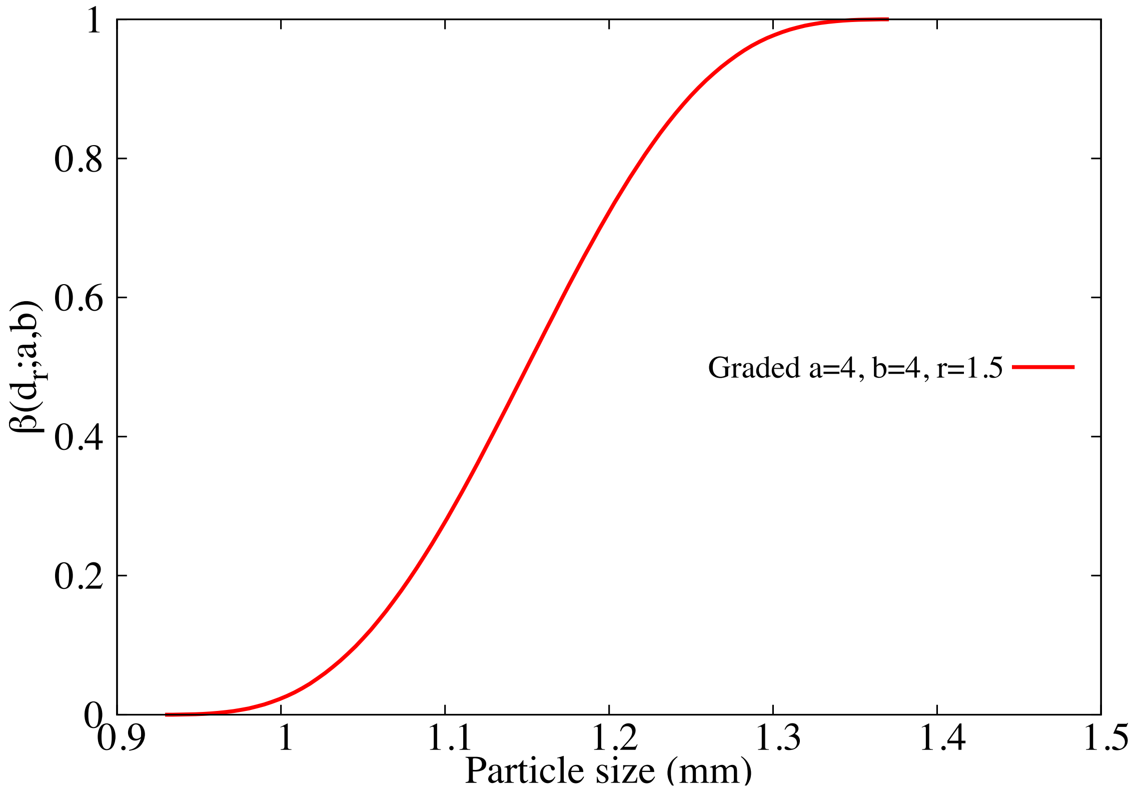

(b) DEM grains generated using the cumulative β distribution

Figure 4.2 DEM sample characteristics

where f_n is the normal contact force; G is the shear modulus; ν is the Poisson's ratio and r is the radius of the grain. A simpler form of stiffness for a spherical grain is defined as

$$k_n = 4ER\,, \tag{4.3}$$

where E is the Young's modulus of the material and R is the radius of the grain. Cambou et al. (2009) observed that the contact model has negligible influence on the run-out behaviour of rapid granular flows. The granular collapse simulations performed using non-linear Hertz-Mindlin contact model and the linear-elastic contact model showed no significant difference in the granular flow behaviour (Utili et al., 2014). Linear-elastic contact model is used in the present study due to its simplicity and lower computation time requirement. The maximum tangential force is limited by the Mohr-Coloumb criterion.

Staron and Hinch (2007) observed that the coefficient of restitution ε dramatically changes the behaviour of the system for $\varepsilon \longrightarrow 1$; in particular, this dramatic change is expected to become more important for increasing values of a. On the contrary, for $\varepsilon \leq 0.8$, the influence of the coefficient of restitution becomes negligible. In the present study, a value of 0.75 is adopted as the coefficient of restitution, similar values of restitution coefficient was adopted by Girolami et al. (2012) and Zenit (2005). The normal damping coefficient C_n is appropriately chosen to achieve the required coefficient of restitution ε:

$$C_n = 2\gamma\sqrt{m_{ij}k_n} \tag{4.4}$$

$$\text{where} \quad \gamma = -\frac{\ln(\varepsilon)}{\sqrt{\pi^2 + \ln^2(\varepsilon)}}, \quad \text{and} \quad m_{ij} = \frac{m_i m_j}{m_i + m_j}. \tag{4.5}$$

The micro-mechanical parameters used in this study are presented in table 4.2. Due to the unsteady nature of the flow, the grains get dispersed on the horizontal plane as discrete bodies start to separate from the main mass, hence the run-out distance is calculated as the position of the farthest grain which has at least one contact with the main mass.

GIMPM with Mohr-Coloumb constitutive model is used to simulate plane strain collapse of granular columns. Crosta et al. (2009) observed that the Mohr-Coloumb with non-associate flow rule is able to capture granular collapse dynamics and models the strong vertical motion. This method does not suffer the limitations of typical shallow water equation techniques. In order to understand the ability and limitations of continuum approaches in capturing the local rheology, it is important to scale the grain scale material properties, such as the inter-particle friction and stiffness, to the continuum scale (macroscopic friction and Young's modulus). Crosta et al. (2009) observed that the friction angle plays a significant role on the run-out behaviour.

Table 4.2 Micro-mechanical parameters used in DEM simulations

Parameter	**Value**
Young's modulus of glass bead	70×10^9 N m^{-2}
Poisson's ratio	0.22 - 0.24
Diameter of glass beads	0.92 to 1.38 mm
Normal and shear stiffness of grains	1.6×10^8 N m^{-1}
Normal and sear stiffness of wall	4×10^8 N m^{-1}
Inter-particle friction coefficient, μ	0.53
Wall friction coefficient	0.466
Coefficient of restitution, ε	0.755

In MPM simulations, the granular flow is assumed to be in critical state and the critical state friction angle is used in the Mohr-Coloumb model. In order to obtain the critical state friction angle of the granular sample, a shear test is performed using 1078 DEM grains. A bi-periodic boundary condition is adopted on the sides of the sample (see figure 4.3a). Two layers of fixed grains (shown in black) is placed at the top and the bottom of the shear sample. A normal pressure 'P' and a horizontal velocity v is applied to the fixed grains at the top of the shear sample. As the normal effective stress is varied, the average shear stress in the sample is measured. The sample is sheared until critical state is reached. The slope of shear stress versus normal effective stress gives the critical state friction angle. A critical state friction angle of 22.2° is obtained. The macroscopic friction angle is in the range observed by Estrada et al. (2008) and Mitchell and Soga (2005). The Young's modulus of the granular assembly is obtained as the initial slope of the stress-strain plot of a uni-axial compression of a granular column using DEM.

Guilkey et al. (2003) suggests using at least four material points per cell for large deformation problems. In the present study, 16 material points per cell is adopted. If the mesh is too fine and the number of particles is too large, the particle size $2lp$ decreases, and the GIMPM interpolation function tends to approach the original MPM function, as shown by Bardenhagen and Kober (2004). Hence, GIMPM loses the merit that it reduces the numerical noise due to material points crossing the background mesh. In addition, the probability of particles crossing the background mesh increases with decrease in the mesh size, hence, more noise may be produced (Abe et al., 2013). The effect of number of material points per cell on the run-out behaviour is discussed in section 4.3.5. In the present study, each material point represents one-fourth of a DEM soil grain. The parameters used for the continuum analyses are presented in table 4.3.

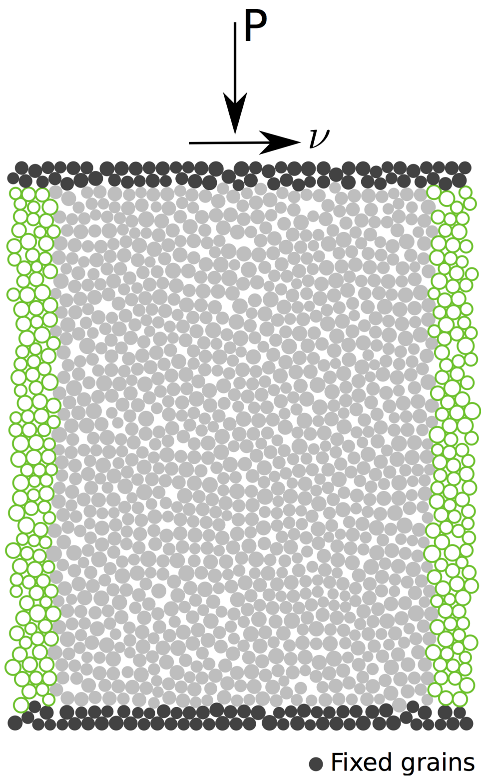

(a) Boundary conditions

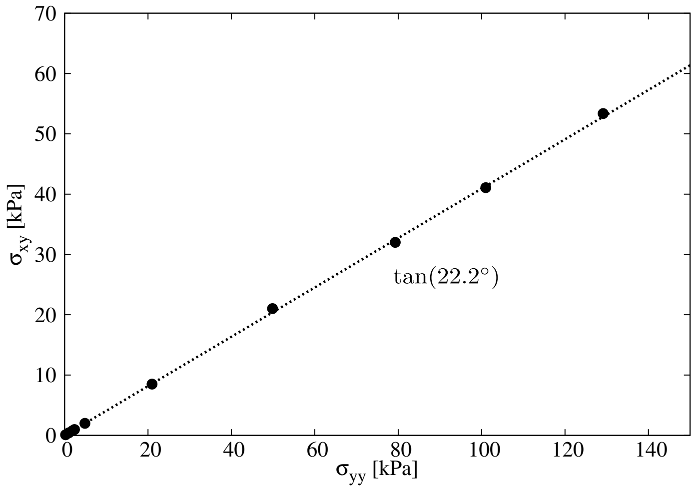

(b) Critical state friction angle from periodic shear test

Figure 4.3 Periodic shear test

Table 4.3 Parameters used in continuum simulations

Parameter	**Value**
Material point spacing	0.575 mm
Number of material points per cell	16
Young's Modulus, E	1.98×10^6 N m^{-2}
Poisson's ratio, ν	0.22 to 0.24
Friction angle, ϕ	$23.2 \pm 0.2°$
Dilatancy angle, Φ	0°
Density, ρ	1800 kg m^{-3}
Wall friction	0.466
Time step increment	1.0×10^{-6} s

4.2.2 Deposit morphology

Two-dimensional plane-strain MPM and DEM simulations of granular column collapse are performed by varying the initial aspect ratio of the column from 0.2 to 10. The normalized final run-out distance, $\Delta L = (L_f - L_0)/L_0$, as a function of the initial aspect ratio ‘a’ of the column is presented in figure 4.4. Similar to the experimental behaviour a power law relation between the run-out and the initial aspect ratio of the column is observed. Two distinct flow regimes can be seen: (a) for ‘a’ < 2.7 a linear relation between the spread and aspect ratio can be observed, and (b) for ‘a’ > 2.7 a power-law relationship exists. In the present study, the following scaling law for the run-out (using DEM) is observed:

$$\frac{L_f - L_0}{L_0} \approx \begin{cases} 1.67a, & a \lesssim 2.7 \\ 2.7a^{2/3}, & a \gtrsim 2.7 \end{cases} \tag{4.6}$$

Both, MPM and DEM simulations are able to capture the linear relationship for ‘a’ < 2.7, and the simulation results agree with the experimental investigation (Lajeunesse et al., 2005). This shows that a simple frictional dissipation model is able to capture the flow dynamics for columns with small aspect ratios. For ‘a’ < 2.7, the normalised run-out distance predicted using DEM simulations are very close to those observed in the experiment. DEM simulations with hexagonal packing shows shorter run-out distances in comparison to randomly packed sample. This difference in the run-out behaviour might be due to the crystallisation and jamming effects in hexagonal packing. The small difference in the final run-out between the DEM and the experimental results can be attributed to the variation in the packing of grains. Also, the experimental data corresponds to granular column collapse in a rectangular channel, where the collapse is not a pure two-dimensional collapse as in the case of numerical simulations.

Significant difference in the final run-out between MPM, which is based on a simple frictional model for dissipation of potential energy, and DEM simulations indicates a change in the mechanism of energy dissipation for columns with large aspect ratios (‘a’ > 2.7). Staron and Hinch (2005) observed that a constant frictional dissipation model cannot describe a power-law relation observed at large aspect ratios. A transition in the run-out behaviour at an aspect ratio of 2.7 indicates a change in the flow kinematics. Similar behaviour in the run-out distance was observed by Bandara (2013) for columns with large aspect ratios ($a \geq 2$).

The longer run-out distance in MPM simulations at large aspect ratios might be influenced by the amount of material mobilised during the collapse. In tall columns, the entire column participates in the flow, in contrast to short columns where the collapse is due to avalanching of flanks (Lajeunesse et al., 2004). It is possible that MPM simulations collapse more resulting in longer run-out distances. Figure 4.5 shows the normalized final height as a function of the initial aspect ratio of the column. Similar to the run-out behaviour, the normalised-height also shows two distinct regimes. The scaling of final height of the column with the initial aspect ratio of the column can be written as

$$\frac{H_f}{L_i} \propto \begin{cases} a, & a \lesssim 0.7 \\ a^{2/3}, & a \gtrsim 0.7 \end{cases} \tag{4.7}$$

The final height predicted by both DEM and MPM simulations match the experimental data for columns with smaller aspect ratio ($a \leq 0.7$). Linear relationship between the final height and the aspect ratio indicates that only a part of the granular column is mobilised during the collapse. For tall columns, both approaches predict similar normalised height. However, the normalised height observed in MPM is higher than in DEM simulations, which is in contrast to the idea of increase in the amount of material mobilised during the collapse in MPM simulations resulting in longer run-out distance. Hence, the longer run-out observed in MPM simulations is due a change in the flow dynamics at higher aspect ratios, which is not captured in MPM simulations. The final height of a column is controlled by the amount of static region in the granular column collapse, while the run-out distance is essentially a function of the flowing mass. Hence, it is important to compare the evolution of flow and the internal flow structure in DEM and MPM simulations.

4.2.3 Flow evolution and internal flow structure

The normalised run-out and height as a function of the aspect ratio indicates that, for a given granular material and substrate properties, the flow dynamics and the final deposit morphology are independent of the volume of granular material released, but depend only on the geometry of the column. A power law relationship is observed between the run-out distance and the initial aspect ratio of the column. A transition in the run-out behaviour at an aspect ratio of 2.7 indicates a change in the flow dynamics.

For short columns (‘a’ < 2.7), the flow is initiated by a failure at the edge of the pile along a well-defined fracture surface. The granular mass fails through avalanching of flanks producing a truncated cone-like deposit (‘a’ < 0.7) or conical deposit (‘a’ > 0.7). The grains located above the failure surface move “*en masse*” leaving a static region underneath the failure surface.

Dimensional analysis of granular column collapse reveals an intrinsic time defined as $\sqrt{H_0/g}$. This intrinsic time is a transient time of order τ_c, at which the flow is fully developed, i.e., the potential energy available at the initial stage of collapse is now fully converted to kinetic energy. Numerical simulation of the velocity profile of a granular column (‘a’=0.4) at critical time τ_c is presented in figure 4.6. At critical time, the velocity field depends only on the

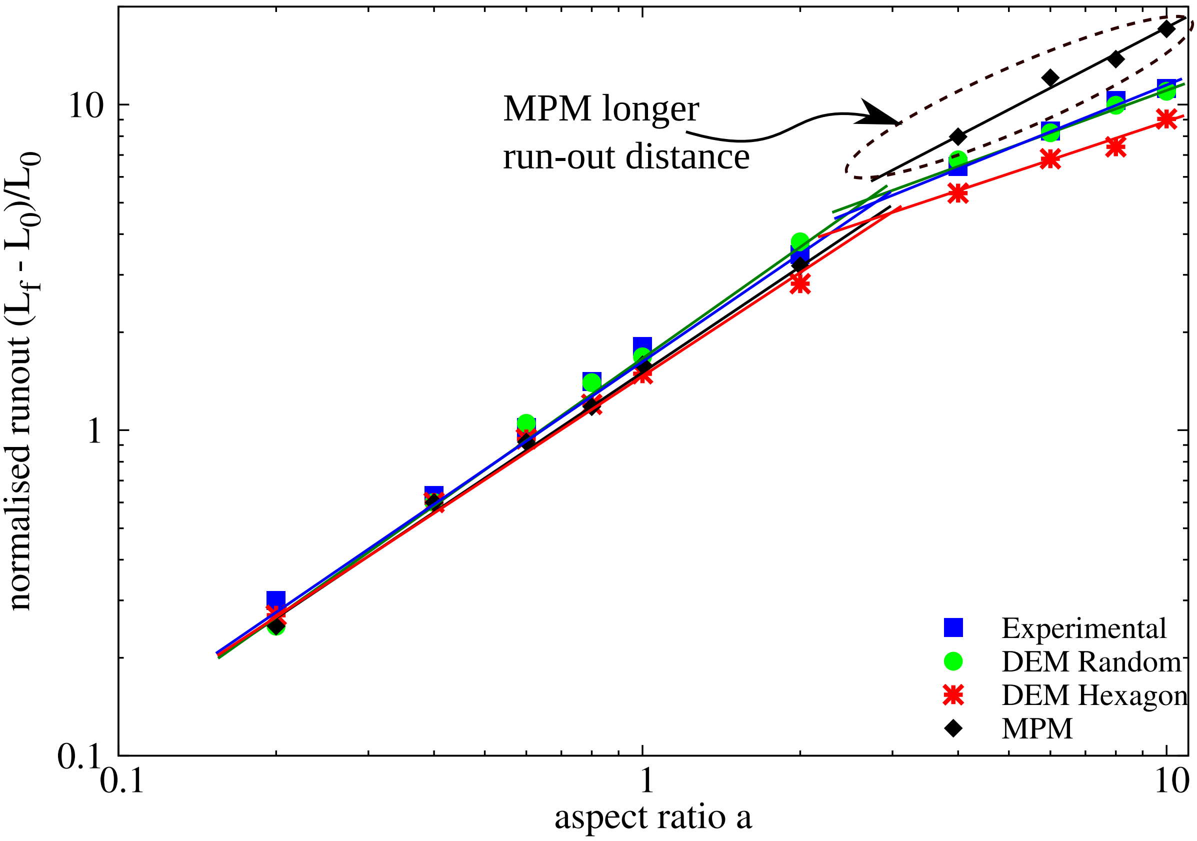

Figure 4.4 Normalised final run-out distance for columns with different initial aspect ratio

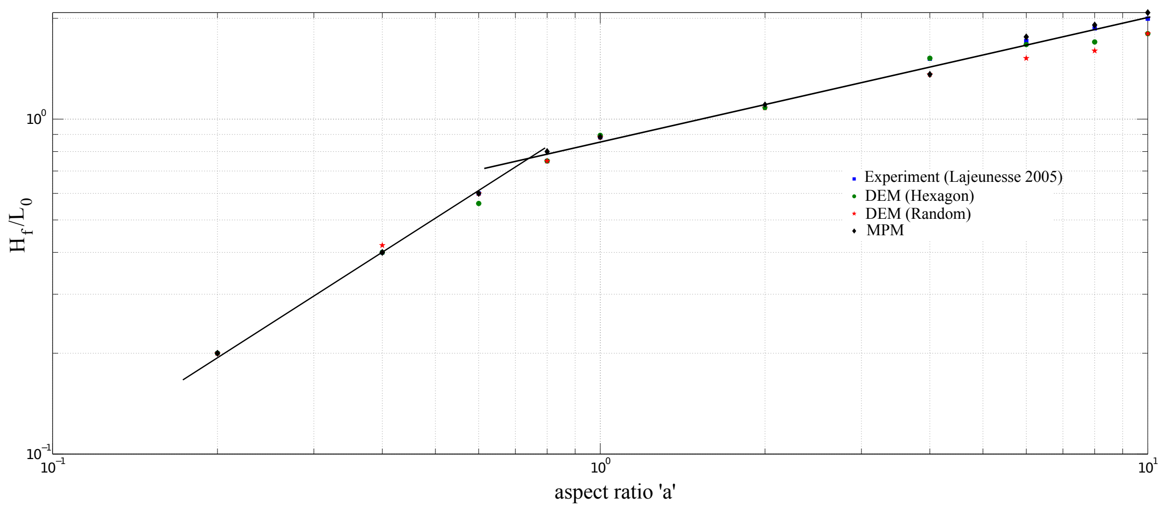

Figure 4.5 Normalised final collapse height for columns with different initial aspect ratio

position of the grain along the sliding mass. The maximum velocity is observed at the front of the flowing mass corresponding to that of a plug flow in horizontal direction. Particulate and continuum simulations show similar run-out distance at the critical time. Both approaches show similar quantity of material destabilised above the failure surface. However, the crystalline arrangement of soil grains in a hexagonal packing results in a different flow mechanics, which also shows the effect of jamming at the flow front. The continuum nature of MPM results in a slightly different geometry of the material destabilised above the failure surface in comparison to DEM simulations. The velocity profile is similar to a steady granular surface flow observed by Lajeunesse et al. (2004).

For columns with lower initial aspect ratios, the run-out distance is proportional to the mass flowing above the failure surface. The spreading results from a Coulomb-like failure of the edges and implies no free fall of the column. Daerr and Douady (1999) also observed active Coulomb yielding in transient granular surface flows. In this case, the effective friction properties of the flow can be simply predicted from the shape of the final deposit. The amount of mass mobilized during the collapse is significantly affected by the angle of the failure surface. Figure 4.6 shows that both numerical techniques predict a distinct failure surface when the flow is fully developed at critical time τ_c. The angle of the failure surface is found to be about 55°. The failure surface begins from the toe of the column and propagates inwards at an angle of 50 to 55°. The formation of the "truncated conical deposit" or "conical deposit" depends only on the initial length of the column, as the angle of the failure surface is found to be independent of the aspect ratio. The failure angle is consistent with the interpretation in terms of *active Coulomb failure* (Lajeunesse et al., 2004), which leads to a predicted failure angle $\theta_y = 45° + \delta/2$, where δ is the friction angle of the granular material. In the present study, the macroscopic friction angle is 22°, which leads to $\theta_y = 45° + 22°/2 = 56°$, which is in good agreement with the numerical simulations and experimental observations by Lajeunesse et al. (2004). The fracture angle has a direct effect on the transition between the truncated cone and the conical deposit occurring at an aspect ratio of 0.7. Schaefer (1990) observed the onset of instabilities in a narrow wedges of 56 to 65^o for Cambridge-type constitutive models that describes granular flows, which is in-line with the failure angle observed in the present study.

The final profile of the granular column with an initial aspect ratio of 0.4 is shown in figure 4.7. Both MPM and DEM show similar run-out behaviour. The continuum approach is able to capture the flow dynamics of short columns, where the failure mechanism is active Coulomb failure. In dense hexagonal packing, the failure surface is steep due to crystallisation effect. The variation in the angle of the failure surface causes a difference in the amount of material destabilised, and in turn the run-out distance. This crystallisation phenomenon is found to have a significant influence on the final deposit of the granular column. Lacaze and

Kerswell (2009) observed that poly-disperse grains are less susceptible to crystallize especially in the case of tall columns.

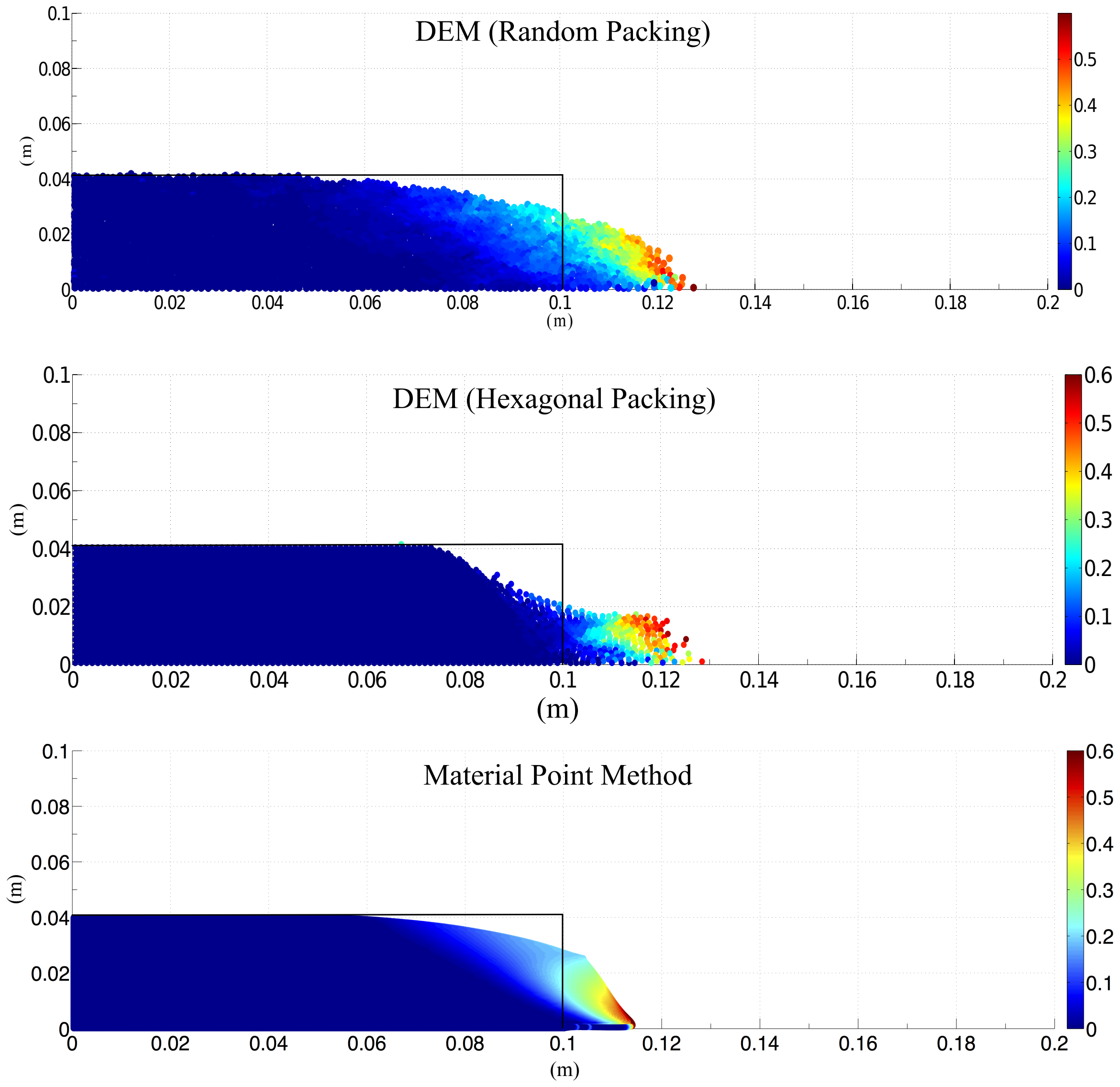

Figure 4.6 Velocity profile of a granular column collapse ($a = 0.4$ & $t = \tau_c$)

For tall columns (‘a’ > 2.7), the flow is still initiated by a well defined failure surface as can be seen in figure 4.8. However, in this case the initial granular column is much higher than the top of the failure surface. Due to gravity most of the grains in the column experience free-fall consuming the column along their way. When they reach the vicinity of the failure surface, the flow gets deviated along the horizontal direction releasing a huge amount of kinetic energy gained during the free fall. For larger aspect ratio ($a > 0.7$), the resulting static region is

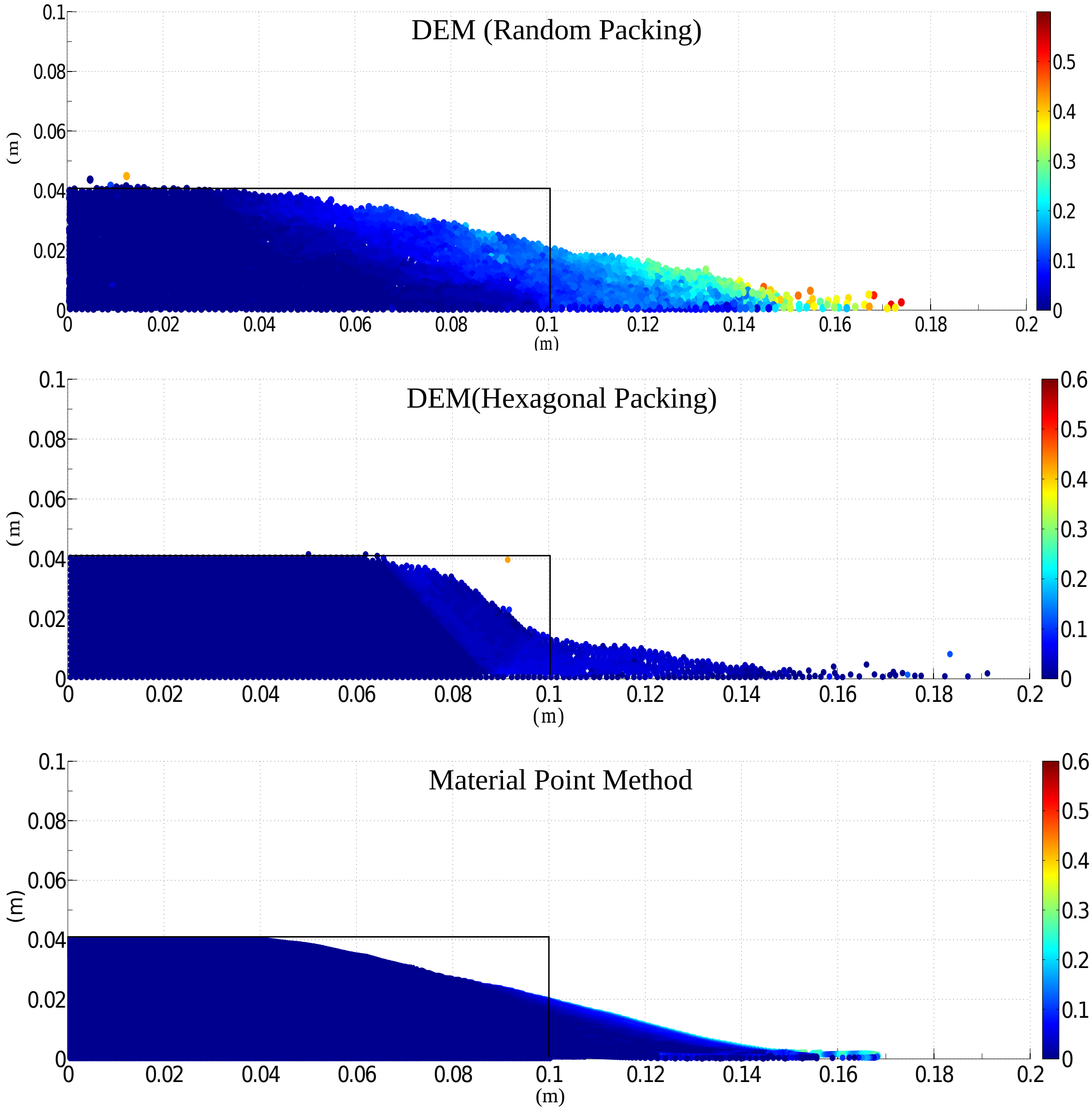

Figure 4.7 Velocity profile of a granular column collapse ($a = 0.4$ & $t = 3 \times \tau_c$)

a cone, the final height of the cone, i.e, H_f lies above the summit of the failure surface. Hence, a different evolution is observed from that of the axis-symmetric geometry (Lube et al., 2005), where the final height coincides with the summit of the failure surface forming a truncated conical deposit. Lajeunesse et al. (2004) observed that the variation in the deposit morphology between the axis-symmetric case and the rectangular collapse to be a geometrical effect rather than as an experimental artefact.

An initial failure surface starting from the toe end of the column at an angle of about 55° can be observed at the critical time τ_c. As the collapse of the granular collapse progresses, successive failure planes parallel to the initial failure surface are formed and shear failure occurs along these planes. The presence of several shear bands in the final profile of the collapsed granular column confirms this behaviour. Crystallisation in hexagonal packing has a significant effect on the run-out distance by forming series of parallel shear bands, resulting in unnatural flow kinematics. This observation throws light on the mechanics of propagation of shear bands in massive landslides such as the Storegga submarine landslide. The flow behaviour becomes similar to that of columns with lower aspect ratio as the flow starts descending along the failure plane. The final profile of the collapsed granular column with an initial aspect ratio of 6 is presented in figure 4.9. For tall columns, the dissipation process is more complex due to the free-fall dynamics. The vertical acceleration of the grains induces a non-trivial mass distribution in the flow during spreading. This mass distribution plays a dominant role in the power-law scaling observed in the run-out (Staron and Hinch, 2007).

Regardless of the experimental configuration and the initial aspect ratio of the columns, the flow is initiated by a well-defined rupture surface, above which the material slides down leaving a static region underneath the failure plane. Depending on the aspect ratio of the column, two asymptotic behaviours are observed. For smaller aspect ratios, the flow is dominated by friction where as the large aspect ratio columns are influenced by the pressure gradient.

To study the influence of aspect ratio on the flow dynamics of granular columns, the flow front $L(t)$ and the maximum height of column $H(t)$ are tracked. The evolution of scaled height (H_f/L_0) and the run-out distance $(L_f - L_0)/L_0$ with time for granular columns with an initial aspect ratio of 0.4 and 6 are presented in figure 4.10. Three distinct regions can be observed in the flow evolution of a granular column collapse regardless of the initial aspect ratio of the column. An initial transient acceleration phase is observed for a time $0.8\tau_c$. This phase is followed by a heap movement of granular materials at the foot with a constant spreading velocity V for about $2\tau_c$. When time 't' $> \tau_c$, the velocity varies linearly with depth in the flowing layer and decreases exponentially with depth near the static layer. This velocity profile is similar to those observed in steady granular surface flows (Lajeunesse et al., 2004). Most of the run-out happens during this phase. The final phase involves deceleration of the flow

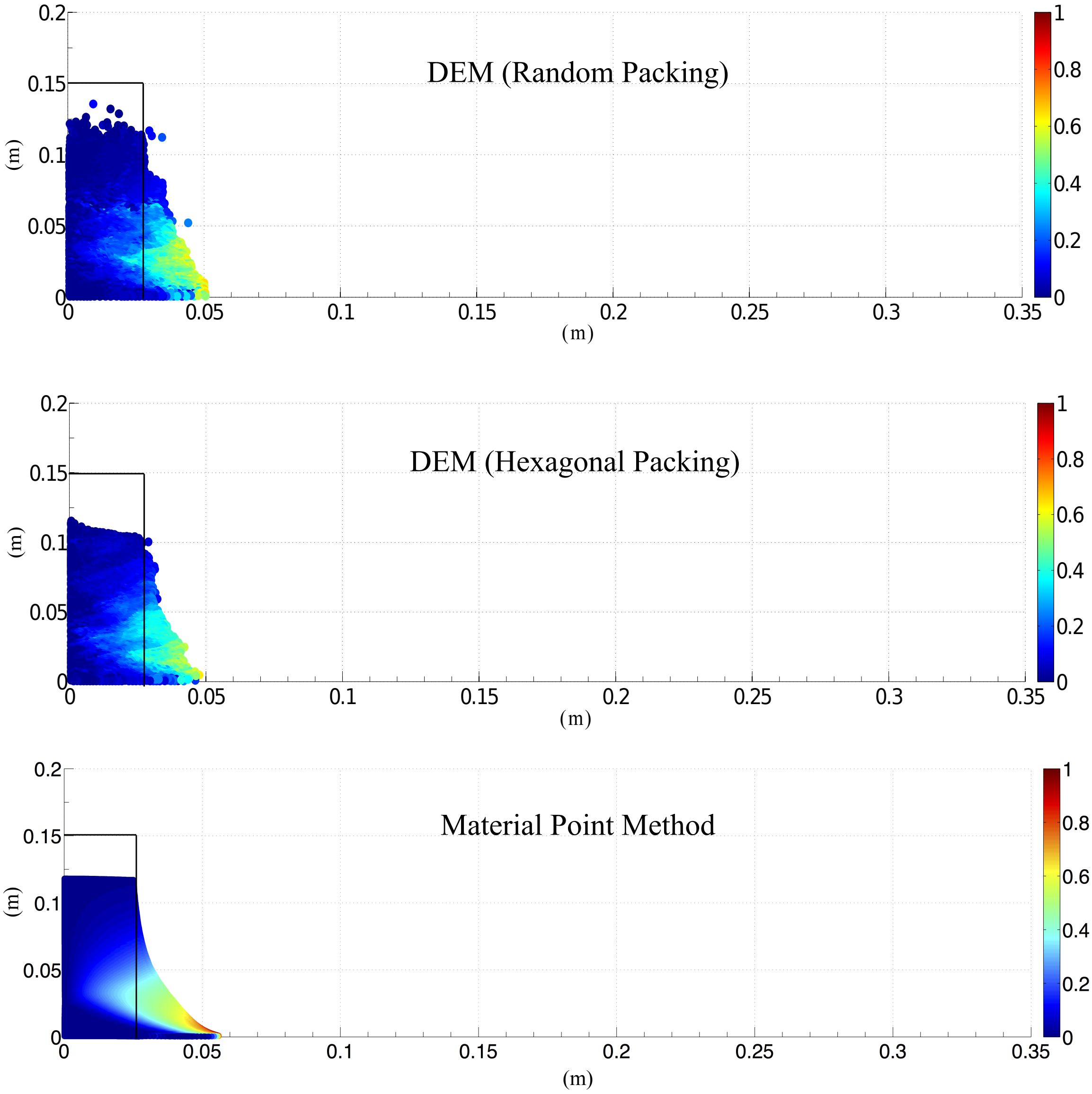

Figure 4.8 Velocity profile of a granular column collapse ($a = 6$ & $t = \tau_c$)

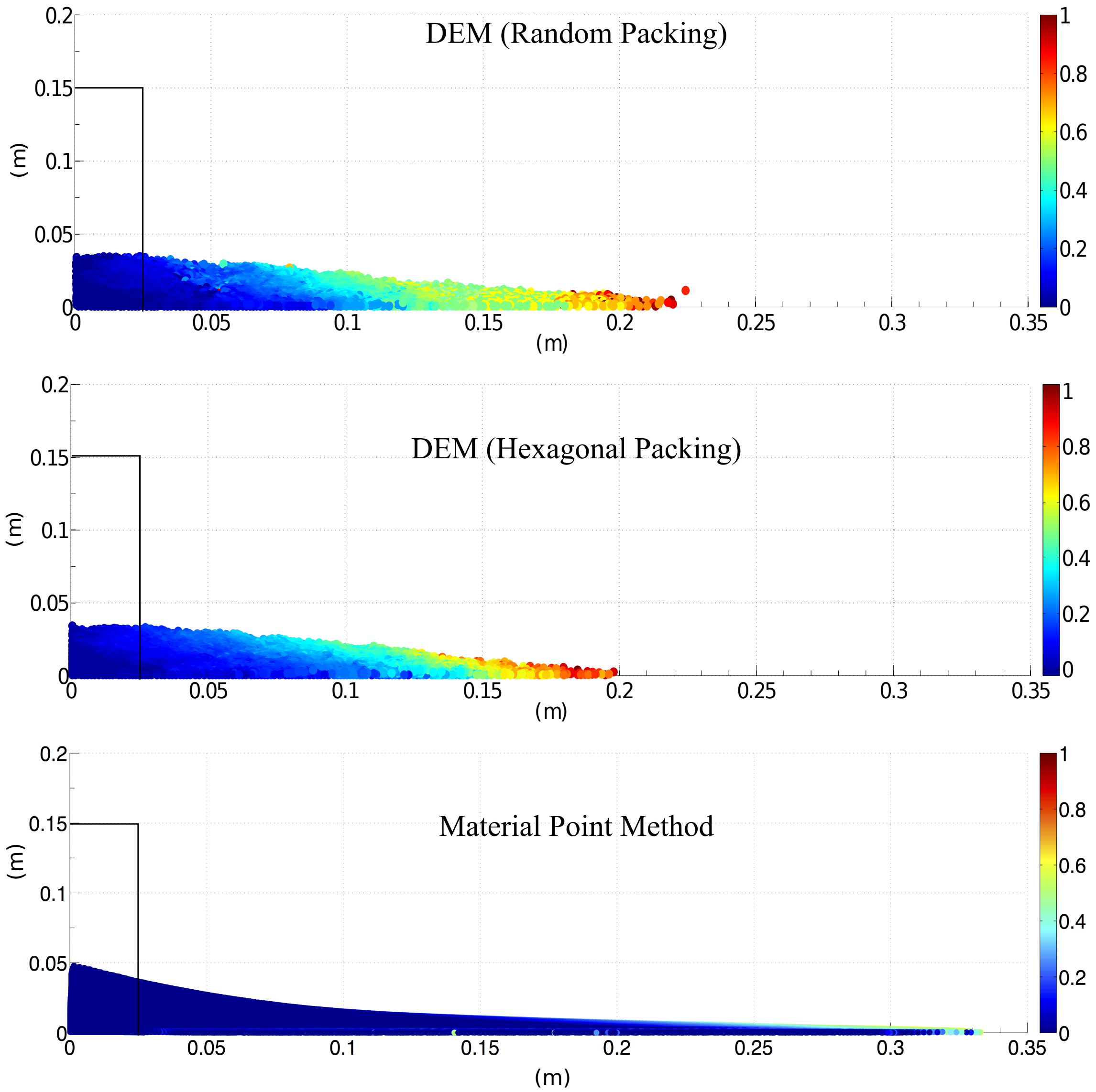

Figure 4.9 Velocity profile of a granular column collapse ($a = 6$ & $t = 3 \times \tau_c$)

front and the flow comes to rest after about $0.6\tau_c$. The spreading of the granular column ceases after a time in the order of about $3\tau_c$, however some motion still persists along the free surface behind the flow front for a much longer time due to internal rearrangement, the duration of which can last up to $t \approx 6\tau_c$.

The critical time is evaluated as the time at which the potential energy available for the flow has been converted to the kinetic energy. In short columns, the critical time observed in both hexagonal and random packing of grains matches the experimental observations. However, the material point method overestimates the critical time by a factor of 0.75, which means that it takes longer for the flow to be fully mobilized. However, the actual run-out duration of the flow is short and the granular mass comes to rest at about $t = 3\tau_c$.

For columns with larger aspect ratios, the continuum and particulate approaches simulate similar flow evolution up to $3\tau_c$, beyond which particulate simulation decelerates and comes to rest, while the flow continues to evolve in MPM simulation resulting in longer run-out distance. The flow comes to rest at time $t = 6\tau_c$. The three phases in a granular flow can be distinctly observed in the flow evolution plot for a column with an initial aspect ratio of 6 (see figure 4.10b). The flow evolution behaviour observed in the case of DEM simulation matches the experimental observation by Lajeunesse et al. (2004). Hexagonal packing predicts longer time for the flow to evolve, which can be attributed to jamming of grains. In MPM simulations, the failure starts at the toe of the column and slowly propagates up to form the failure surface. This results in slower initiation of the flow. Whereas in DEM, the initial stage of collapse is characterised by free-fall under gravity. It can be observed that MPM overestimates the critical time by 50%. Although, MPM and DEM simulations show the same run-out at time $t = 3\tau_c$, the flow evolution between both the approaches is different. MPM simulations continue to accelerate beyond $3\tau_c$ and ceases to flow at $6\tau_c$. In order to understand the difference in the flow dynamics in the case of material point method, it is important to study the mechanism of energy dissipation.

4.2.4 Energy dissipation mechanism

The energy dissipation mechanism during the collapse provides useful insights into the flow dynamics. In the case of small aspect ratios, the columns undergo no free fall. The spreading mainly results from the failure of the edges, while the top of the column remains essentially undisturbed in the central area. Staron and Hinch (2007) showed that the amount of energy dissipated during the spreading δE can be easily recovered using the simple shape of the final

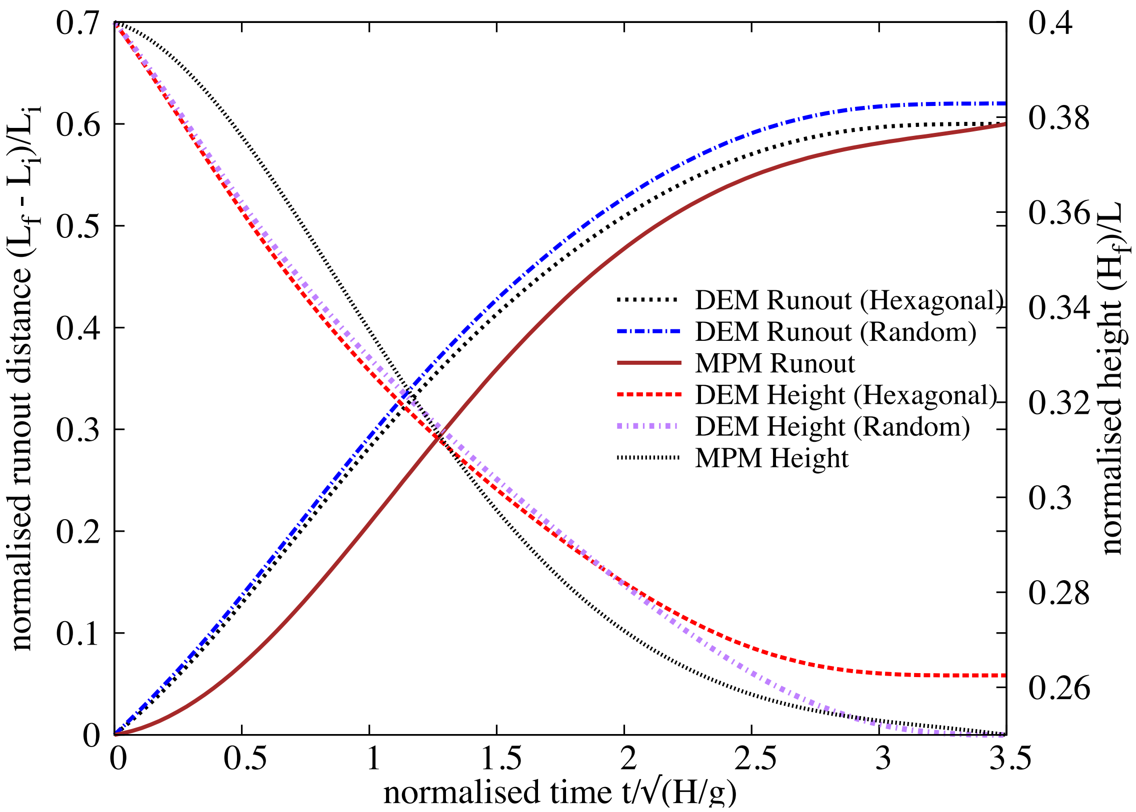

(a) Flow evolution of a column with $a = 0.4$

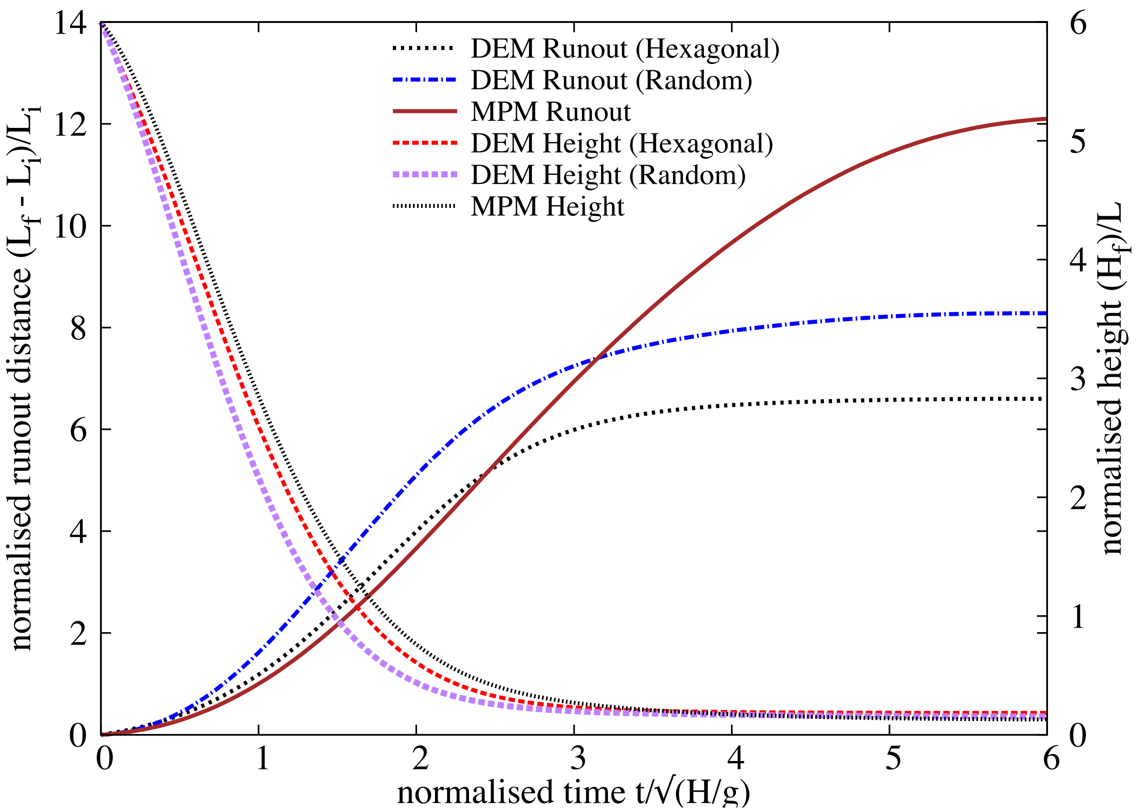

(b) Flow evolution of a column with $a = 6$

Figure 4.10 Flow evolution of granular column collapse

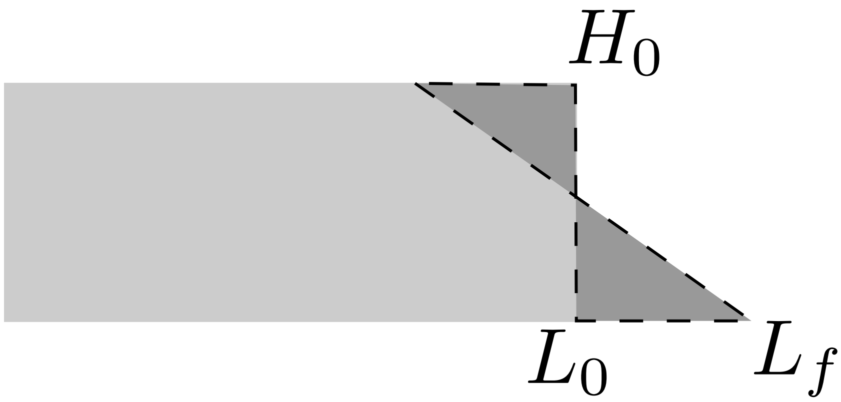

Figure 4.11 Scheme of collapse for small aspect ratio columns. The amount of energy δE lost in the process can be evaluated from the run-out distance $L_f - L_0$ (after Staron and Hinch (2007)).

deposit and volume conservation (see figure 4.11). The difference of potential energy between the initial and the final states gives

$$\delta E = \frac{1}{6} g \rho (L_f - L_0) H_0^2 \,, \tag{4.8}$$

where ρ is the density of the packing. It is assumed that this energy is dissipated by the work of frictional forces W_μ over the total run-out distance by the center of mass G of the spreading material. Staron et al. (2006) considers two regions of dissipation: the amount of mass destabilised $\frac{1}{4}(L_f - L_0)H_0$ over two thirds of the runout distance $2(L_f - L_0)/3$ (considering the triangular shape of the final deposit and the initial and the final positions of the center of mass). The effective coefficient of friction μ_e characterizes the mean dissipation in the flow. The work of friction forces is

$$W_\mu = \frac{1}{6} \mu_e g \rho (L_f - L_0) H_0^2 \,, \tag{4.9}$$

Equating δ_E and W_μ gives $\mu_e(L_f - L_0) = H_0$. The scaling of the runout leads directly to the relation $\mu_e = \lambda^{-1}$, which is the numerical constant, which depends on the material properties (Balmforth and Kerswell, 2005), in the power-law relation between the run-out and the initial aspect ratio. The amount of energy δE dissipated during the spreading is compared with $W = N_p g m_p r_p$, where N_p is the total number of grains, m_p is their mass, and r_p is the total horizontal distance run by each of them. We observe that the dissipation energy δE is proportional to W. Staron and Hinch (2007) observed that the coefficient of proportionality gives a measure of the effective friction and observed a power law dependence between μ_e and internal friction angle μ: $\mu_e = 0.425\mu^{0.2}$. In this study, an effective friction angle μ_e of $21°$ is observed, which is very close to the critical state friction angle of $22°$ used in MPM simulations. This proves that the energy dissipation mechanism modelled in a continuum sense as a frictional dissipation process captures the flow kinematics observed in DEM and experiments, for short columns.

Figure 4.12a shows the time evolution of the normalised potential energy (E_p/E_0) and kinetic energy (E_k/E_0) for granular columns with an initial aspect ratio 'a' = 0.4. The normalised potential and kinetic energy are computed as

$$E_p = \sum_{p=1}^{N_p} m_p g h_p\,, \tag{4.10}$$

$$E_{ki} = \frac{1}{2}\sum_{p=1}^{N_p} m_p v_p^2\,, \tag{4.11}$$

where N_p is the total number of grains, m_p is the mass of a grain 'p', h_p is the height and v_p is the velocity of the grain 'p'. The cumulative dissipation energy is computed as

$$\frac{E_d}{E_0} = 1 - \frac{E_k}{E_0} - \frac{E_p}{E_0}\,. \tag{4.12}$$

It can be observed that both MPM and DEM show similar energy dissipation mechanism. The DEM simulation shows 3% more potential energy dissipation in comparison with MPM simulations. This small difference in the potential energy is due to grain rearrangements. This shows the ability of continuum approach in capturing the flow kinematics of columns with small aspect ratios ($a \leq 2.7$).

The evolution of normalised kinetic and potential energy of a tall column collapse ('a' of 6) is shown in figure 4.12b. It can be observed that the initial potential energy stored in the grains is converted to kinetic energy which is dissipated as the granular material flows down. Three successive stages can be identified in the granular column collapse. In first stage, similar to short columns, the flow is initiated by a well defined failure surface. However, the centre of gravity of the granular column is much higher than the top of the failure surface, which results in free fall of grains under gravity consuming the column along their way. In this stage which lasts for $(t < 0.8\tau_c)$, the initial potential energy stored in the grains is converted into vertical motion. In the second stage, when the grains reach the vicinity of the failure surface, they undergo collisions with the bottom plane and the neighbouring grains, thus causing the flow to deviate along the horizontal direction releasing a large amount of kinetic energy gained during the free fall (see figure 4.9). In the third stage, the grains eventually leave the base area of the column and flow sideways (Lajeunesse et al., 2004). As the process involves collective dynamics of all the grains, it is difficult to predict the exact trajectory of a grain, however, the overall dynamics can be explained.

DEM simulations model both collisional and frictional dissipation process during the collapse of tall columns. However, MPM simulations assume that the total initial potential energy stored in the system is completely dissipated through friction over the entire run-out distance, this results in longer run-out distance. Figure 4.12b shows the evolution of energy with time. At the initial stage of collapse, characterised by free fall of grains under gravity, DEM simulation due its particulate nature shows a rapid reduction in the potential energy in comparison with MPM, where the failure begins from the toe of the column. The continuum nature of MPM simulations results in slower initiation of collapse (see figure 4.10b). It can be also observed from figure 4.12b that dissipation energy in MPM is 25% less than DEM simulations. In order to understand the mechanism of energy dissipation, it is important to separate the contribution from the cumulative frictional and collisional parts. The frictional dissipation (basal and internal friction) observed in DEM is almost identical to the frictional dissipation observed in MPM (figure 4.12b). The difference in the dissipation energy is due to the collisional regime, which occurs at $0.8\tau_c$. The total dissipation and the frictional dissipation curves diverge around $0.8\tau_c$ where the grains near the vicinity of the failure surface undergo collisions with the bottom plane and the neighbouring grains resulting in collisional dissipation of the stored potential energy. DEM simulation show drop in the peak kinetic energy at $\approx 0.8\tau_c$, which is at the beginning collisional dissipation stage. MPM lacks this collision dissipation mechanism, which results in longer run-out distances for columns with large aspect ratios.

$\mu(I)$ rheology, discussed in **??**, describes the granular behaviour using a dimensionless number, called the *inertial number I*, which is the ratio of inertia to the pressure forces. Small values of I corresponds to critical state of soil mechanics and large values of I corresponds to the fully collisional regime of kinetic theory. $\mu(I)$ rheology is adopted in MPM simulations to understand the characteristics of the flow regime. Mohr-Coulomb model was used along with $\mu(I)$ rheology. The friction angle is changed according to a friction law (Da Cruz et al., 2005) that is dependent on the inertial number I as $\mu = \mu_{min} + bI$ where $\mu_{min} = 0.22$ and b = 1. Figure 4.13 shows the flow evolution of granular column collapse for aspect ratio ‘a’ of 0.4 and 6 using $\mu(I)$ rheology. For short columns, the evolution of flow based on $\mu(I)$ rheology is identical to the MPM simulation using Mohr-Coloumb model. However, for tall columns, $\mu(I)$ rheology evolves at the same rate as the DEM simulations up to $t = 0.8\tau_c$, after which MPM simulation continues to accelerate due to lack of collisional dissipation, while the DEM simulation decelerates with time.

Figure 4.23b shows that the short column attains a maximum inertial number of 0.012, which is in the dense granular flow regime, inertial number $I \approx 10^{-3}$ to 0.1 (Da Cruz et al., 2005). However, the maximum inertial number $I \approx 0.04$, for tall is still within the dense granular flow regime. DEM simulations, however, showed a collisional regime that has inertial

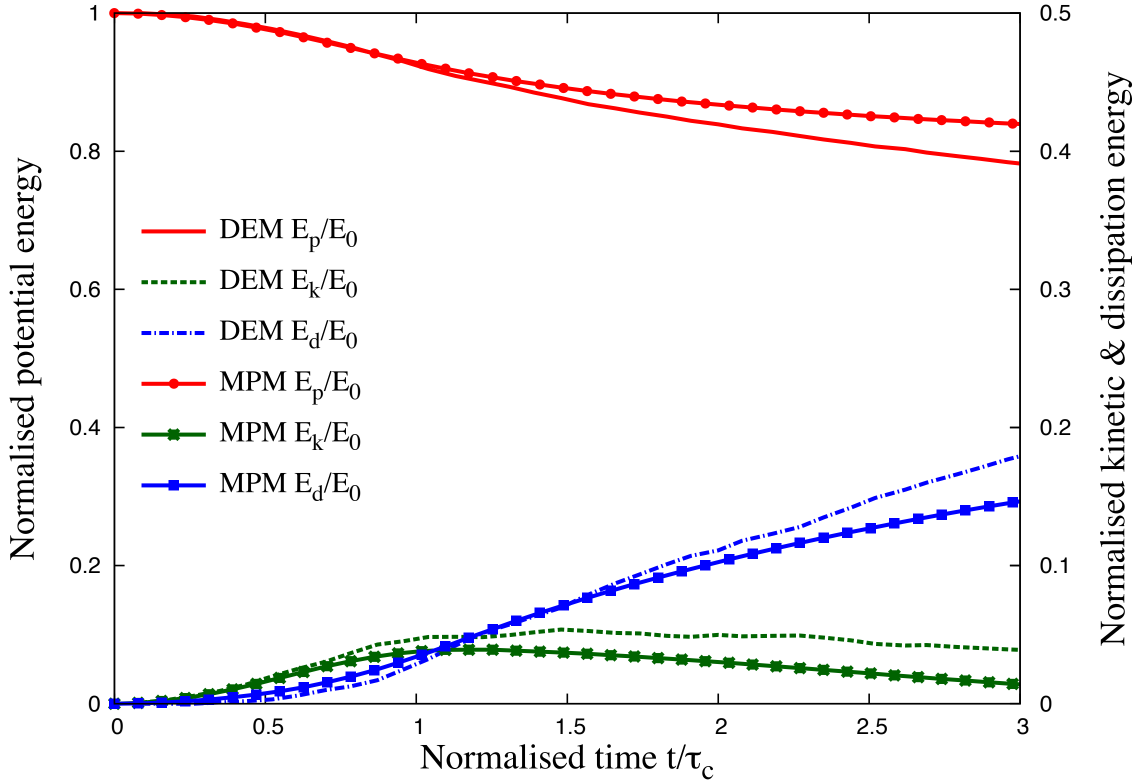

(a) Energy evolution of a column with $a = 0.4$

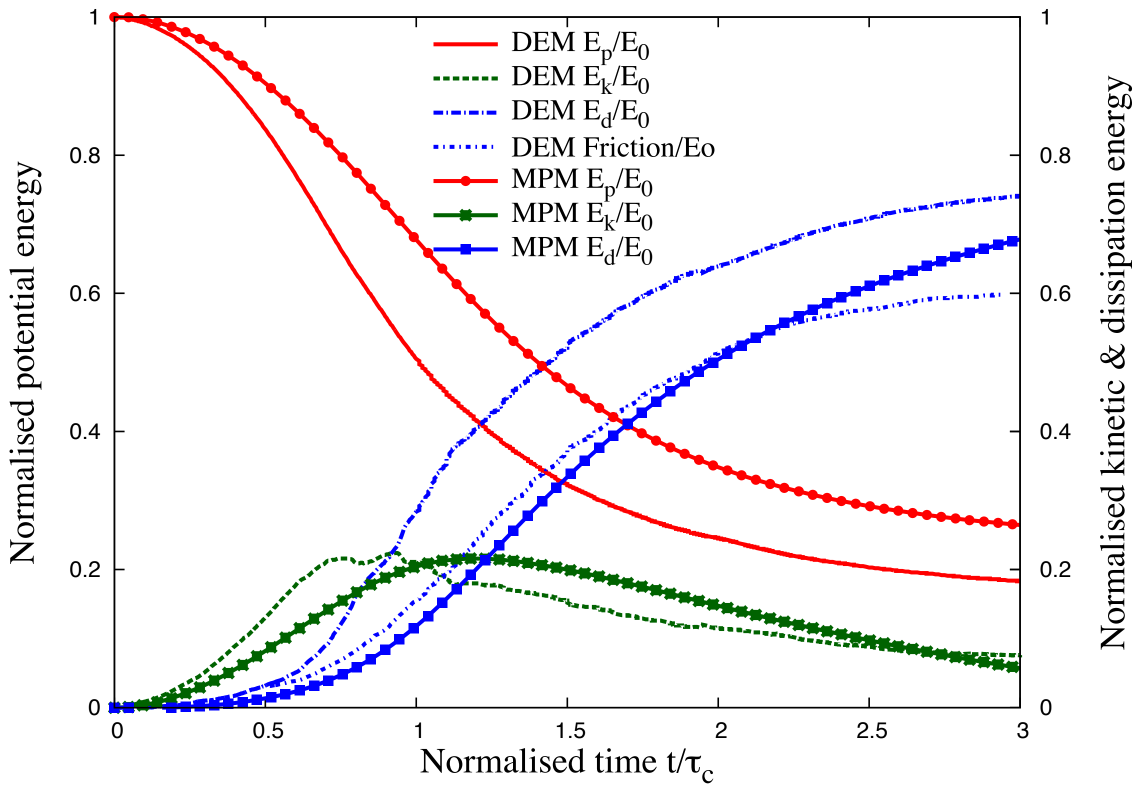

(b) Energy evolution of a column with $a = 6$

Figure 4.12 Energy evolution of granular column collapse

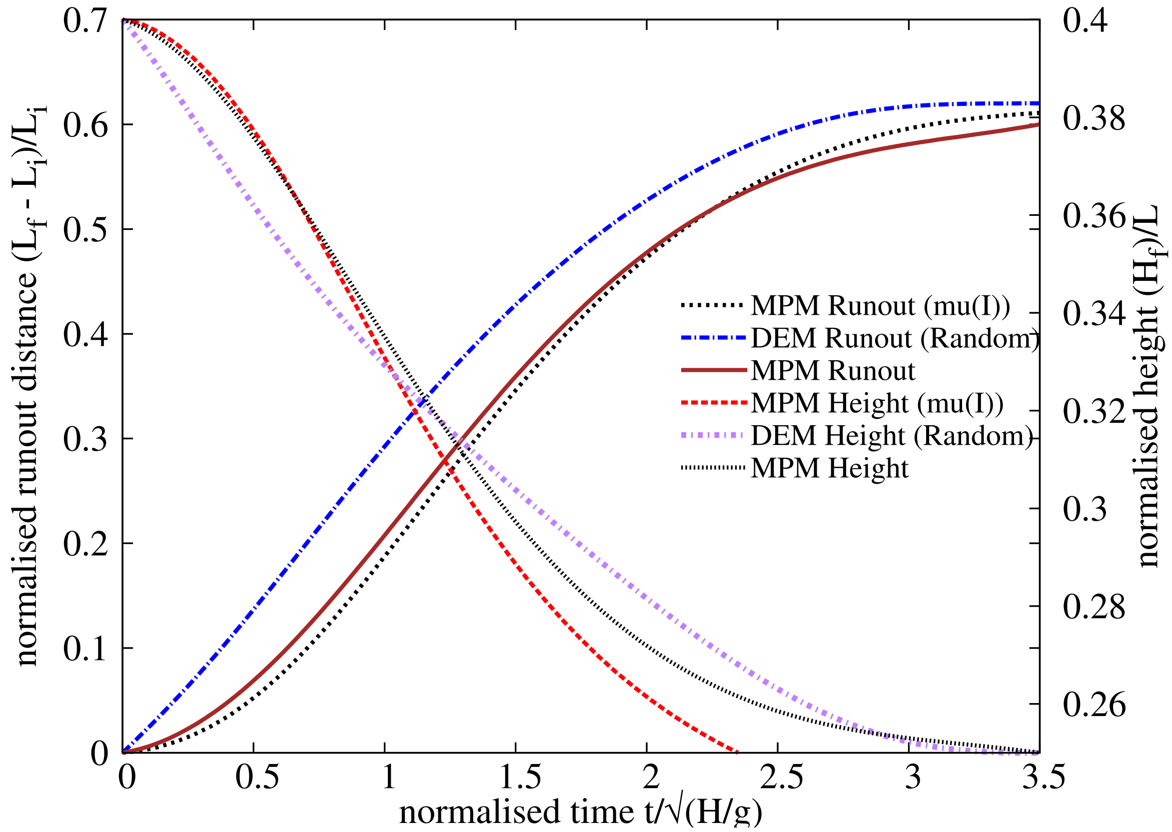

(a) Flow evolution of a column with $a = 0.4$ using $\mu(I)$ rheology

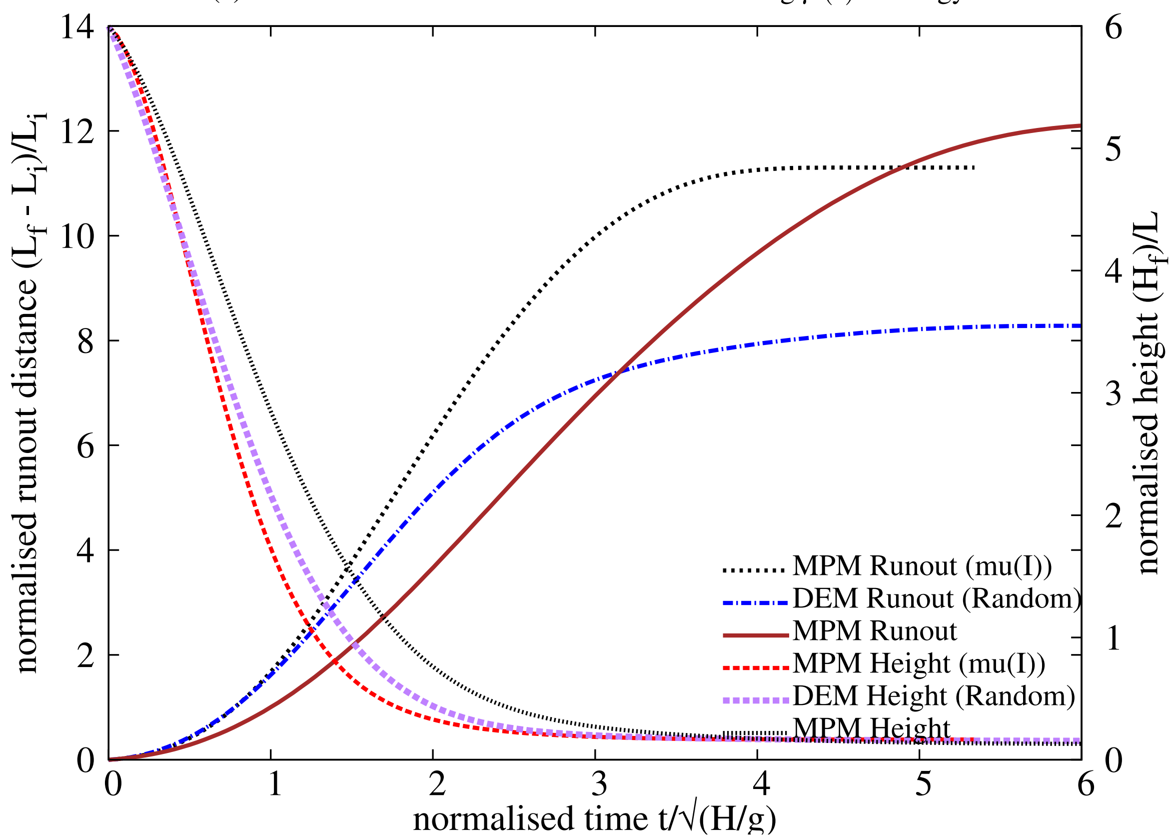

(b) Flow evolution of a column with $a = 6$ using $\mu(I)$ rheology

Figure 4.13 Flow evolution of granular column collapse using $\mu(I)$ rheology number higher than 0.1. This shows that continuum approach using frictional laws are able to capture the flow kinematics at small aspect ratios, however are unable to precisely describe the flow dynamics of tall columns, which is characterised by an initial collisional regime.

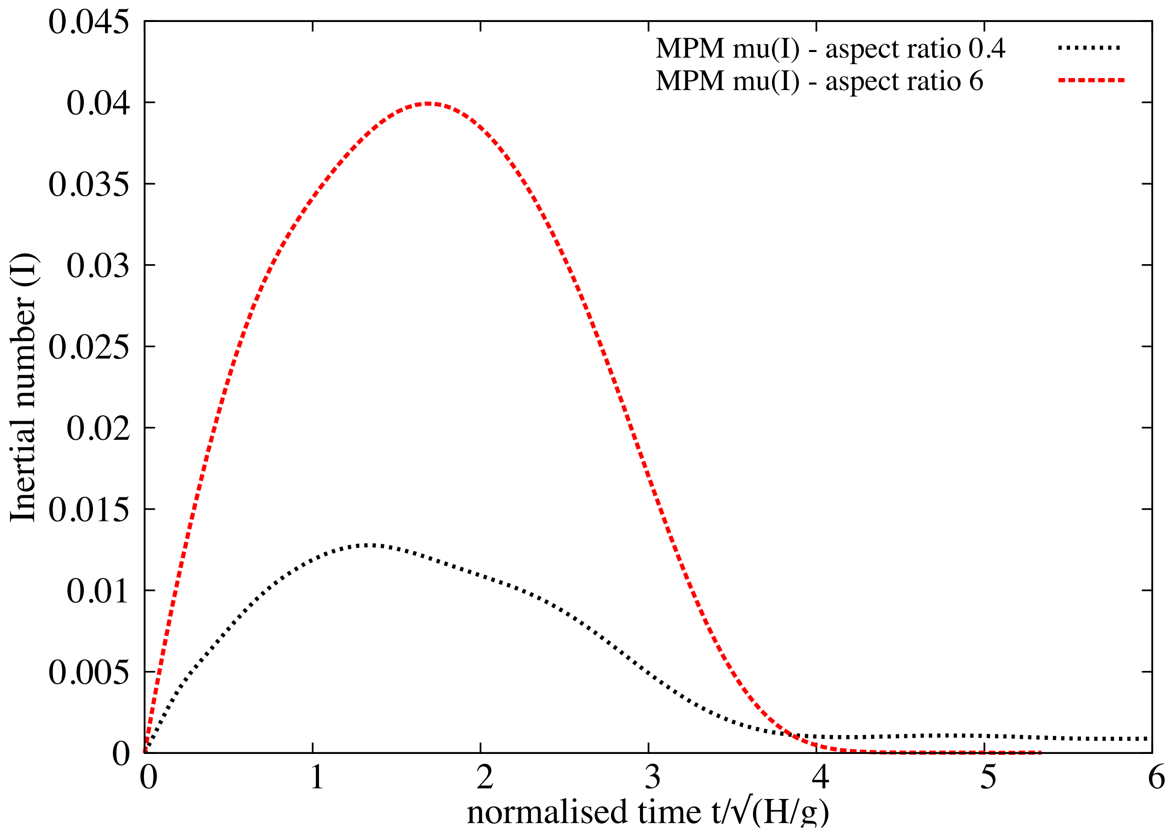

Figure 4.14 Evolution of inertial number with time for columns with $a = 0.4$ and $a = 6$

4.2.5 Role of initial grain properties

Lube et al. (2005) observed that the run-out distance scales with the initial aspect ratio of the column, independent of the material properties. The run-out evolution after the initial transition regime is a frictional dissipation process, and the lack of influence of material properties on the run-out behaviour is inconsistent with frictional dissipation in continuum modelling of granular flow behaviour. Balmforth and Kerswell (2005) observed that the material properties have almost no influence on the exponent of the normalised run-out as a function of the initial aspect ratio. The numerical constant of proportionality, however, showed clear material dependence. This corroborates the conclusions of Lajeunesse et al. (2004) and softens that of Lube et al. (2005). Daerr and Douady (1999) also observed strong influence of initial packing density and the internal structure on the behaviour of granular flows.

It should be noted that the collapse experiment is highly transient and no clear stationary regime is observed. On the contrary, the acceleration and the deceleration phases cover nearly the whole duration of the spreading. This makes it difficult to analyse the flow structure and its relation with other characteristic of the system. The knowledge of the final run-out is not a sufficient characterization of the deposit: one also needs to know how the mass is distributed during the flow to understand the dynamics and the dissipation process. This is expected to be true in natural contexts as well as in experiments. While the inter-grain friction does not affect the early vertical dynamics, nor the power-law dependence, it controls the effective frictional properties of the flow, and its internal structure (Staron and Hinch, 2007). It is interesting to note that the details of the structure of the flow do not influence the final run-out dependence, and thus seem to play a marginal role in the overall behaviour of the spreading. This could explain why simple continuum model with a frictional dissipation could reproduce the run-out scaling for columns with small aspect ratios.

The run-out behaviour of a loose (79% packing density) and a dense (83% packing density) granular column (a = 0.8) are studied to understand the influence of material properties. The evolution of normalised run-out with time for two different initial packing densities are presented in figure 4.15. At the initial stage of collapse $t = \tau_c$, the flow evolution is identical in both dense and loose conditions. However, the dense column flows 30% longer than the loose condition. Both the columns come to rest at around $t = 4\tau_c$. The columns, however, show similar evolution of the normalised height. This shows that only a part of the column is destabilised during the collapse.

Figure 4.17 show the evolution of potential and kinetic energy with time. Similar potential energy evolution in both dense and loose conditions reveals that there is no change in the overall mechanism of collapse. The dense condition has slightly higher peak kinetic energy than the loose column. In the free-fall phase, the dense column shows a steeper increase in the horizontal kinetic energy in comparison to the loose column. This indicates that dense granular mass is pushed farther away more quickly than the loose column. Loose column exhibits higher vertical kinetic energy which may be due to particle rearrangement resulting in densification of the granular mass. Figure 4.16 shows that the loose sample densifies as the flow evolves. Both dense and loose granular columns dilate during the initial stage of collapse, this is due to grains experiencing shear along the fracture surface. In both cases, the granular mass attains similar packing density at the end of the flow. Dense granular column dilates, while the loose column compacts to achieve the same critical density. The dense condition has higher mobilised potential energy during the initial stage of collapse, which yields higher horizontal kinetic energy for the flow. However in loose condition, a higher proportion of the available energy is lost during compaction. This behaviour in addition to higher mobilised potential

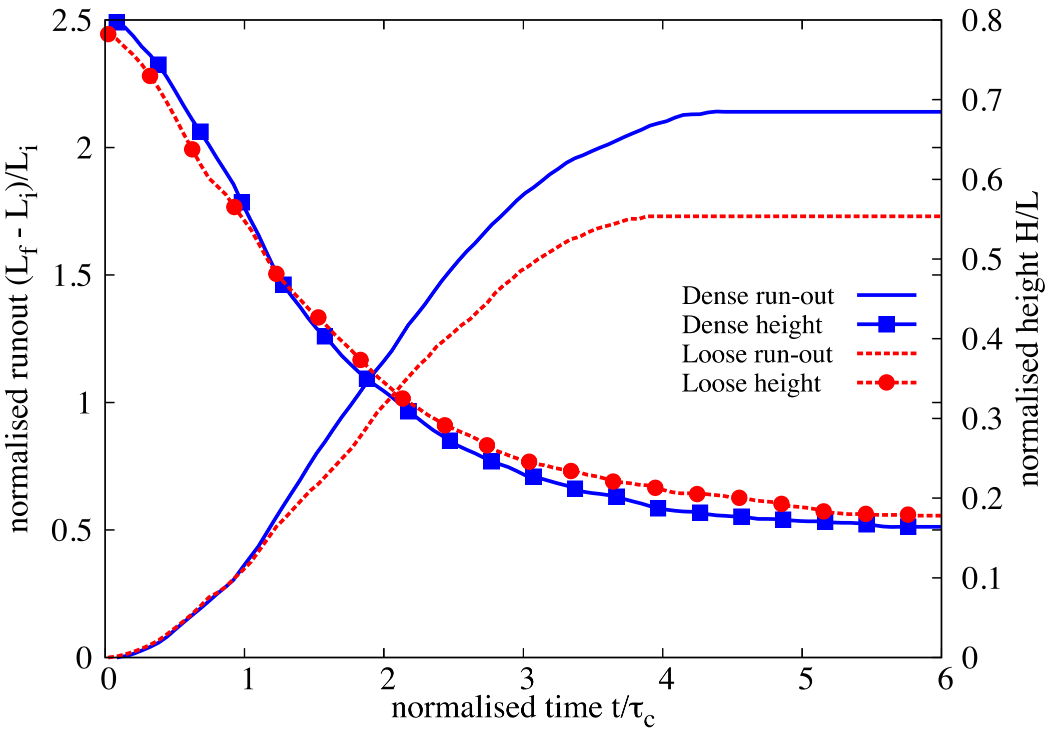

Figure 4.15 Effect of density on run-out evolution $a = 0.8$

energy results in longer run-out distance in dense granular column. Lajeunesse et al. (2004) observed that the flow comes to rest at around $3\tau_c$, but the grains continue to re-arrange until $6\tau_c$, similar behaviour is observed in DEM simulations.

In order to remove the effect of crystallisation on the run-out behaviour, a highly poly-disperse sample ($r = d_{max}/d_{min} = 6$) is used. The flow kinematics of a dense (relative density $D_r = 74\%$) and a loose ($D_r = 22\%$) granular column with aspect ratio of 0.8 is studied. Similar to the previous case, the dense granular column exhibits longer run-out distance (see figure 4.18. Due to compaction of grains in loose condition, almost 20% of the initial potential energy available for collapse is lost in densification due to grain rearrangements in comparison to the dense condition (see figure 4.20). The compaction of grains in loose column and the dilation in dense column results in significantly different flow structure, especially at the flow front (figure 4.19). As the loose column densifies, more granular mass is pushed to the flow front resulting in higher vertical effective stress. The loose column exhibits a more parabolic final deposit profile in comparison to the dense column, which shows a triangular deposit at the front.

In short column, only a part of the granular column above the failure surface participates in the flow. However, it appears that the collapse for large aspect ratios mixes two very different dynamics: the first stage shows a large vertical acceleration, while the second stage consists

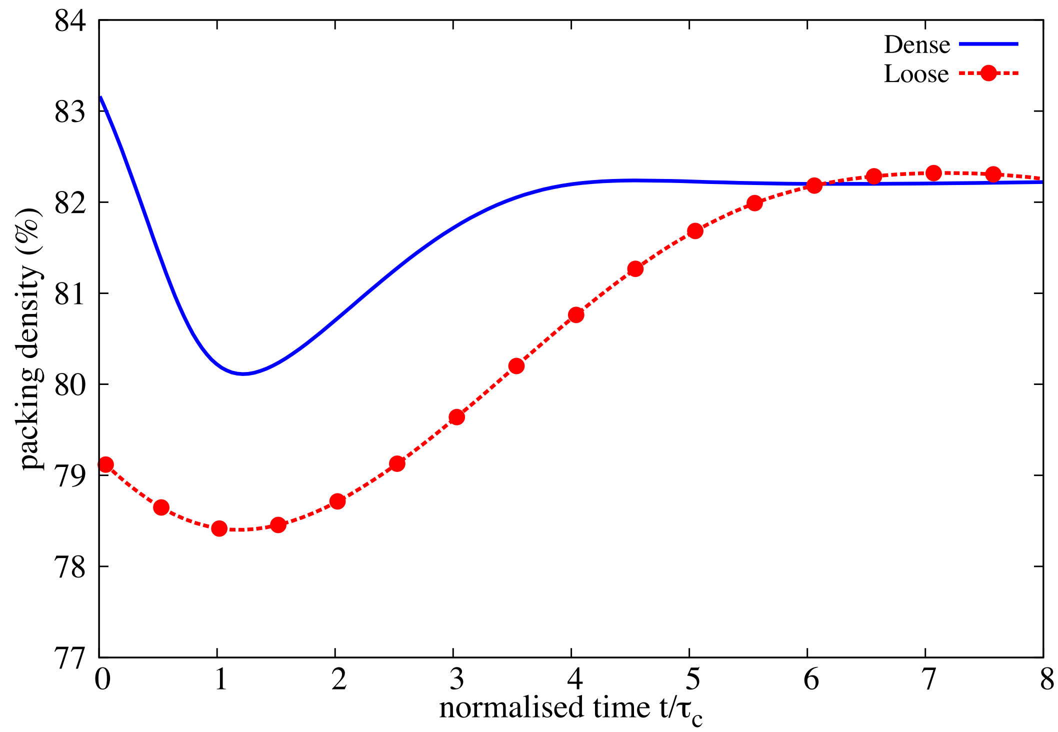

Figure 4.16 Evolution of local packing density $a = 0.8$

of a “conventional” horizontal granular flows. The effect of density on the run-out behaviour of tall columns is investigated. Similar to short columns, the dense granular column with an aspect ratio of 6 shows higher run-out distance in comparison to the loose condition. The dense granular column flows almost twice as much as that of the loose column. Unlike short columns, the evolution of run-out is different even at the initial stage of the collapse. The dense granular column, which has higher initial potential energy show a rapid increase in the run-out due to free-fall and higher mobilised potential energy. During this stage of collapse, the dense granular column has 15 % higher normalised kinetic energy available for the horizontal push. This results in longer run-out distance for dense granular column in comparison to initially loose granular column.

The initial packing fraction and the distribution of kinetic energy in the system has a significant influence on the flow kinematics and the run-out behaviour, this suggests that triggering mechanisms play a crucial role in the case of natural flows. This stresses the necessity of accounting for initiation mechanisms while modelling the run-out behaviour using continuum approaches to predict realistic granular flow behaviour.

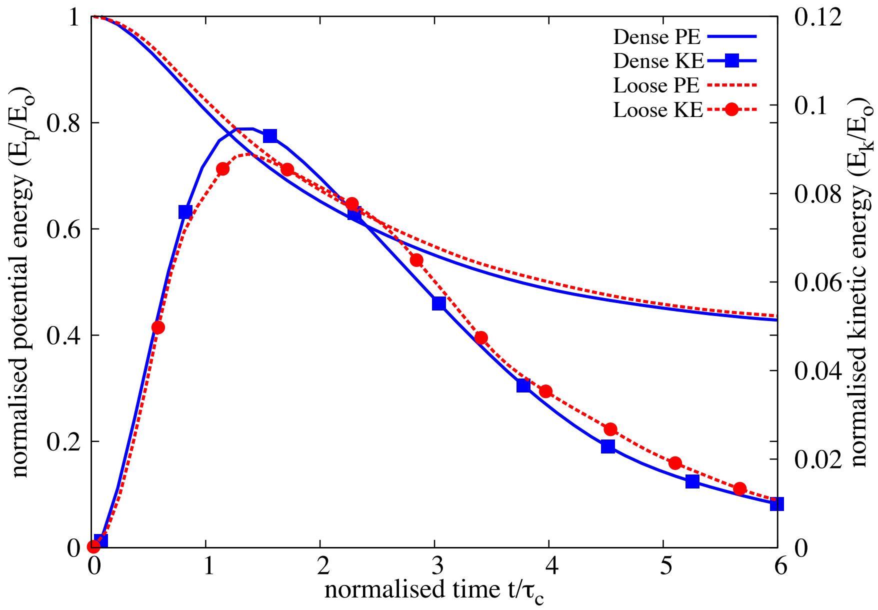

(a) Evolution of potential and kinetic energy

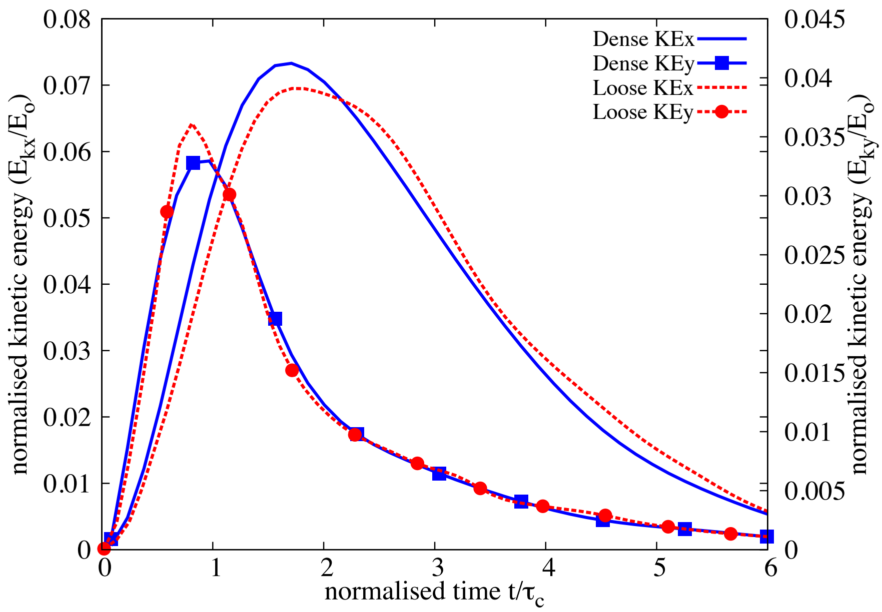

(b) Effect of kinetic energy

Figure 4.17 Effect of density on energy evolution $a = 0.8$

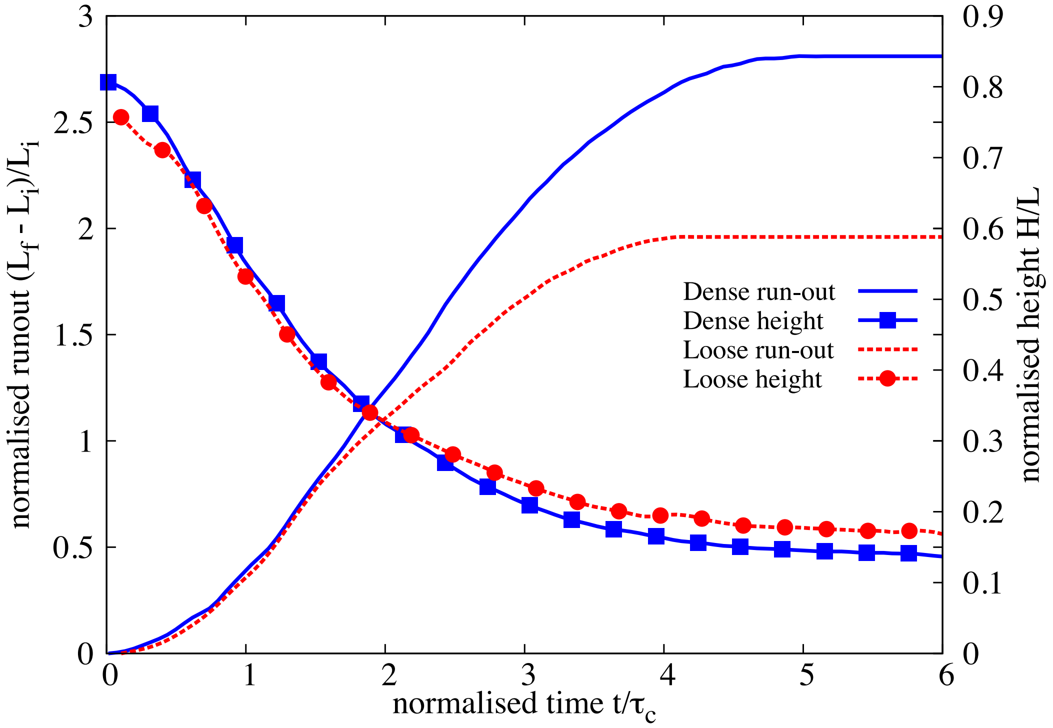

Figure 4.18 Effect of density on run-out evolution $a = 0.8$ (poly-dispersity ‘r’ = 6)

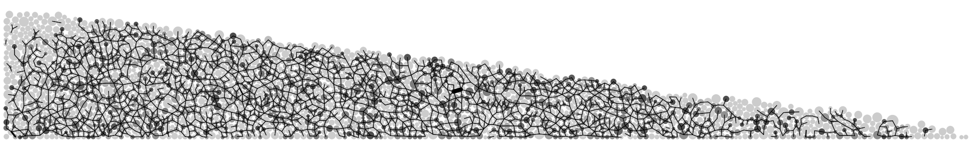

(a) Dense initial packing

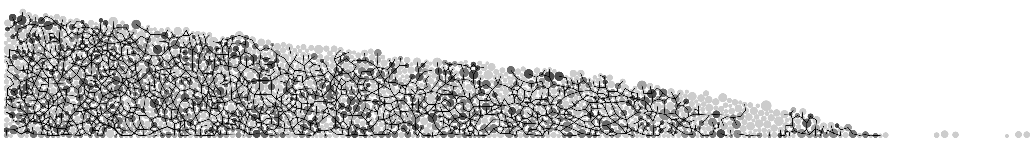

(b) Loose initial packing

Figure 4.19 Snapshots of granular column collapse $t = 6\tau_c$

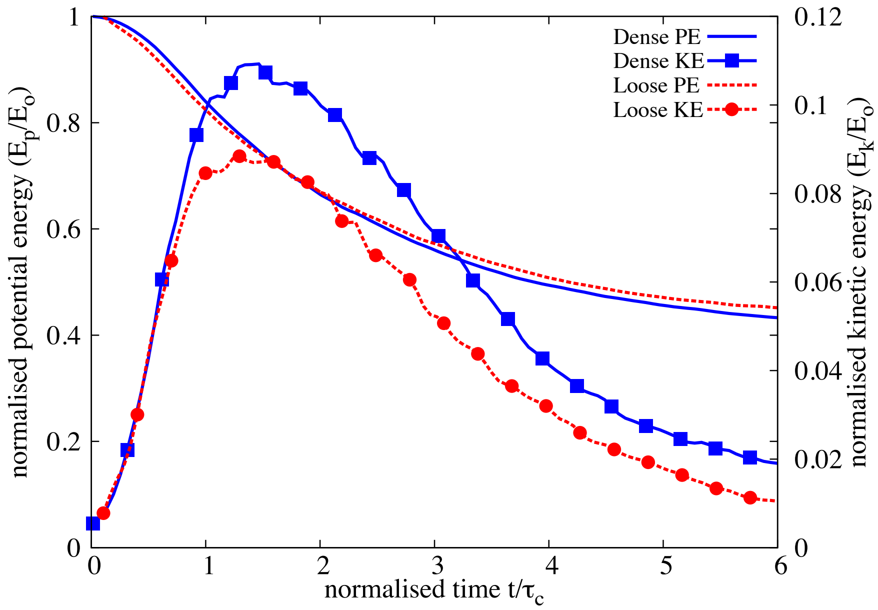

(a) Evolution of potential and kinetic energy

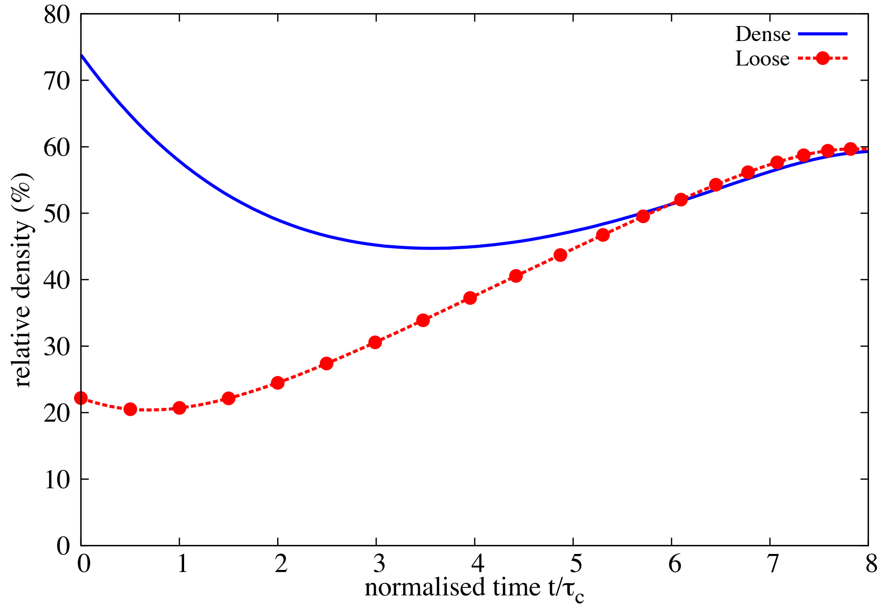

(b) Evolution of packing density

Figure 4.20 Effect of density on energy and packing fraction evolution $a = 0.8$ (poly-dispersity ‘r’ = 6)

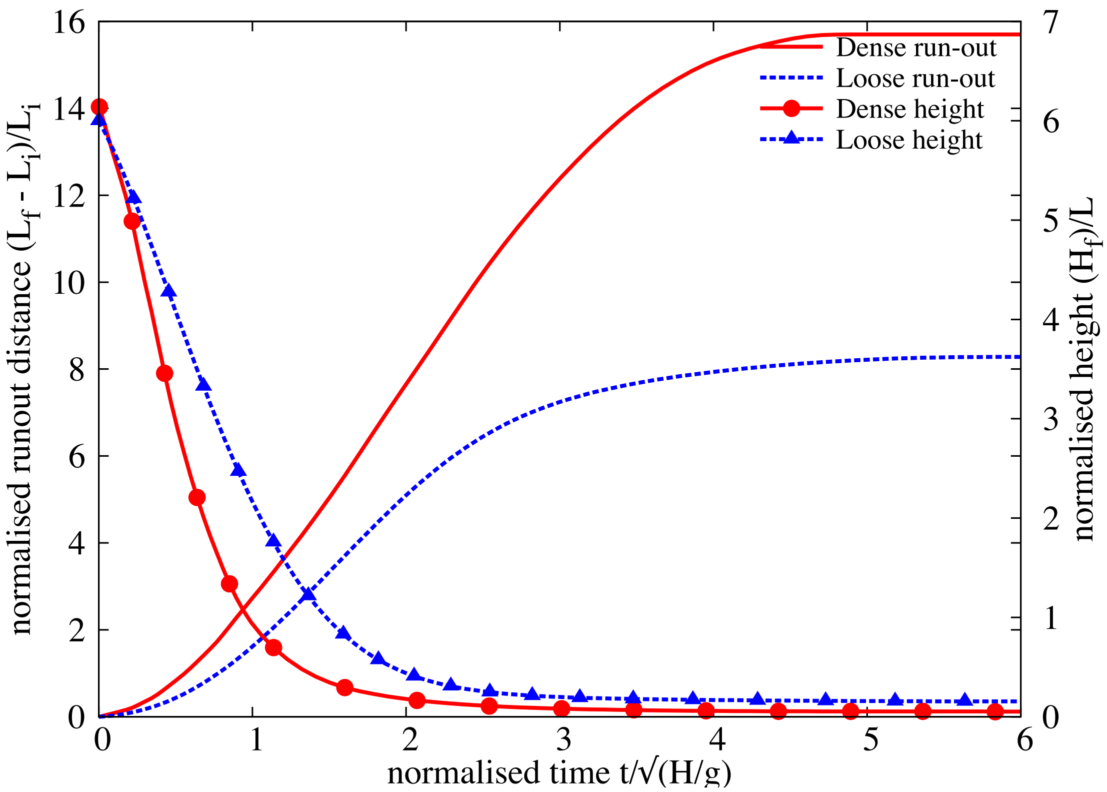

(a) Effect of density on run-out evolution

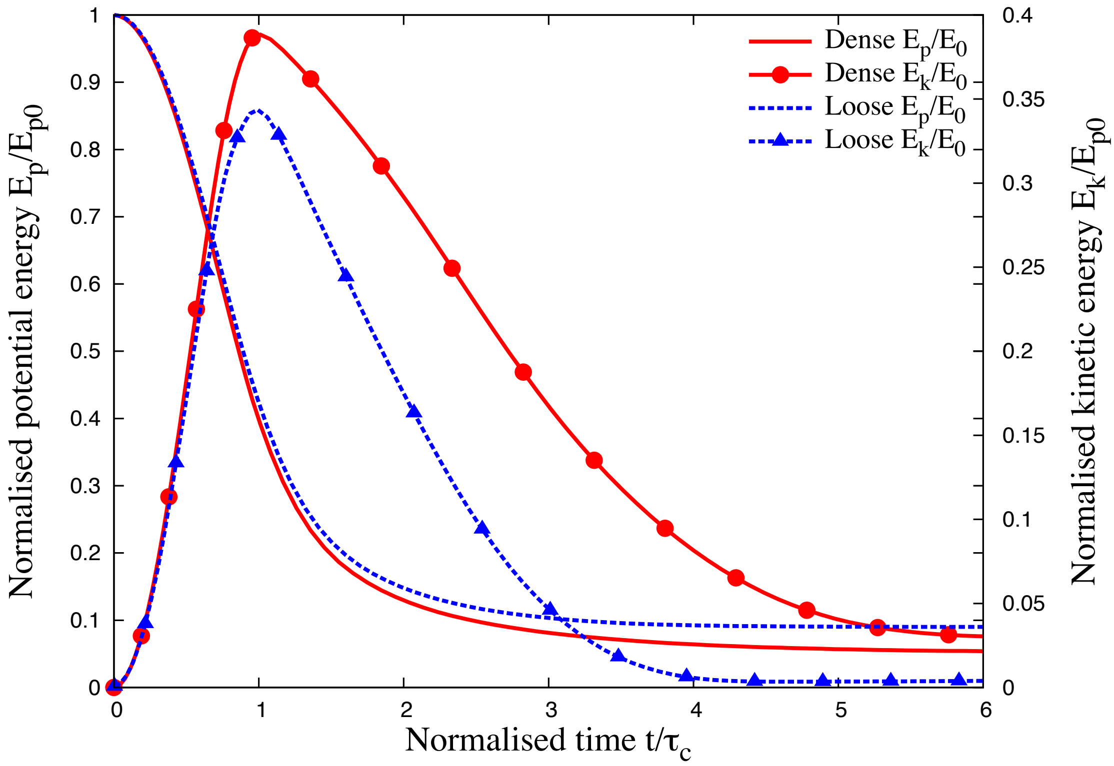

(b) Effect of density on energy evolution

Figure 4.21 Effect of density on run-out behaviour and energy evolution $a = 0.6$

4.3 Slopes subjected to impact loading

Transient granular flows occur very often in nature. Well-known examples are rockfalls, debris flows, and aerial and submarine avalanches. In the geotechnical context, transient movements of large granular slopes is a substantial factor of risk due to their destructive force and the transformations they may produce in the landscape. Natural granular flows may be triggered as a result of different processes such as gradual degradation, induced by weathering or chemical reactions, liquefaction and external forces such as earthquakes. Most contemporary research on granular materials deals with the steady-state flow. Transients and inhomogeneous boundary conditions are much less amenable to observation and analysis, and have thus been less extensively studied despite their primary importance in engineering practice. In most cases of granular flow, an initially static pile of grains is disturbed by external forces, it then undergoes an abrupt accelerated motion and spreads over long distances before relaxing to a new equilibrium state. The kinetic energy acquired during destabilisation is dissipated by friction and inelastic collisions.

This section investigates the ability of MPM, a continuum approach, to reproduce the evolution of a granular pile destabilised by an external energy source. In particular, a central issue is whether power-law dependence of the run-out distance and time observed with respect to the initial geometry or energy can be reproduced by a simple Mohr-Coulomb plastic behaviour for granular slopes subjected an impact energy. Effect of different input parameters, such as the distribution of energy and base friction, on the run-out kinematics are studied by comparing the data obtained from DEM and MPM simulations.

4.3.1 Numerical set-up

The DEM sample is composed of ~ 13000 disks with a uniform distribution of diameters by volume fractions ($d_{max} = 1.5 d_{min}$). The mean grain diameter and mass are $d \simeq 2.455$ mm and $m \simeq 0.0123$ kg, respectively. The grains are first poured uniformly into a rectangular box of given width and then the right-hand side wall is shifted further to the right to allow the grain to spread. A stable granular slope is obtained when all grains come to rest; see figure 4.22. This procedure leads to a mean packing fraction $\simeq 0.82$. Soil grains with mean density of 2600 kg m^{-3} and internal friction coefficient of 0.4 between grains is adopted.

The initial static pile is set into motion by applying a constant horizontal gradient $v_{0x}(y) = k(y_{max} - y)$ with $k > 0$. Such a configuration mimics the energy transfer mechanism of a horizontal quake along the bottom of the pile. The evolution of pile geometry and the total kinetic energy as a function of the initial input energy E_0 is studied. The run-out distance L_f is the distance of the rightmost grain, which is still in contact with the main mass when the

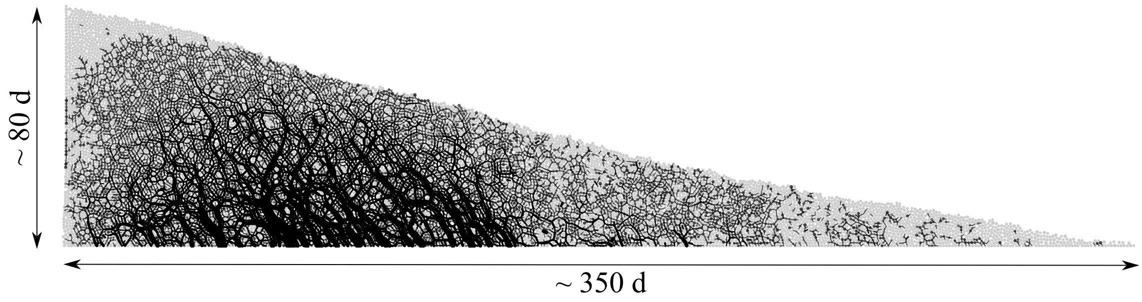

Figure 4.22 Initial geometry and dimensions of the pile

pile comes to rest. The run-out will be normalized by the initial length L_0 of the pile, as in the experiments of collapsing columns. The total run-out duration t_f is the time taken by the pile to reach its final run-out distance L_f.

For grain scale simulations, classical DEM and Contact Dynamics approach are used. This research is done in collaboration with Patrick Mutabaruka, University of Montpellier, who performed Contact Dynamics (CD) simulations that are presented in this section. A detailed description of the Contact Dynamics method can be found in Jean (1999); Moreau (1993); Radjai and Dubois (2011); Radjai and Richefeu (2009). The CD method is based on implicit time integration of the equations of motion and a nonsmooth formulation of mutual exclusion and dry friction between particles. The CD method requires no elastic repulsive potential and no smoothing of the Coulomb friction law for the determination of forces. For this reason, the simulations can be performed with large time steps compared to discrete element simulations. The unknown variables are particle velocities and contact forces, which are calculated at each time step by taking into account the conservation of momenta and the constraints due to mutual exclusion between particles and the Coulomb friction. An iterative research algorithm based on a non-linear Gauss-Seidel scheme is used. The only contact parameters within the CD method are the friction coefficient μ, the normal restitution coefficient ε_n and the tangential restitution coefficient ε_t between grains.

In MPM simulations the material point spacing is same as the mean grain diameter in DEM. A mesh size of 0.0125m is adopted with 25 material points per cell. The effect of mesh size and the number of material points per cell is investigated in section 4.3.5. A Mohr-Coulomb model with no dilation is used to simulate the continuum behaviour of the granular pile. Periodic shear tests using CD, see figure 4.23a, reveals a macroscopic friction coefficient of 0.22. The evolution of inertial number with friction is presented in figure 4.23b. The natural units of the system are the mean grain diameter d, the mean grain mass m and gravity g. For this reason, the length scales are normalised by d, time by $(d/g)^{1/2}$, velocities by $(gd)^{1/2}$ and energies by mgd.

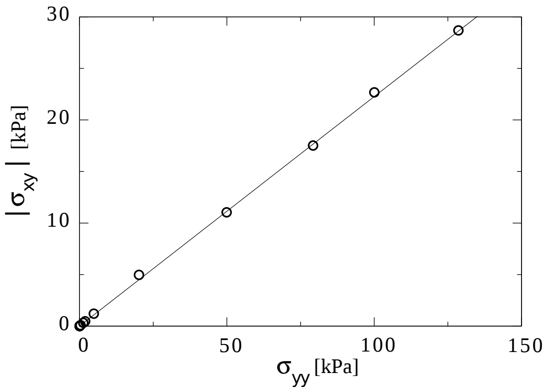

(a) Evaluating the critical state friction angle from periodic shear test.

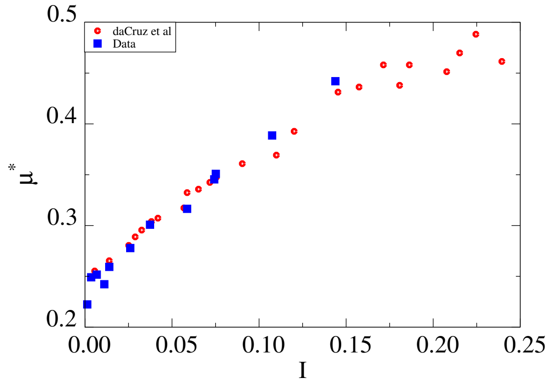

(b) Evolution of Inertial number with friction μ

Figure 4.23 Periodic shear test using CD (Mutabaruka, 2013).

4.3.2 Evolution of pile geometry and run-out

Figure 4.24 shows the initial evolution of granular slope subjected to an initial impact energy $E_0 = 61$ (in dimensionless units) using MPM. As the granular slope is sheared along the bottom, the shear propagates to the top leaving a cavity in the vicinity of the left wall. This cavity gets partially filled as the granular mass at the top collapse behind the flowing mass due to inertia. Similar behaviour is observed during the initial stages of the flow evolution using DEM and CD techniques (see figure 4.25). Due to inertia, the grains at the top of the granular heap roll down to fill the cavity, while the pile continues to spread.

The flow involves a transient phase with a change in the geometry of the pile followed by continuous spreading. The gradient input energy applied to the granular slope mimics a horizontal quake. Despite the creation of a cavity behind the flowing mass, the granular heap remains in contact with the left wall irrespective of the input energy. Figure 4.26a shows the normalized run-out distance $(L_f - L_0)/L_0$ and total run-out time t_f as a function of the input energy E_0. Two regimes characterized by a power-law relation between the run-out distance and time as a function of E_0 can be observed. In the first regime, corresponding to the range of low input energies $E_0 < 40\ mgd$, the run-out distance observed varies as $L_f \propto (E_0)^{\alpha}$ with $\alpha \simeq 0.206 \pm 0.012$ over nearly one decade. Overall, the run-out distance predicted by the continuum approach matches the DEM simulations. At very low energies, DEM simulations show longer run-out distance due to local fluidisation. The difference in the run-out between DEM and CD arise mainly from the scales of description and the inelastic nature of Contact Dynamics. Similar behaviour between DEM and CD approaches was observed by Radjai et al. (1997).

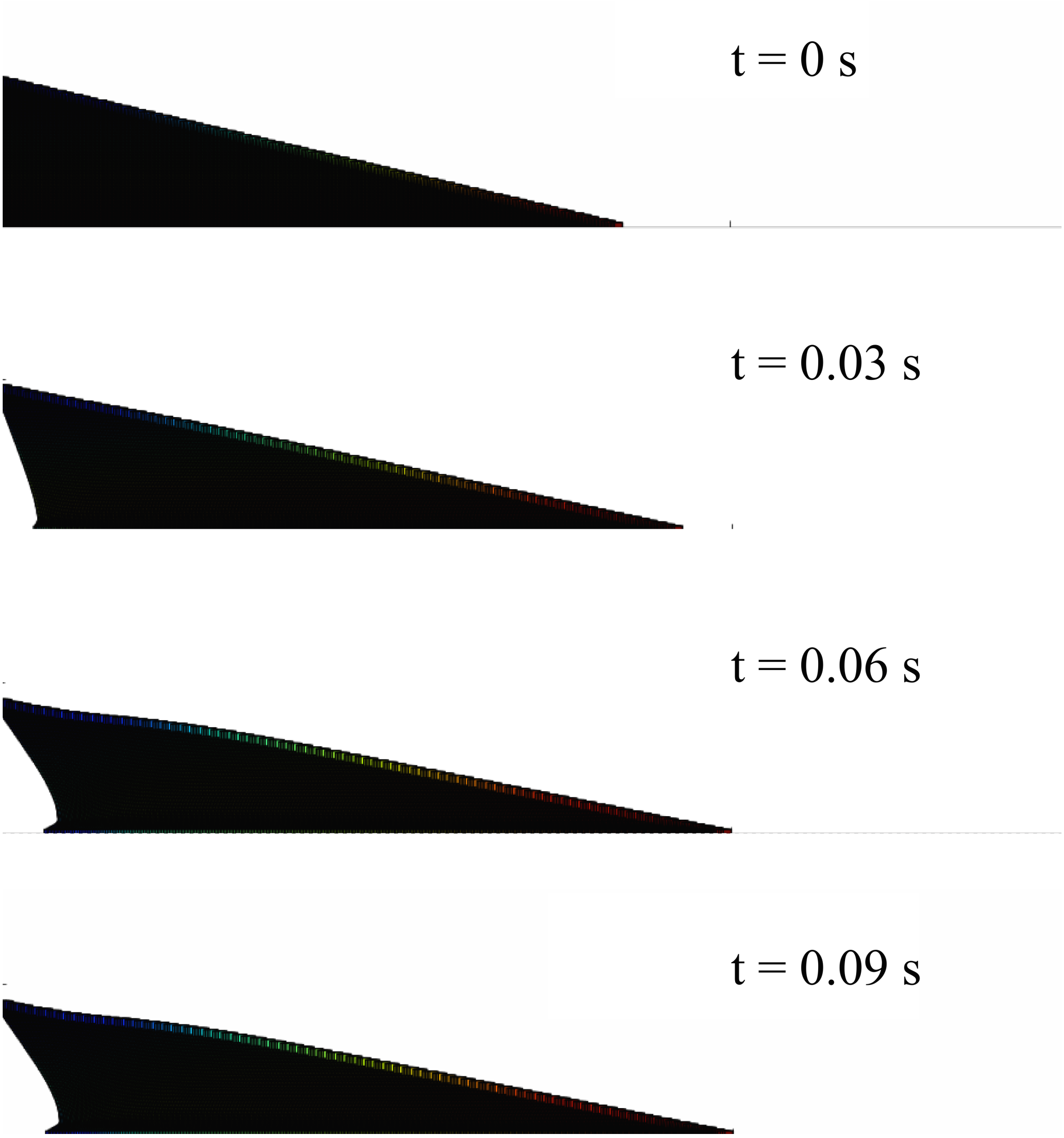

Figure 4.24 MPM simulation of the initial stages of granular pile subjected to a gradient impact energy.

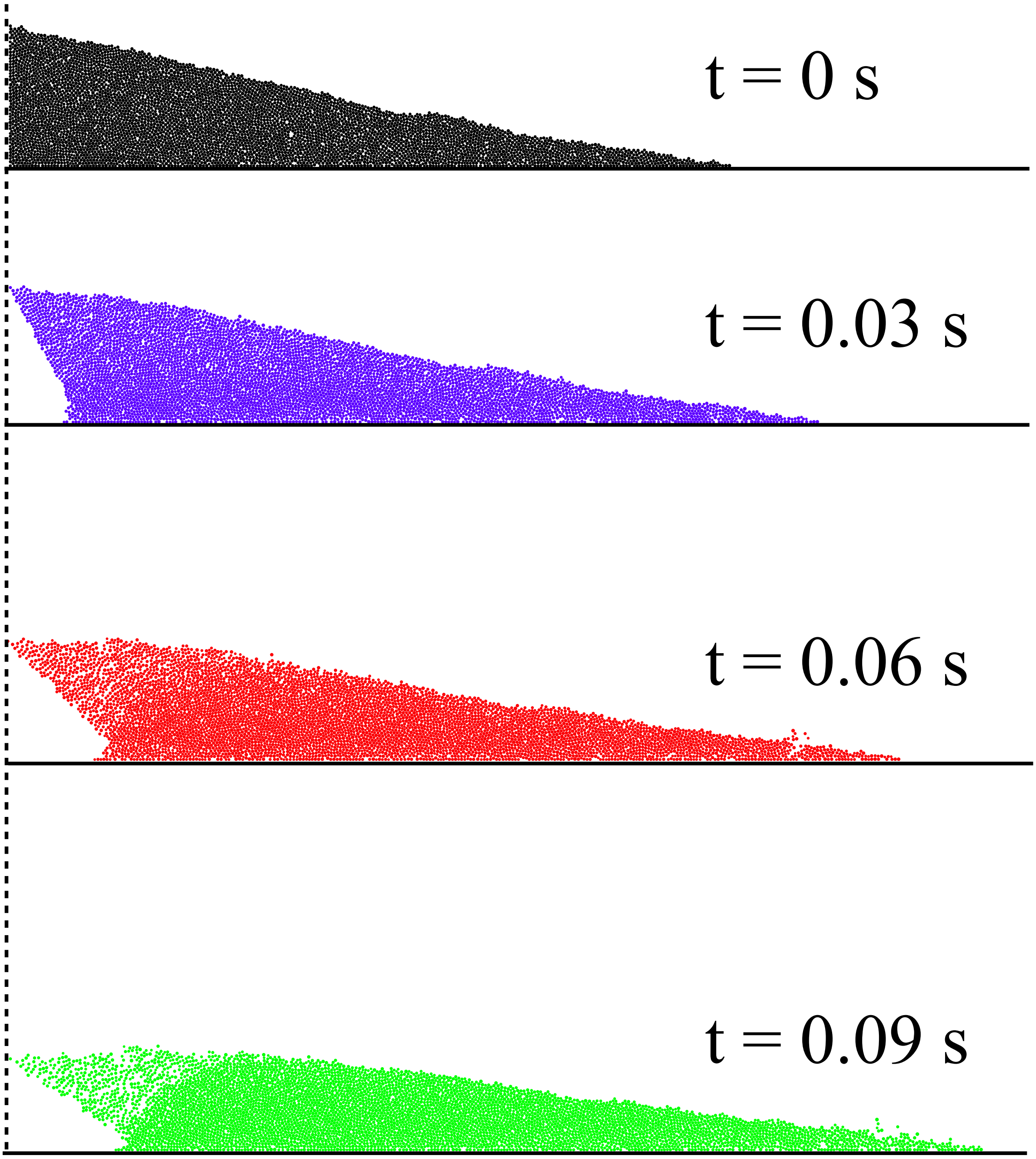

Figure 4.25 CD simulation of the initial stages of granular pile subjected to a gradient impact energy. (Mutabaruka, 2013).

While the run-out exhibits a power-law relation with the initial input energy, DEM simulations show that the flow duration remains constant at a value $t_f \simeq 60\ (d/g)^{0.5}$ irrespective of the value of E_0. The constant run-out time, in grain-scale simulations, indicates the collapse of grain into the cavity left behind the pile. An average run-out speed can be defined as $v_s = (L_f - L_0)/t_f$. According to the data, $v_s \propto (E_0)^{0.52\pm0.012}$. The error on the exponent represents the confidence interval of linear fits on the logarithmic scale. Since the initial average velocity varies as $v_0 \propto (E_0)^{0.5}$, this difference between the values of the exponents suggests that the mobilized mass during run-out declines when the input energy is increased.

In the second regime, corresponding to the range of high input energies $E_0 > 40\ mgd$, the run-out distance varies as $L_f \propto (E_0)^{\alpha'}$ over one decade with $\alpha' \simeq 0.56 \pm 0.04$ while the duration increases as $t_f \propto (E_0)^{\beta'}$ with $\beta' \simeq 0.33 \pm 0.02$. Hence, in this regime the average run-out speed varies as $v_s \propto (E_0)^{0.498\pm0.01}$. This exponent is close to the value 0.5 in $v_0 \propto (E_0)^{0.5}$, and hence, within the confidence interval of the exponents In the second regime, both DEM and MPM predict almost the same run-out behaviour. However, MPM predicts longer duration with increase in the input energy.

It is worth noting that a similar power-law dependence of the run-out distance and time were found in the case of granular column collapse with respect to the initial aspect ratio. In the column geometry, the grains spread away owing to the kinetic energy acquired during gravitational collapse of the column. Topin et al. (2012) found that the run-out distance varies as a power-law of the available peak kinetic energy at the end of the free-fall stage with an exponent $\simeq 0.5$. This value of exponent is lower than the run-out evolution observed in the second regime. This is, however, physically plausible since the distribution of kinetic energies at the end of the collapse is more chaotic than in this case where the energy is supplied from the very beginning in a well-defined shear mode. As pointed out by Staron et al. (2005), the distribution of kinetic energies is an essential factor for the run-out distance.

4.3.3 Decay of kinetic energy

The non-trivial evolution of the pile geometry in two regimes suggests that the energy supplied to the pile is not simply dissipated by shear and friction along the bottom plane. It is important to split the kinetic energy into vertical and horizontal components (K_{Ex} and K_{Ey}) of the velocity field. Although, the input energy is in the x component, a fraction of energy is transferred to the vertical component of the velocity field and dissipated during the transient phase. The evolution of kinetic energy is studied to understand the behaviour of granular flow that is consistent with the evolution of the pile shape.

The evolution of total kinetic energies E_k with time for different values of the input energy E_{ki} based on MPM simulations are shown in figure 4.27. MPM simulations shows two distinct

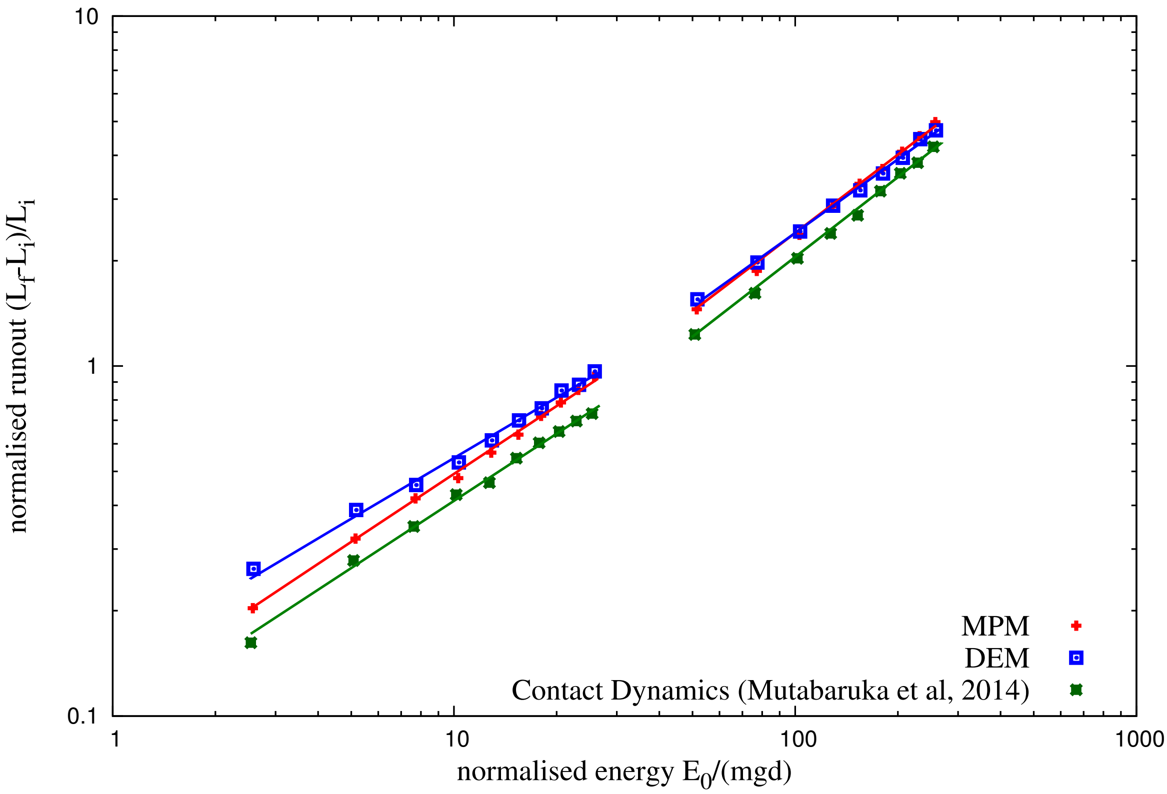

(a) Run-out distance as a function of normalised input kinetic energy

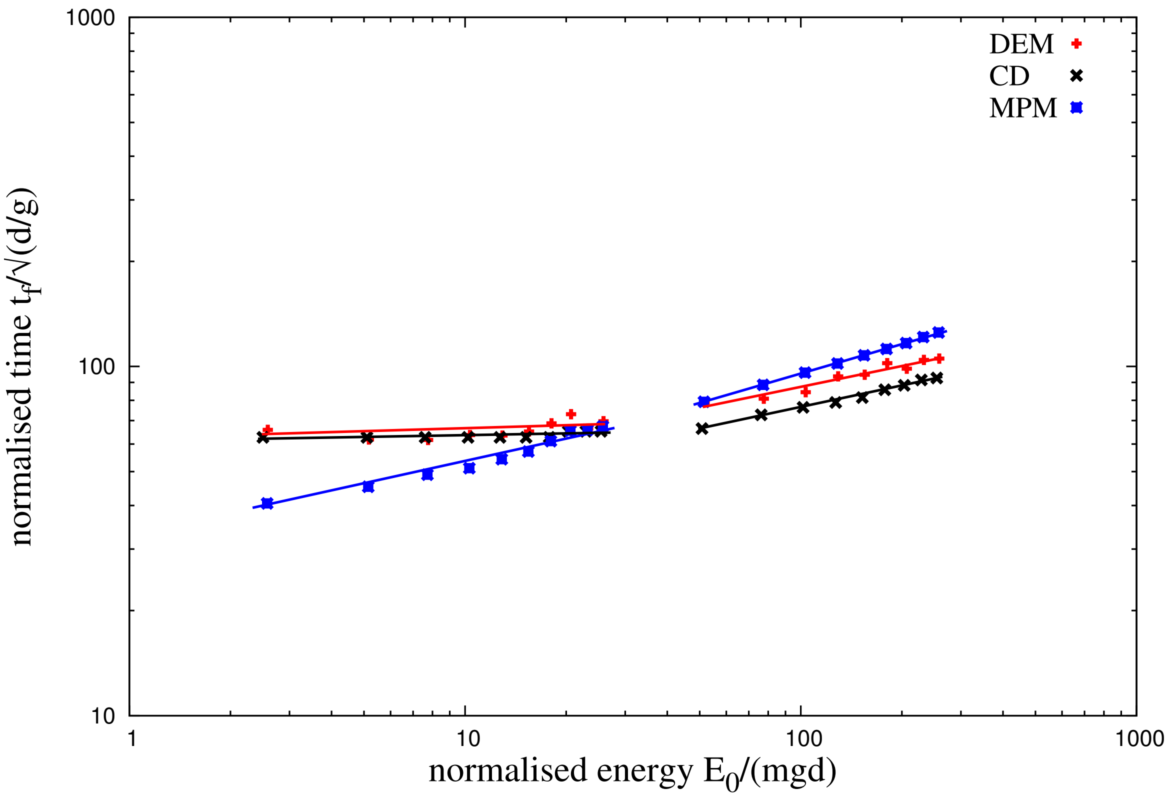

(b) Duration of run-out as a function of normalised input kinetic energy

Figure 4.26 Run-out behaviour of a pile subjected a gradient impact energy regimes in the normalised kinetic energy plot as a function of normalised time in figure 4.27b. However, DEM simulations (see figure 4.28) show that the energy evolution corresponding to low energy regime nearly collapse on to a single time evolution. This is consistent with the observation of run-out time t_f independent of the input energy. In contrast, MPM simulations predict a power law relation between the run-out duration and input energy. However, the plots corresponding to the high energy regime (figure 4.27), collapse only at the beginning of the run-out i.e. for $t < t_1 \simeq 7.5\ (d/g)^{0.5}$. Although MPM simulations show longer duration of run-out (figure 4.27), the total kinetic energy is completely dissipated at $t = 60\sqrt{d/g}$. DEM simulations predict $t = 80\sqrt{d/g}$ for the kinetic energy to be completely dissipated. This is due particle rearrangement at the free surface (figure 4.29). The granular mass densifies as the flow progresses, after the initial dilation phase for $t = 20\sqrt{d/g}$.

Figure 4.30 displays the evolution of kinetic energy in the translational (E_x and E_y) degrees of freedom. E_x decays similar to the total energy dissipation, but E_y increases and passes through a peak before decaying rapidly to a negligible level. The transient is best observed for E_y, which has significant values only for $t < t_1$. This energy represents the proportion of kinetic energy transferred to the y component of the velocity field due to the destabilisation of the pile and collapse of grains in the cavity behind the pile. Higher proportion of vertical acceleration E_{ky}/E_0 is observed for lower values of input energy E_0. This means that, at lower input energies a larger fraction of the energy is consumed in the destabilisation process. Whereas at a higher input energies, most of the energy is dissipated in the spreading phase. For this reason, the total duration t_1 of this destabilisation phase is nearly the same in both regimes and its value is controlled by the gravity rather than the input energy. The height of the pile being of the order of 80 d, the total free-fall time for a particle located at this height is $\simeq 12\ (d/g)^{0.5}$, which is of the same order as t_1. DEM simulations show that the contribution of the rotational energy during the transient stage and the spreading stage is negligible.

To analyse the second phase for higher input energies, the kinetic energy E'_{kx0} available at the end of the transient phase is considered. This energy is responsible for most of the run-out and hence it is expected to control the run-out distance and time. Figure 4.31 shows the evolution of E_{kx} normalized by E'_{kx0} as a function of time. The plots have seemingly the same aspect but they show different decay times. A decay time τ can be defined as the time required for E_{kx} to decline by a factor $1/2$. Figure 4.32 shows the same data in which the time t' elapsed since t_1, normalized by τ. Interestingly, now all the data nicely collapse on to a single curve. However, this curve can not be fitted by simple functional forms such as variants of exponential decay. This means that the spreading of the pile is not a self-similar process in agreement with the fact that the energy fades away in a finite time t'_f.

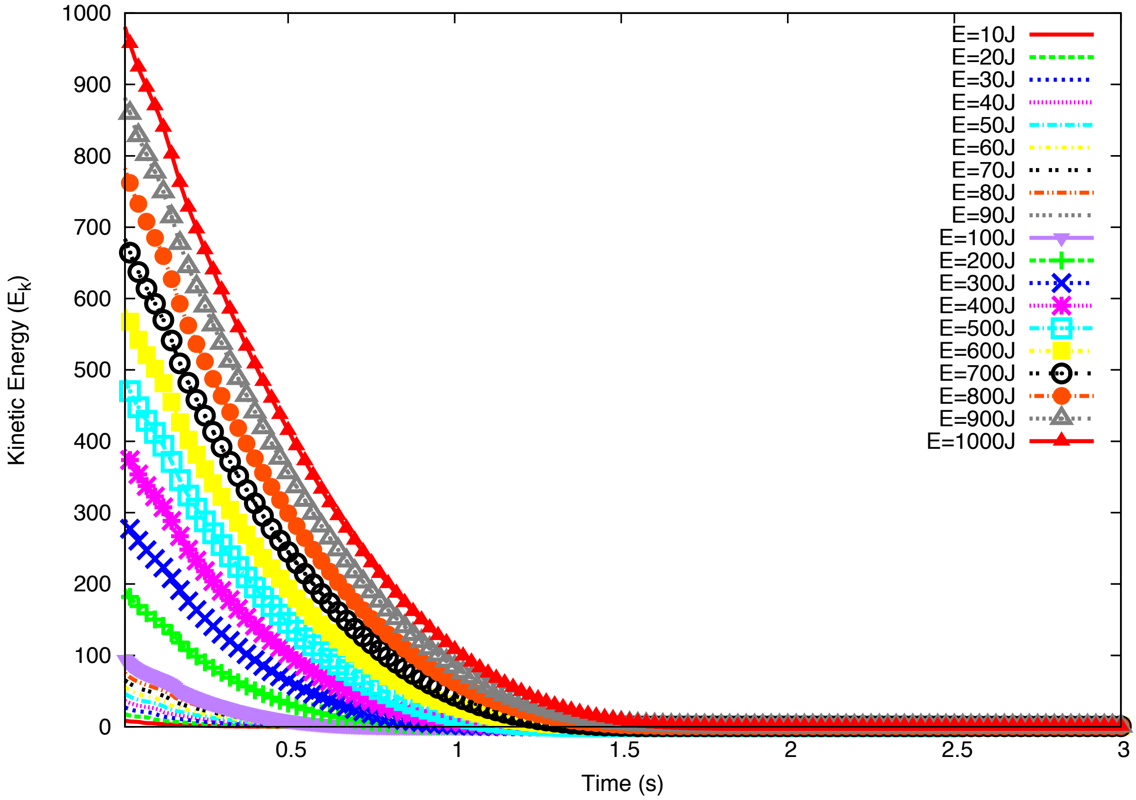

(a) Evolution of total kinetic energy with time

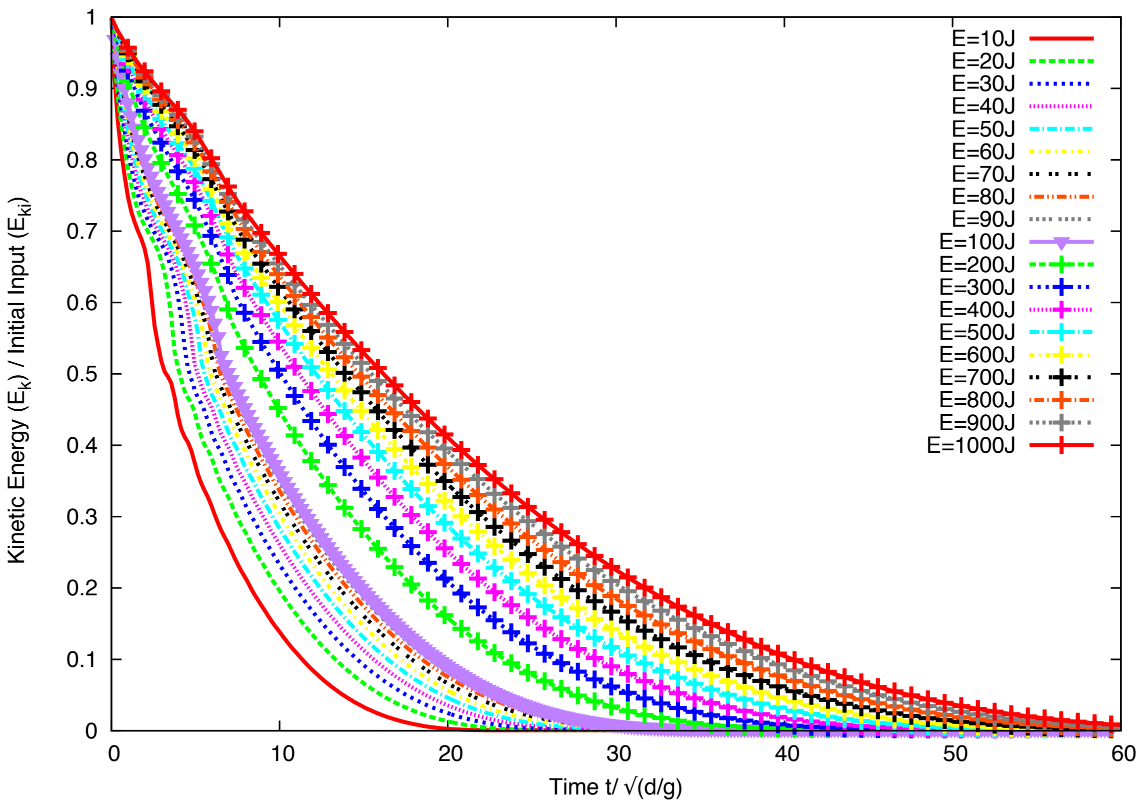

(b) Evolution of normalised kinetic energy with normalised time

Figure 4.27 Evolution of kinetic energy with time (MPM)

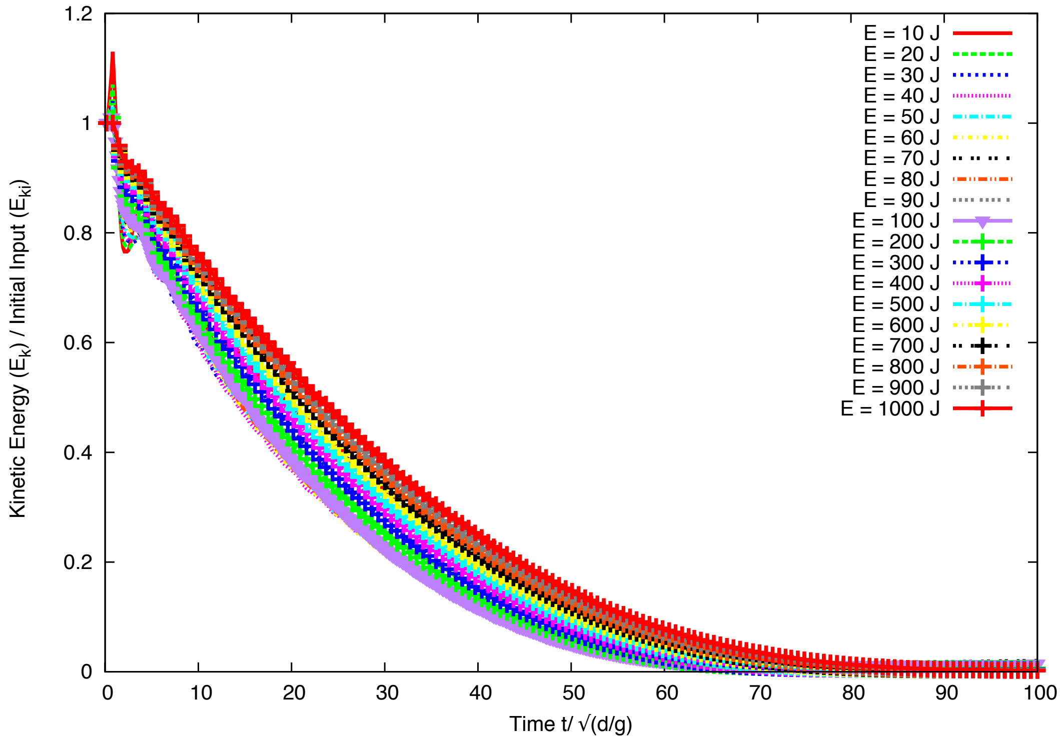

Figure 4.28 Evolution of normalised kinetic energy with normalised time

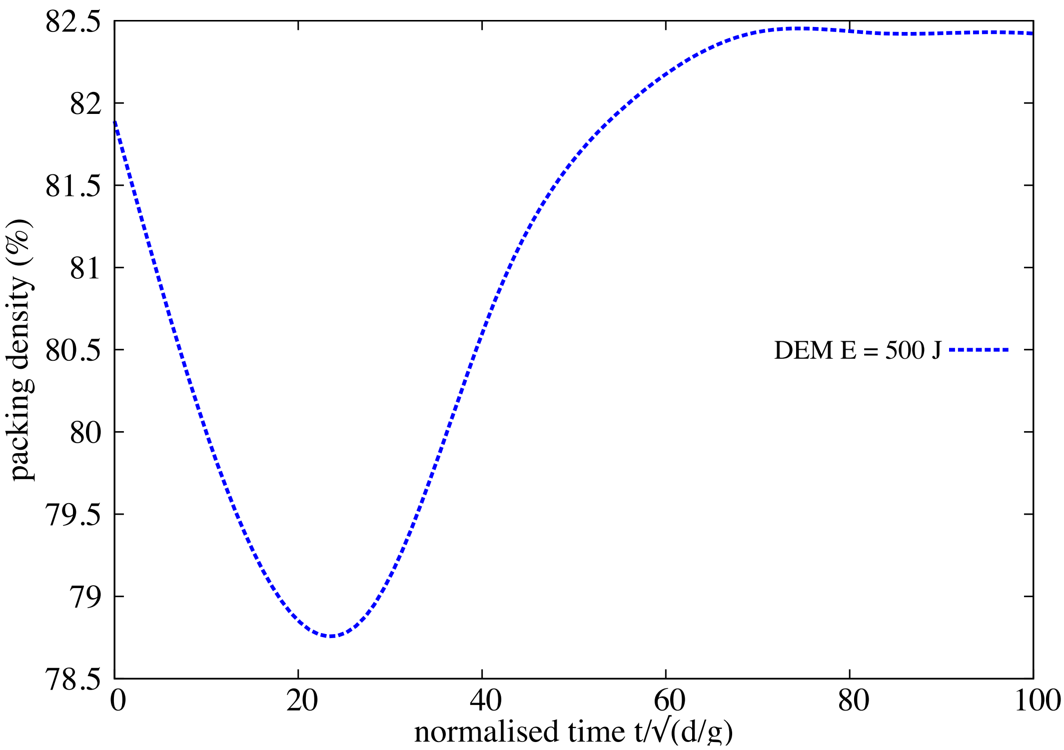

Figure 4.29 Evolution of packing density with time $E_0 = 152mgd$ (DEM)

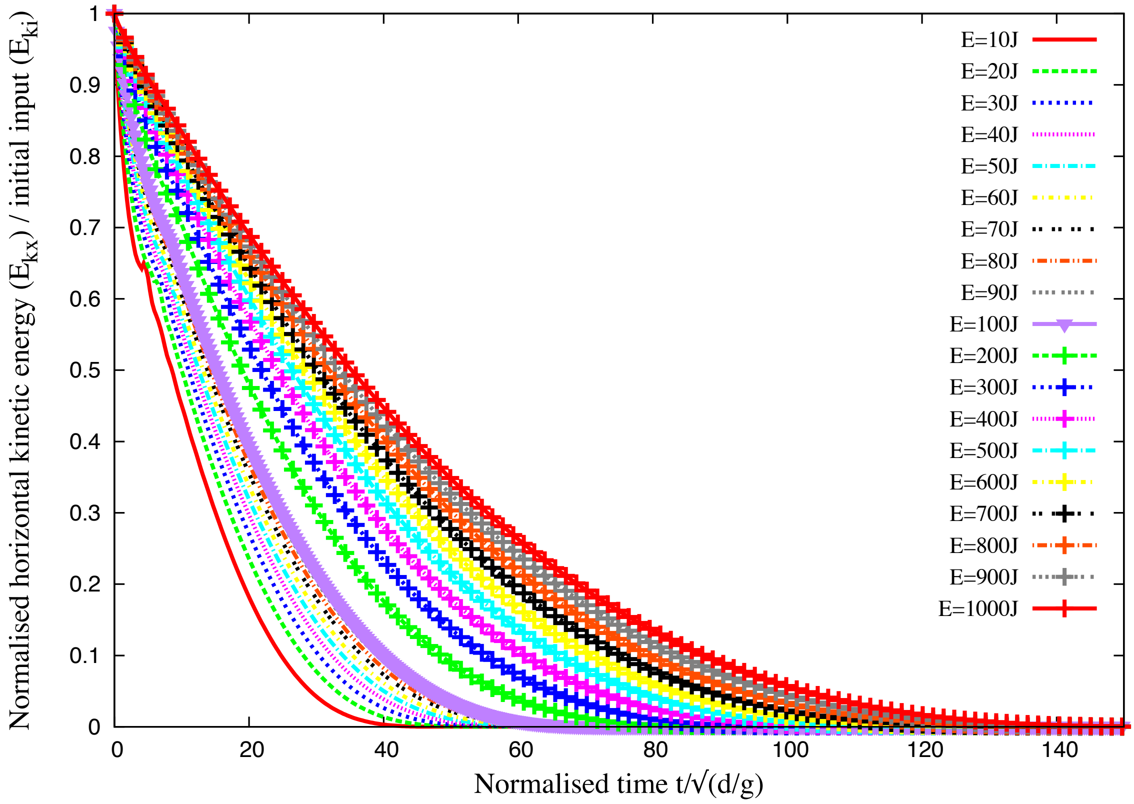

(a) Evolution of normalised horizontal kinetic energy with time

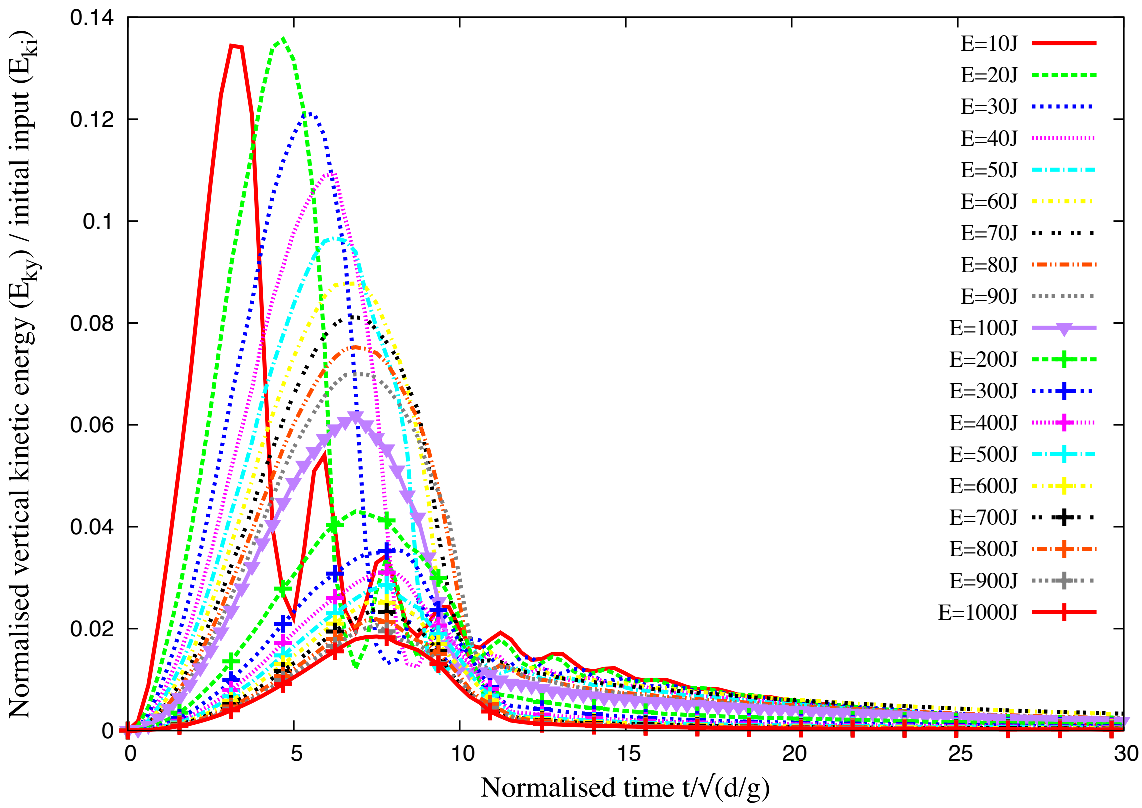

(b) Evolution of normalised vertical kinetic energy with time

Figure 4.30 Evolution of vertical and horizontal kinetic energy with time (MPM)

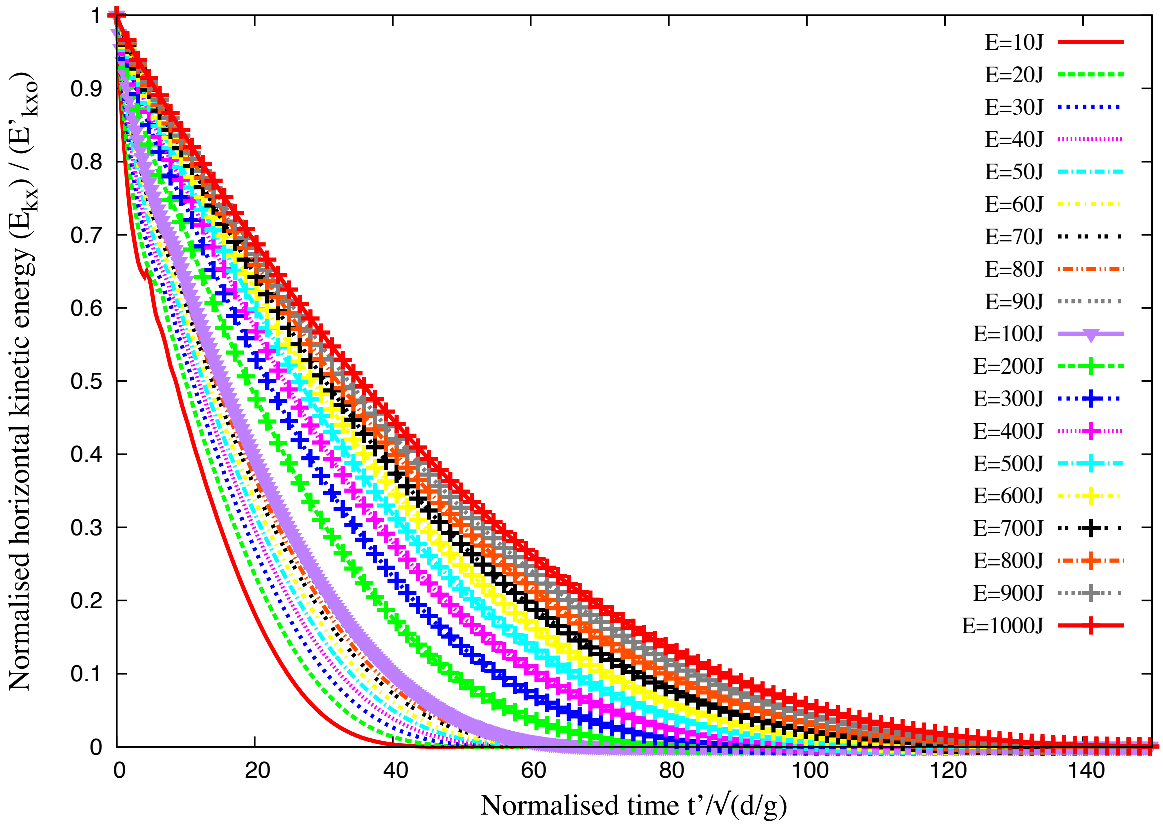

Figure 4.31 Evolution of kinetic energy in the *x* component of the velocity field normalized by the available kinetic energy at the end of the transient as a function of time elapsed since the same instant (MPM).

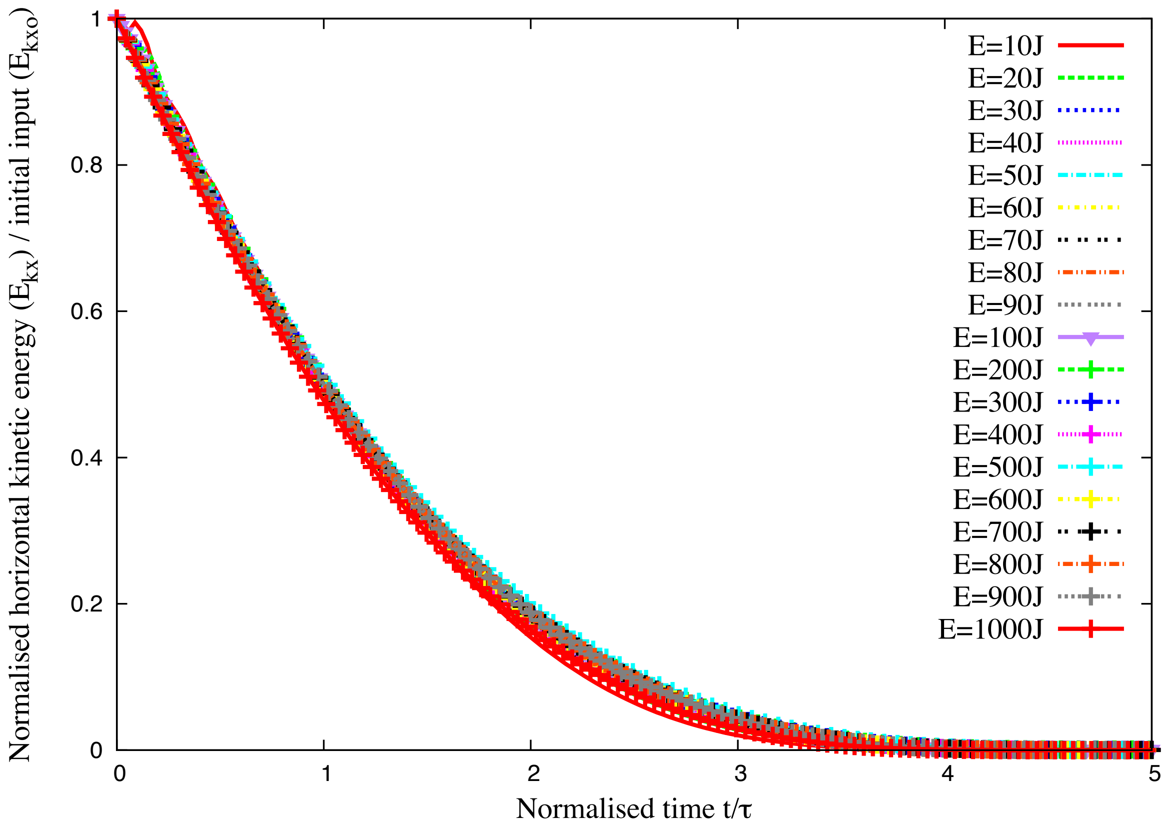

Figure 4.32 Evolution of kinetic energy in the x component of the velocity field normalized by the available kinetic energy at the end of the transient as a function of normalized time (MPM).

The scaling of the data with the decay time τ suggests that the run-out time t'_f, since the beginning of the second phase, might be a simple function of τ. Figure 4.33a shows both t'_f and τ as a function of E'_{x0}, where a power-law relation can be observed for both time scales. The run-out time $t'_f \propto (E'_{x0})^{\beta'}$ has the same exponent $\beta' \simeq 0.33 \pm 0.02$ as t_f as a function of E_0. For the decay time we have $\tau \propto (E'_{x0})^{\beta''}$ with $\beta'' \simeq 0.38 \pm 0.03$. The relation between the two times can thus be expressed as (see figure 4.33b)

$$t'_f = k\,\tau\,(E'_{x0})^{\beta''-\beta'}\,, \tag{4.13}$$

where $k \simeq 5 \pm 0.4$ and $\beta'' - \beta' \simeq -0.06 \pm 0.05$. This value is small enough to be neglected within the confidence interval of the data. It is therefore plausible to assume that the run-out time is a multiple of the decay time and the spreading process is controlled by a single time. A weak dependence on the energy E'_{kx0} is consistent with the fact that the energy available at the beginning of the second phase is not dissipated in the spreading process (calculated from the position of the tip of the pile) since the pile keeps deforming by the movements of the grains at the free surface even when the tip comes to rest. This can explain the small difference between the two exponents as observed here.

4.3.4 Effect of friction

The run-out distance, duration of flow, and the dissipation of kinetic energy are controlled by the input energy and collective dynamics of the whole pile. However, the run-out behaviour is expected to depend also on the base friction. A series of simulations with different values of base friction was performed using MPM to analyse the influence of friction on the run-out behaviour. The influence of friction on the run-out behaviour is shown in figure 4.34a. The exponent of the power-law relation between the run-out and input energy has a weak dependence on the base friction, however, the proportionality constant is affected by the change in the base friction. This behaviour is similar to that observed in granular column collapse with varying initial properties (Balmforth and Kerswell, 2005; Lajeunesse et al., 2005).

CD simulations using different values of coefficient of restitution show no difference in the run-out behaviour. At large input energies, the pile remains in a dense state so that multiple collisions inside the pile occur at small time scales compared to the deformation time. When the restitution coefficients are increased, more collisions occur during a longer time interval but the overall energy dissipation rate by collisions remains the same. This effect is a seminal example of collective effects which erase the influence of local parameters at the macroscopic scale.

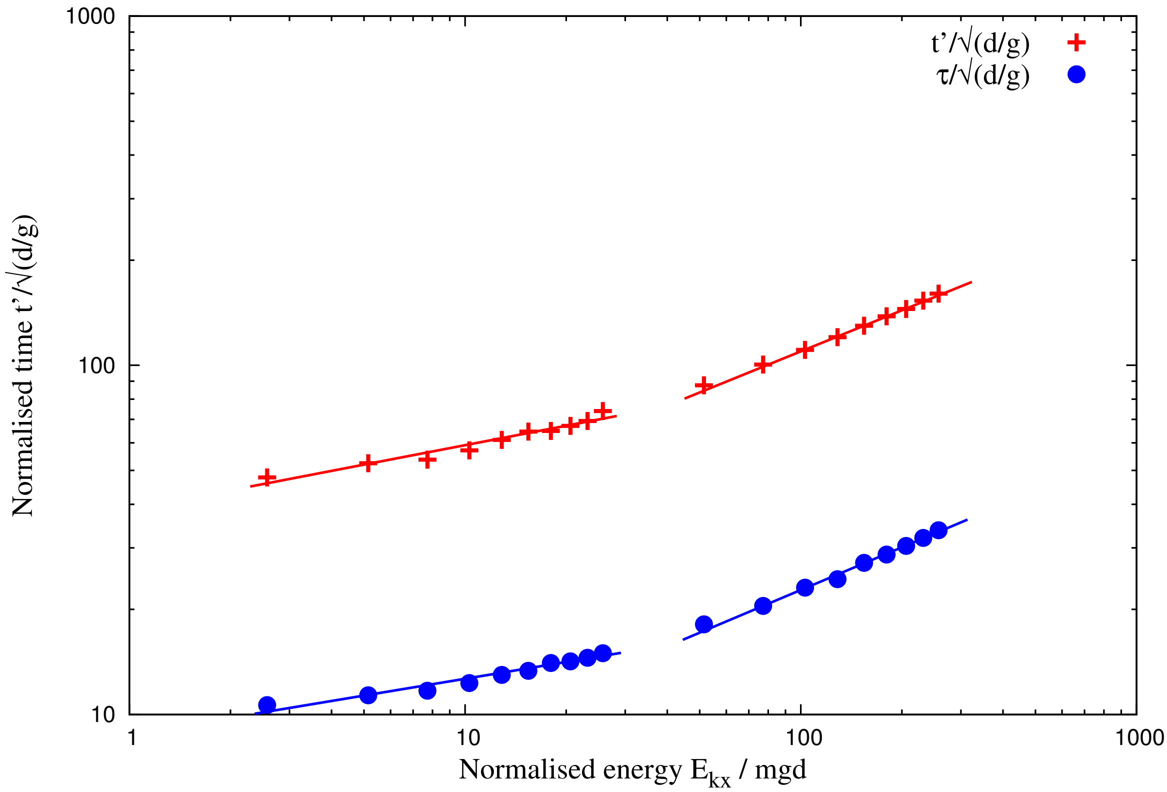

(a) Power law evolution of t'_f and τ as a function of kinetic energy E'_{kx0}.

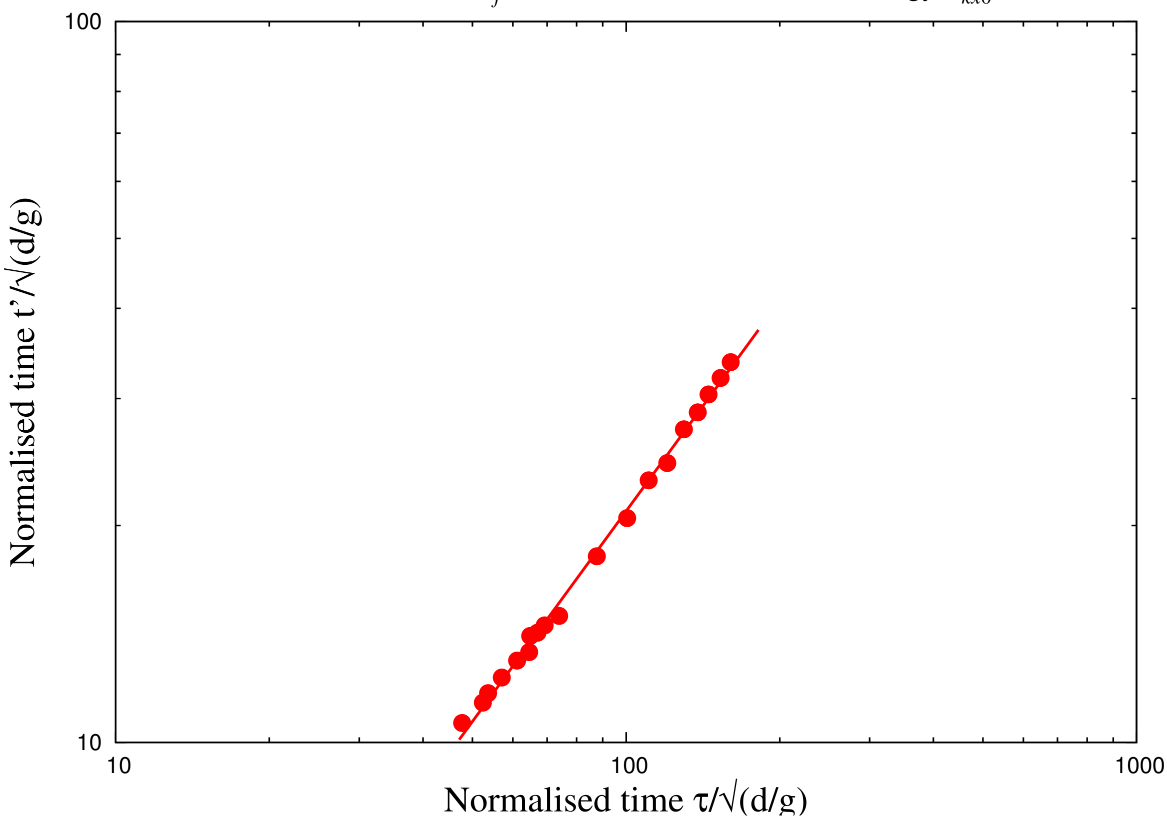

(b) Linear relationship between decay time and run-out time after the transient as a function of the normalised kinetic energy E_{kx0}.

Figure 4.33 Decay time and run-out time as a function of the normalised kinetic energy E_{kx0}.

In contrast with the restitution coefficients, the effect of friction coefficient, however, is quite important for the run-out. MPM simulations with varying friction coefficient shows that, both the run-out distance and the decay time decrease as the friction coefficient is increased. This effect is much more pronounced at low values of the friction coefficient. The run-out time, for example, is reduced by a factor of ≈ 4 as μ_s is increased from 0.1 to 0.2 while the change in the run-out and duration is less effected with increase in friction coefficient. This “saturation effect" can be observed in a systematic way in simple shear tests. The dissipation rate may reach a saturation point where the dilation of granular materials and rolling of the grains change in response to increase in friction coefficient (Estrada et al., 2008).

Effect kinetic energy distribution

Staron et al. (2005) observed that the distribution of kinetic energy in the granular system is an essential factor for the run-out distance. In order to understand the influence of energy distribution on the run-out behaviour, granular pile subjected to two different velocity fields were studied. A uniform velocity $V_{xo}(y) = V_0$ is applied to the entire pile, in contrast to the gradient impact velocity. Snapshots of flow kinematics at initial stages are shown in figure 4.35 (MPM simulations) and figure 4.36 (DEM). It can be observed from the figures that the continuum behaviour is identical to that of grain-scale simulations. As each grain experiences the same velocity, grains located at the top of the slope are pushed farther away and unlike the gradient input velocity, the cavity left behind the granular mass is not filled by the soil grains at the top.

Figure 4.37a shows the influence of velocity distribution on the run-out behaviour. At low input energy, the gradient velocity distribution shows significanly longer run-out in comparison to uniform velocity distribution. Section 4.3.3 shows that at low input energies a larger fraction of the energy is consumed in the destabilisation process. Which means that the amount energy available for flow is less, in uniform velocity distribution, this energy is even smaller as the initial velocity is distrubted uniformly throughout the granular mass. However at higher input energy, where most of the energy is dissipated during the spreading phase, the run-out distance has a weak dependence on the distribution of velocity in the granular mass. The duration of the flow shows similar behaviour to the run-out, however, a slope subjected to a gradient velocity flows quicker than a slope subjected to a uniform impact velocity. Gradient velocity distribution provides more input energy at the initial stage to overcome the frictional resistance at the base. This shows that the material property and the distribution of kinetic energy in the system has a non-trivial influence on the flow kinematics and the internal flow structure.

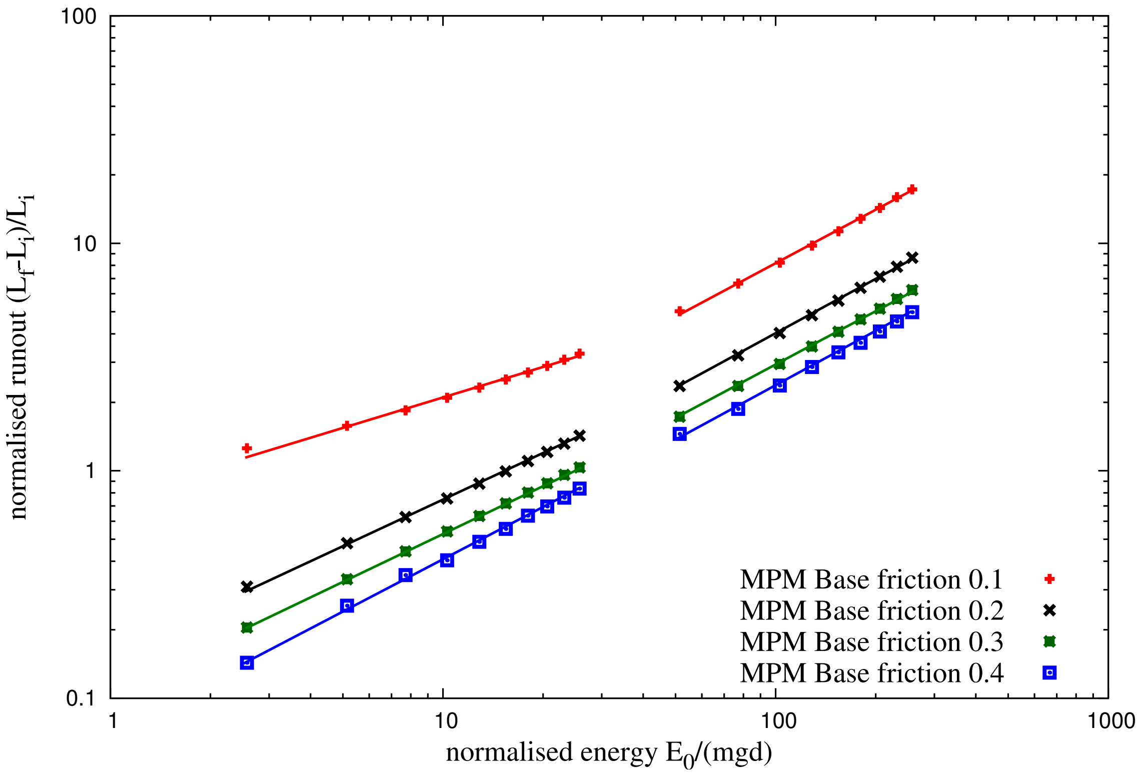

(a) Effect of friction on the run-out distance

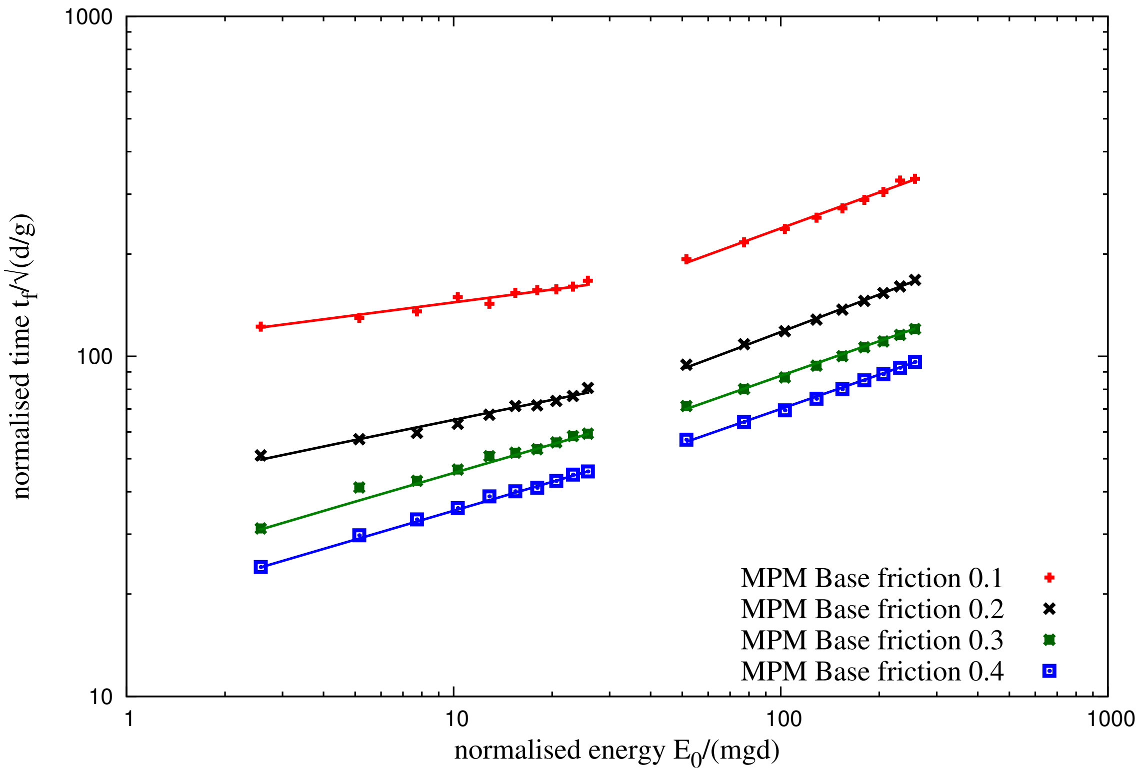

(b) Effect of friction on the duration of run-out.

Figure 4.34 Effect of friction on the run-out behaviour

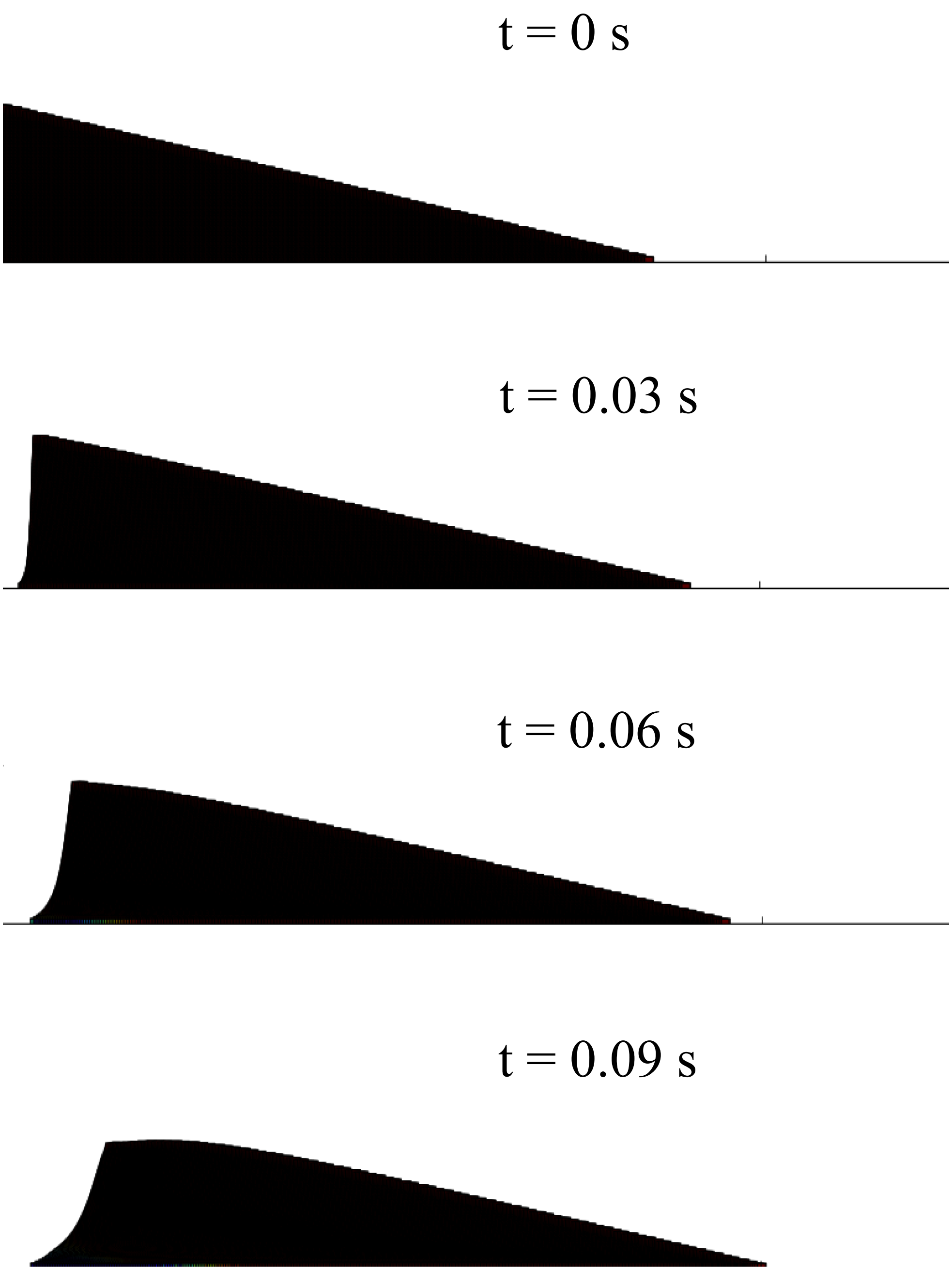

Figure 4.35 Snapshots of MPM simulations of the evolution of granular pile subjected to a gradient impact energy $E_0 = 61\ mgd$.

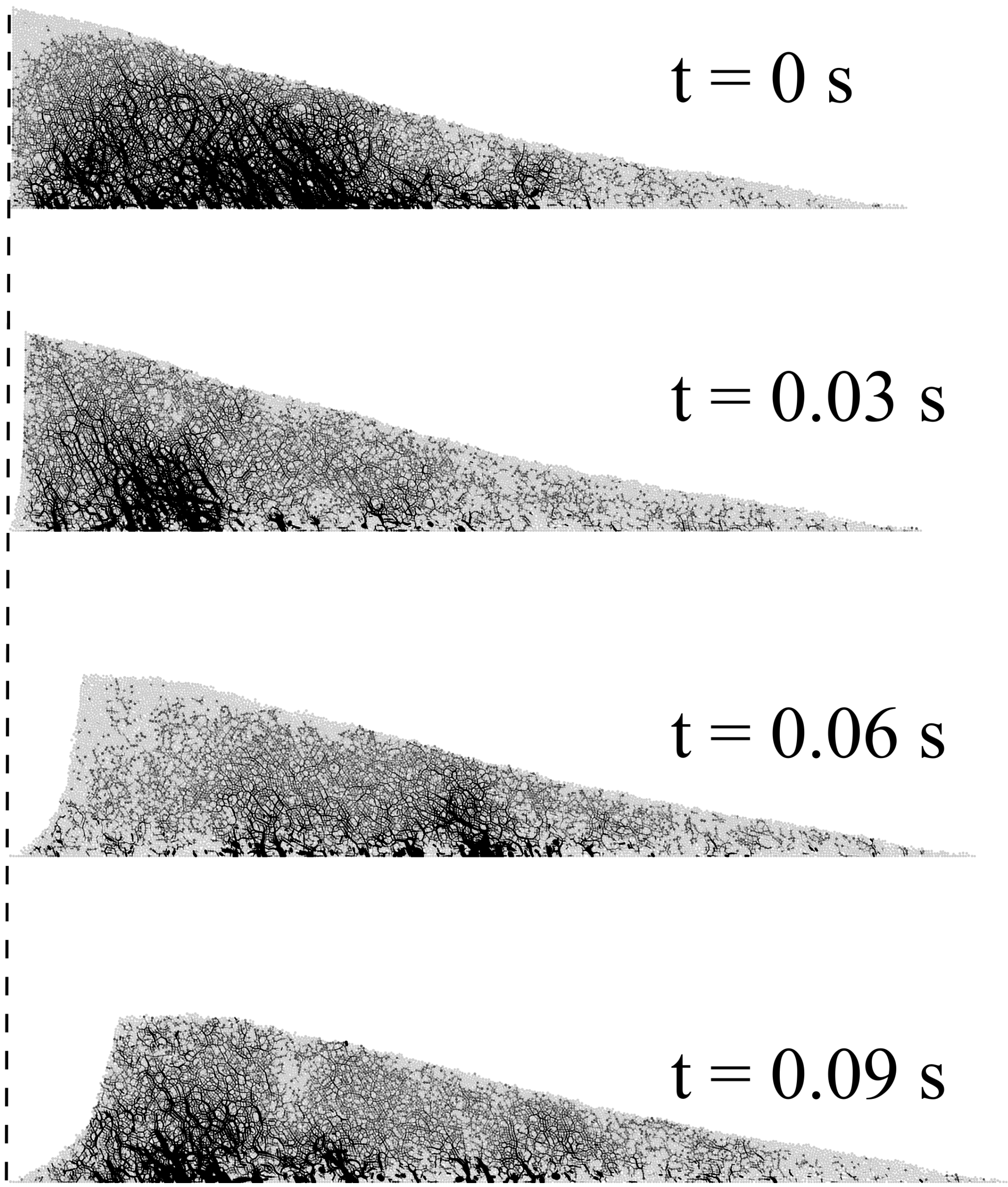

Figure 4.36 Snapshots of DEM simulations of the evolution of granular pile subjected to a gradient impact energy $E_0 = 61\ mgd$.

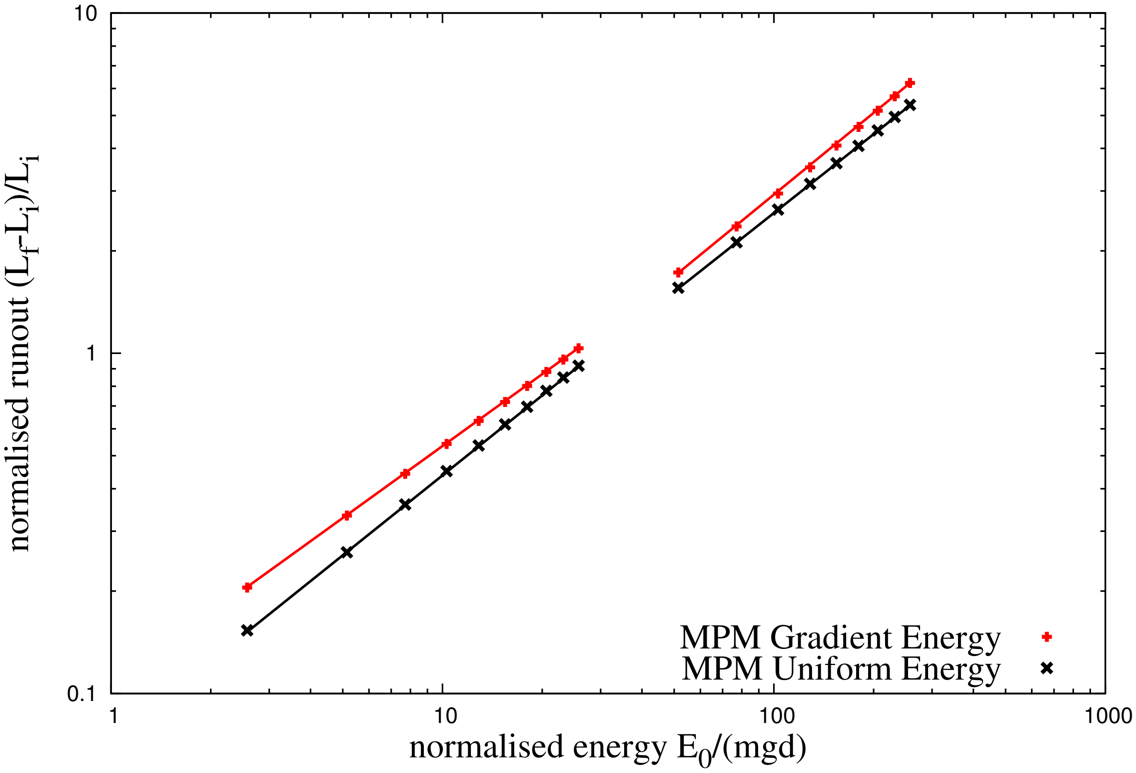

(a) Run-out distance as a function of normalised input kinetic energy

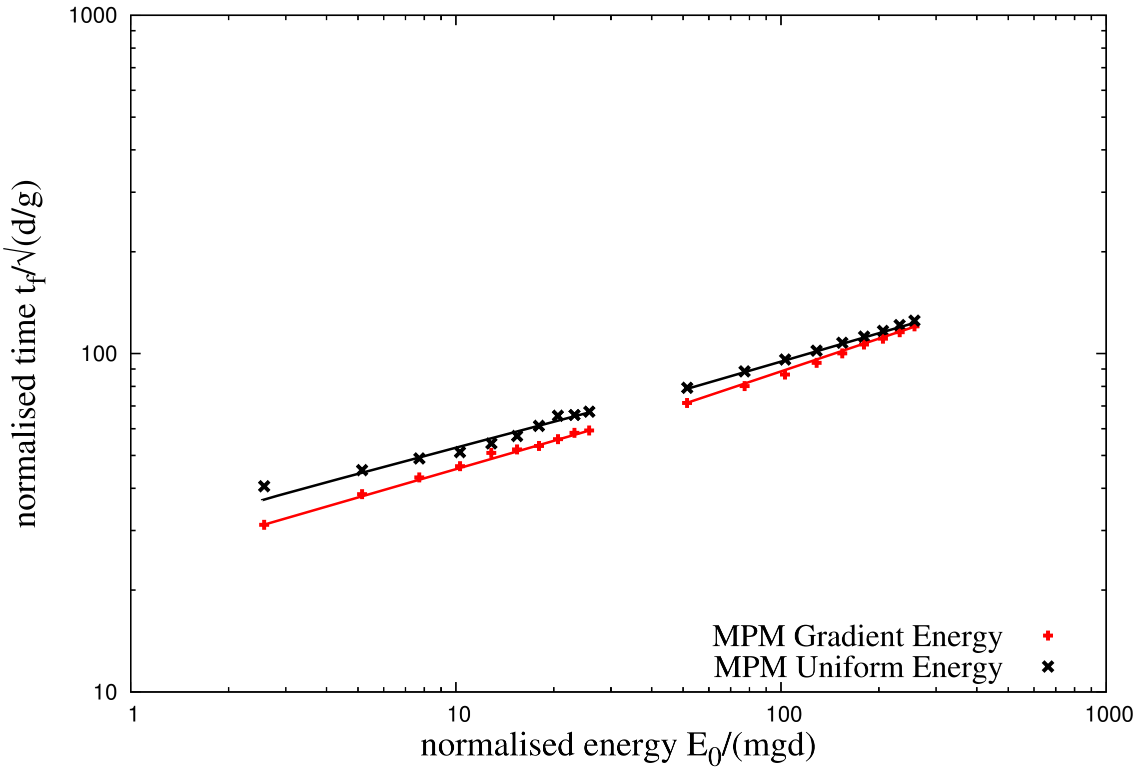

(b) Duration of run-out as a function of normalised input kinetic energy

Figure 4.37 Effect of input velocity distribution on the run-out behaviour

4.3.5 Effect of mesh size and number of material points per cell

Abe et al. (2013) observed that for a coarse mesh, the numerical error decreases with increase in the number of material points per cell. In contrast, they observed an opposite trend for the fine meshes (0.01 m). The influence of numerical noise due to particles crossing the background mesh was not observed when the mesh size is greater than 0.05 m. Coetzee et al. (2005) also found that the numerical error decreases with increase in mesh refinement.

In the present study, the effect of mesh size and the number of material points per cell on the run-out behaviour is investigated. For a mesh size of 0.0125 m, the number of material points per cell (PPC) is varied as 4, 16, 25, 36, 64, 81 and 100. The effect of number of material points on the run-out behaviour is presented in figure 4.38. At a low input energy of 50 J, 4 and 16 material points per cell result in longer run-out distance, where as the run-out distance converges when the number of PPC is more than 25. While at a high input energy of 500 J, both 4 and 16 PPC predict almost the same run-out distance, but is higher than the run-out predicted with more than 25 material points per cell.

The evolution of the granular pile during the initial stage of flow is show in figure 4.39 for different number of material points per cell. At low input energy, fewer material points per cell results in larger separation of the spreading mass from the left wall. Distinct shear bands can be observed for more than 16 PPC. The flow structure remains unchanged with increase in PPC of more than 25. At a higher input energy (see figure 4.40), almost all cases predict similar flow structure, except in the case of 4 PPC.

Figure 4.41 shows the evolution of kinetic energy with time for varying number of material points per cell. At low input energy, the horizontal kinetic energy evolution is identical for all cases. A slightly quicker run-out evolution during the spreading phase can be observed for the case of 4 PPC. However, increase in the number of material points per cell significantly affects the evolution of the vertical kinetic energy E_{ky}. At low energy, a large proportion of the input energy is dissipated in the destabilisation process. This results in material points falling behind the spreading mass to the fill the cavity. Fewer number of material points per cell results in cell crossing noise as the material points filling the cavity experience free-fall due to gravity. The effect of cell-crossing noise can be seen in the osciallation of vertical kinetic energy for fewer material points per cell. However, at high input energy, most of the input velocity is dissipated during the spreading process. This means that only a small fraction of energy is available in the vertical component resulting in almost similar behaviour for all cases. Four material points per cell predicts a higher peak vertical kinetic energy in comparison with other cases, unlike the low energy case, no oscillations were observed for the high input energy.

The effect of mesh size on the flow kinematics is studied by comparing two mesh sizes: 0.01 m and 0.0125 m (see figure 4.42). It can be observed that the run-out distance converges

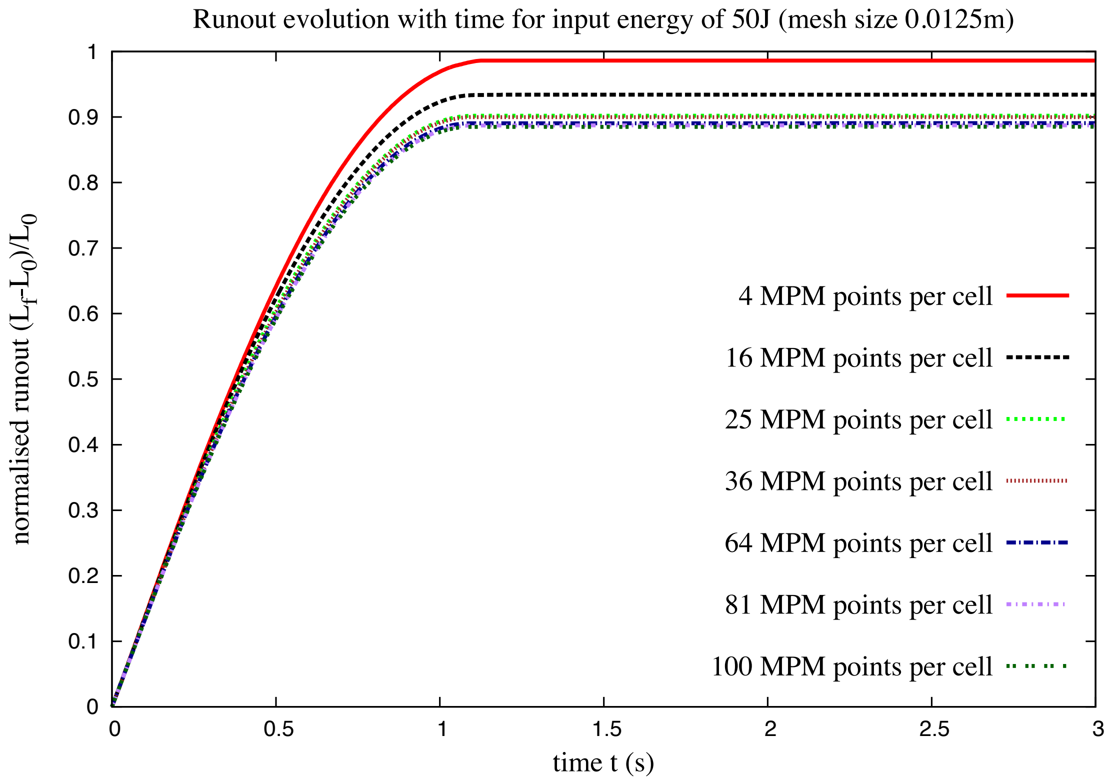

(a) $E_0 = 12.7mgd$

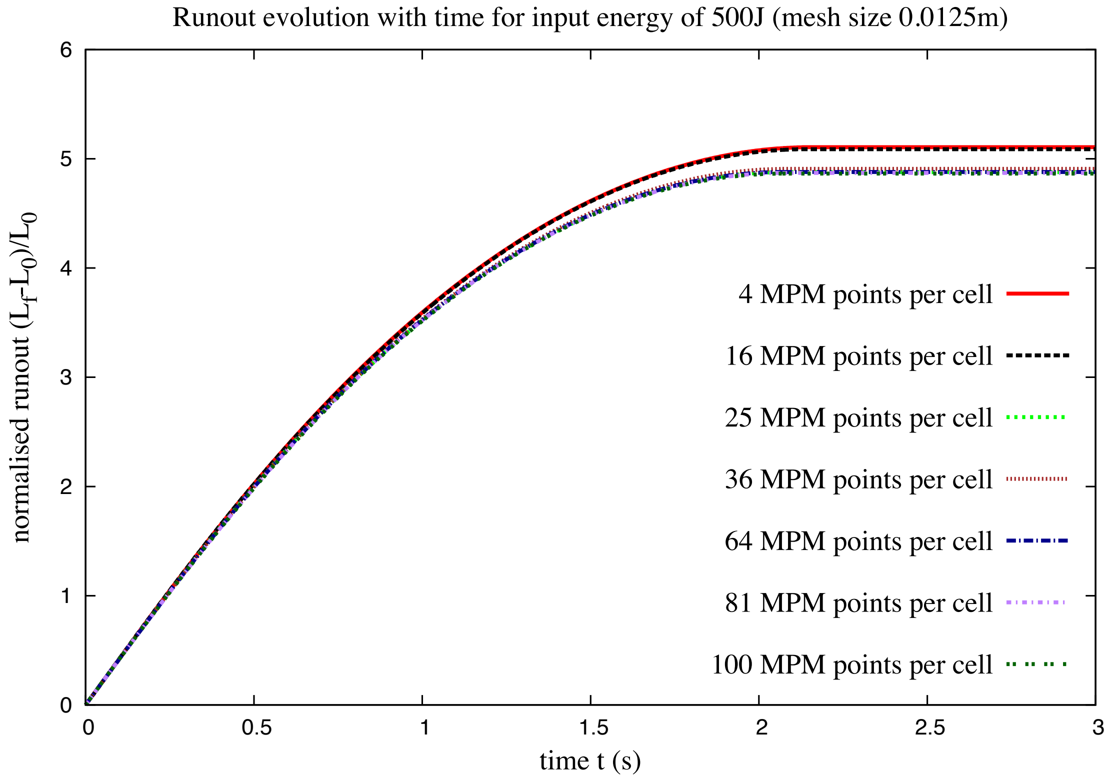

(b) $E_0 = 152mgd$

Figure 4.38 Evolution of run-out with time for varying material points per cell.

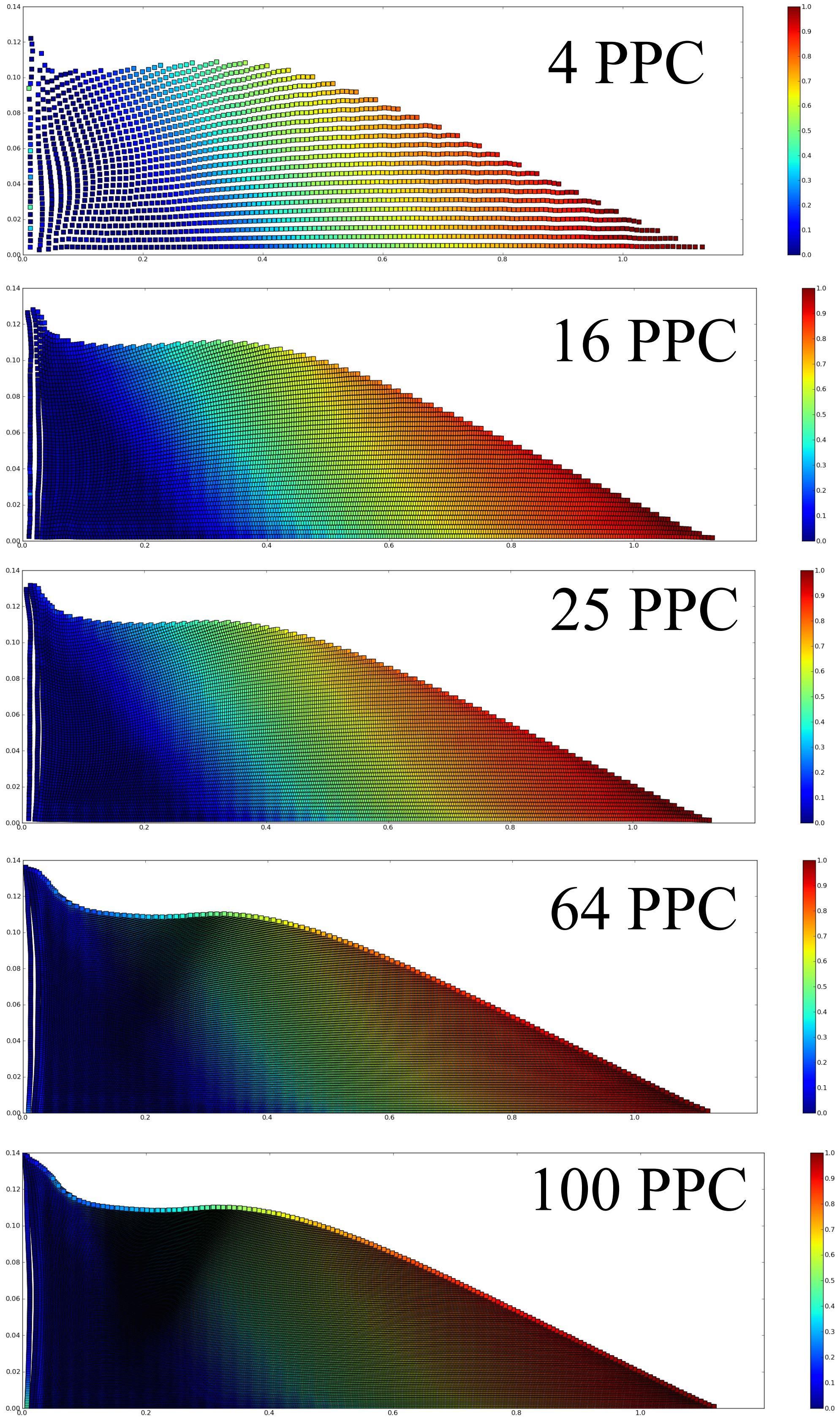

Figure 4.39 Effect of number of material points on cell on the run-out behaviour $E_0 = 12.7mgd$. Velocity profile (m/s) of granular pile subjected to gradient impact loading.

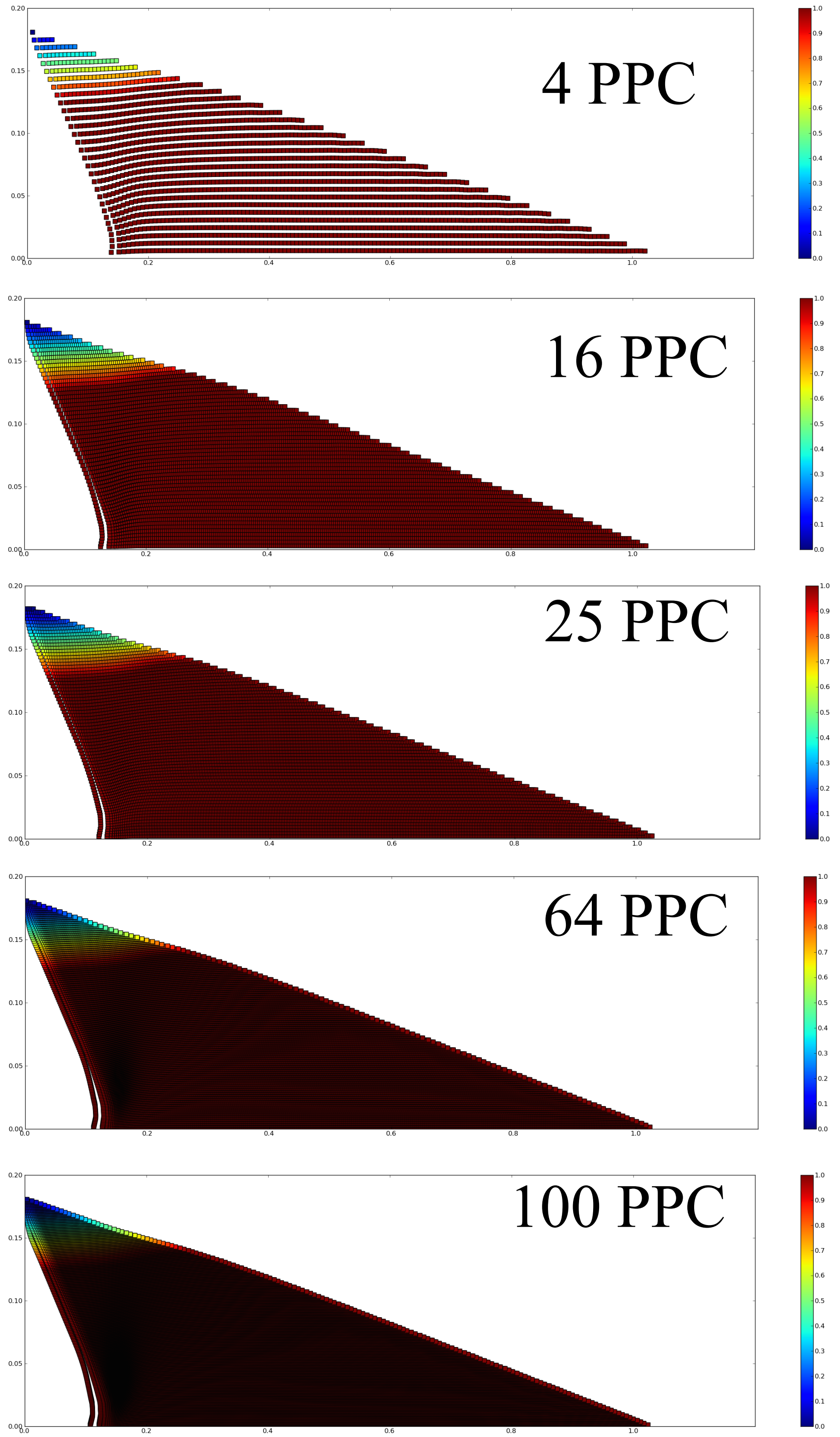

Figure 4.40 Effect of number of material points on cell on the run-out behaviour $E_0 = 152mgd$. Velocity profile (m/s) of granular pile subjected to gradient impact loading.

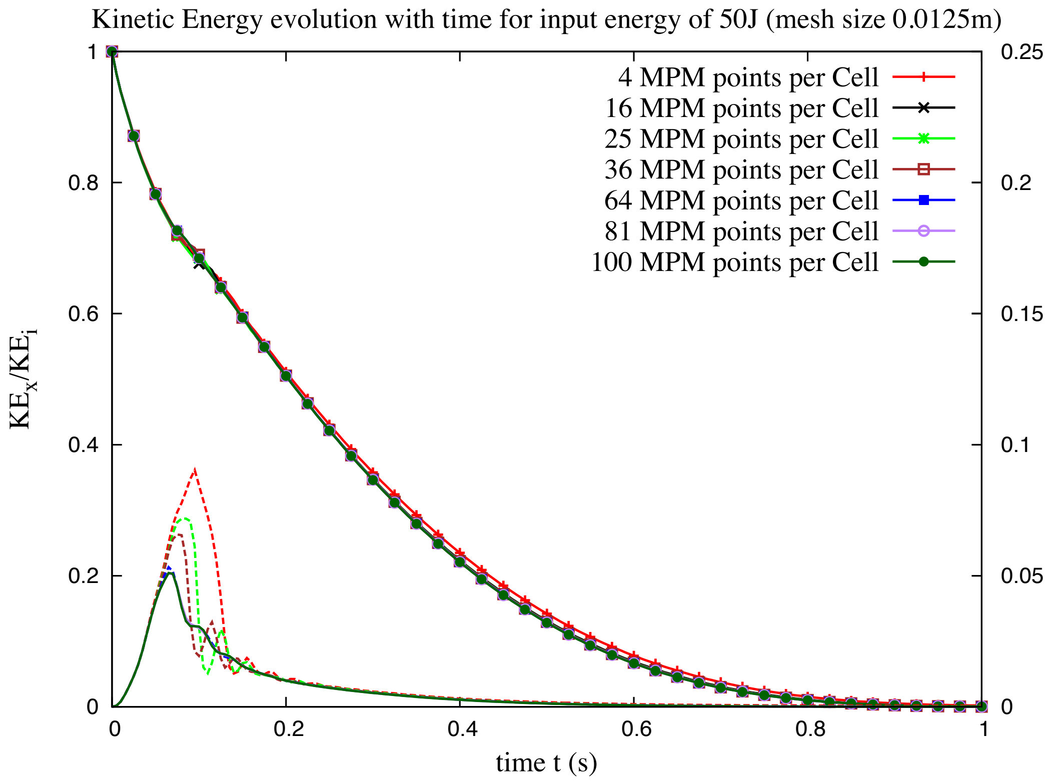

(a) $E_0 = 12.7mgd$.

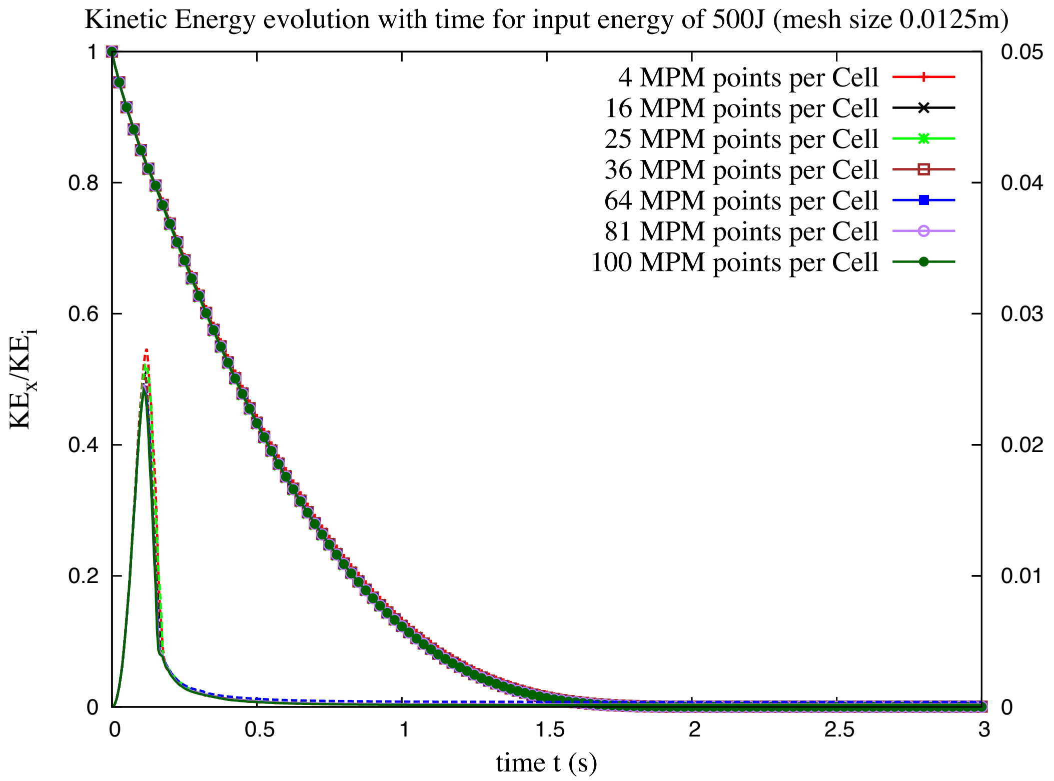

(b) $E_0 = 152mgd$

Figure 4.41 Evolution of kinetic with time for varying material points per cell with increase in the number of material points per cell in both cases. Less than 1% difference in the run-out distance was observed between a mesh size of 0.0125 m and 0.01 m. The final run-out duration is almost unaffected by the increase in the number of material points per cell.

This shows that the run-out distance is affected by the number of material points per cell. However, the duration of the run-out is independent of the number of material points per cell. The computation time increases with increase in the number of material points per cell and decrease in the mesh size. However, the run-out distance converges with increase in number of material points per cell. Hence, an optimum number of 25 material points per cell was adopted in this case. In summary, for conducting a successful MPM analysis, a careful selection of the mesh size and the number of particles is necessary.

4.3.6 Comparison with granular column collapse

Figure 4.43 shows the run-out behaviour of granular column collapse and the slope subjected to impact velocities as a function of normalised kinetic energy. In the case of column collapse, the peak energy at τ_c is used as the energy available for the flow. It can be observed that MPM and DEM predict similar run-out behaviour for low energy regime (short columns), which undergo frictional failure along the flanks. However MPM predicts longer run-out for high energy regime (corresponding to a > 2.7), where the granular column experiences significant collisional dissipation. The lack of a collisional energy dissipation mechanism in MPM results in over prediction of run-out distances. In the case of granular column subjected to impact velocity, the dissipation is friction and MPM is able to predict the run-out response in good agreement with DEM simulations. At very low energy, DEM simulations show longer run-out in the case of slope subjected to impact due to local destabilisation at the flow front. Both granular flows, column collapse and slope subjected to impact, show power-law relation with the energy. This shows that the power-law behaviour is a granular flow characteristic.

4.4 Summary

Multi-scale simulation of dry granular flows were performed to capture the local rheology, and to understand the capability and limitations of continuum models in realistic simulation of granular flow dynamics. MPM with a simple frictional dissipation model is able to capture the flow kinematics of dry granular flows. However, the lack of collisional dissipation in MPM is a limitation in modelling the collapse of tall columns. Both DEM and MPM simulations show a power-law dependence of the run-out and time with the initial aspect ratio of the column.

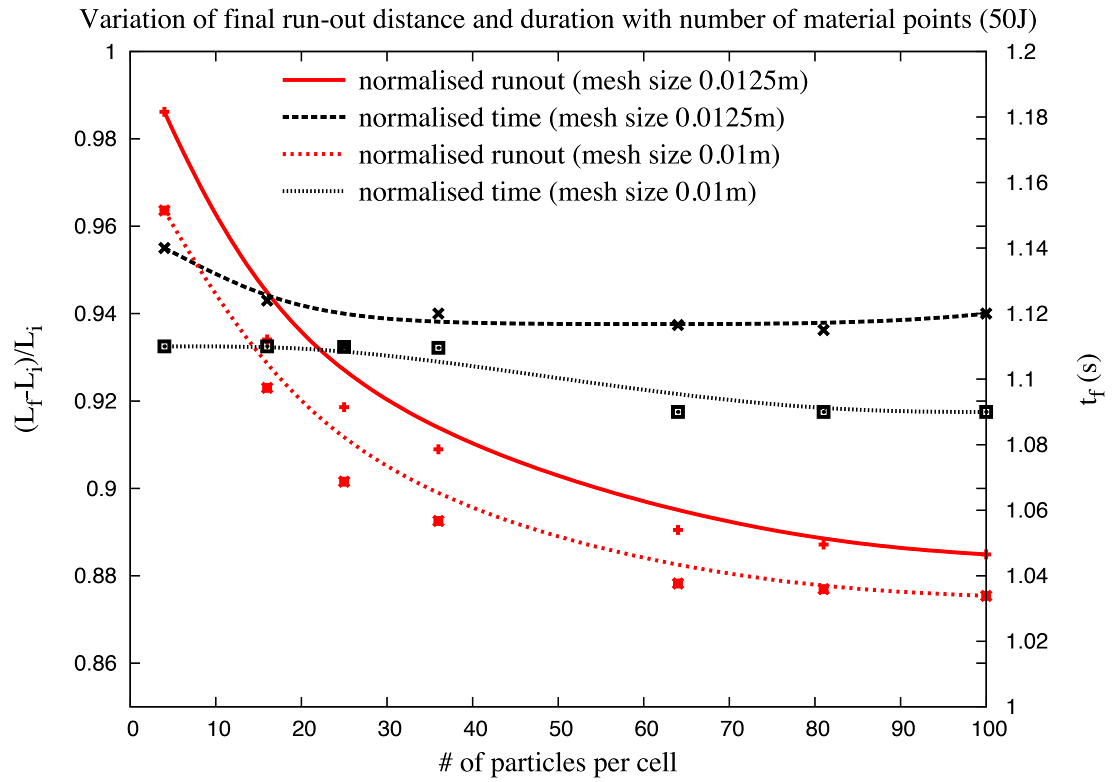

(a) $E_0 = 12.7mgd$.

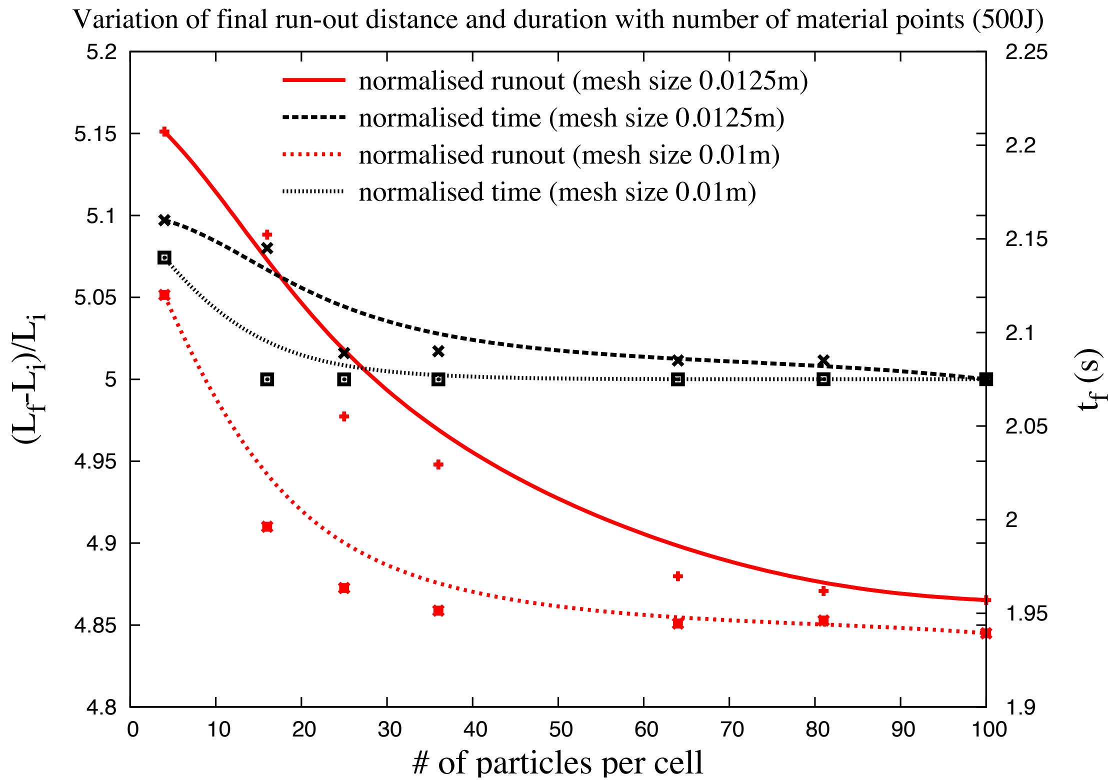

(b) $E_0 = 152mgd$.

Figure 4.42 Evolution of run-out and duration of flow for varying material points per cell.

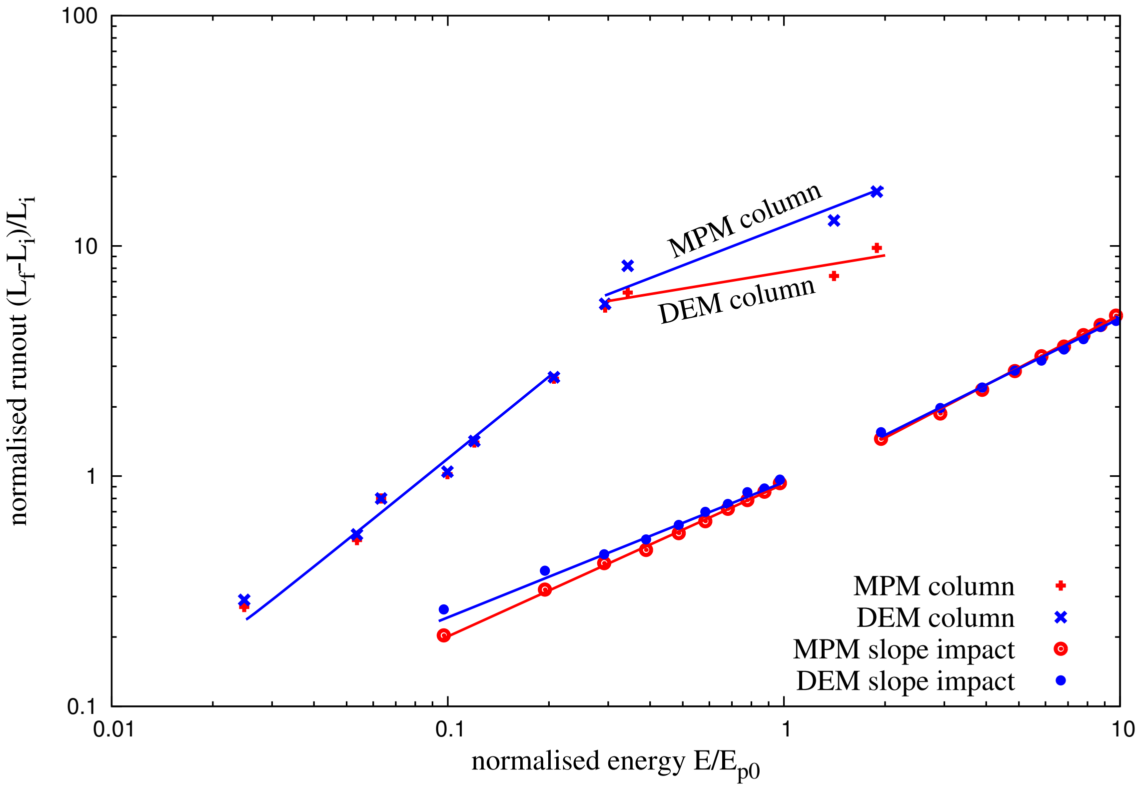

Figure 4.43 Comparison of column collapse with slope subjected to impact loading.

The initial configuration and the material properties have a significant influence on the run-out behaviour.

Natural granular flows are triggered by different mechanisms. The distribution of kinetic energy in the granular mass is found to have an effect on the flow kinematics. A multi-scale analyses of granular slope subjected to impact velocity reveals a power-law dependence of the run-out distance and time as a function of the input energy with non-trivial exponents. This reveals that the power-law behaviour is a generic feature of granular dynamics. The values of the exponents are not simple functions of the geometry.

We also observe two regimes with different values of the exponents: a low-energy regime and a high-energy regime. The low energy regime reflects mainly the destabilisation of the pile, with a run-out time independent of the input energy. Whereas, the second regime is governed by the spreading dynamics induced by higher input energy. The evolution of granular slope in the high-energy regime can be described by a characteristic decay time and the energy available at the end of the first stage, where the pile is destabilised. MPM is successfully able to simulate the transient evolution with a single input parameter, the macroscopic friction angle. This study exemplifies the ability of MPM, a continuum approach, in modelling complex granular flow dynamics and opens the possibility of realistic simulation of geological-scale flows on complex topographies.

References

Abe, K., Soga, K., and Bandara, S. (2013). Material Point Method for Coupled Hydromechanical Problems. *Journal of Geotechnical and Geoenvironmental Engineering*, page 04013033.

Balmforth, N. J. and Kerswell, R. R. (2005). Granular collapse in two dimensions. *Journal of Fluid Mechanics*, 538:399–428.

Bandara, S. (2013). *Material Point Method to simulate Large Deformation Problems in Fluid-saturated Granular Medium*. PhD thesis, University of Cambridge.

Bardenhagen, S. and Kober, E. (2004). The generalized interpolation material point method. *Computer Modeling in Engineering and Sciences*, 5(6):477–496.

Cambou, B., Jean, M., and Radjaï, F. (2009). *Micromechanics of granular materials*. Wiley-ISTE.

Coetzee, C. J., Vermeer, P. A., and Basson, A. H. (2005). The modelling of anchors using the material point method. *International Journal for Numerical and Analytical Methods in Geomechanics*, 29(9):879–895.

Crosta, G. B., Imposimato, S., and Roddeman, D. (2009). Numerical modeling of 2-D granular step collapse on erodible and nonerodible surface. *J. Geophys. Res.*, 114(F3):F03020.

Da Cruz, F., Emam, S., Prochnow, M., Roux, J. N., and Chevoir, F. (2005). Rheophysics of dense granular materials: Discrete simulation of plane shear flows. *Physical Review E - Statistical, Nonlinear, and Soft Matter Physics*, 72(2):1–17.

Daerr, A. and Douady, S. (1999). Two types of avalanche behaviour in granular media. *Nature*, 399(6733):241–243.

Estrada, N., Taboada, A., and Radjai, F. (2008). Shear strength and force transmission in granular media with rolling resistance. *Physical Review E*, 78(2):021301.

Girolami, L., Hergault, V., Vinay, G., and Wachs, A. (2012). A three-dimensional discrete-grain model for the simulation of dam-break rectangular collapses: comparison between numerical results and experiments. *Granular Matter*, pages 1–12.

Guilkey, J., Harman, T., Xia, A., Kashiwa, B., and McMurtry, P. (2003). An Eulerian-Lagrangian approach for large deformation fluid structure interaction problems, Part 1: algorithm development. *Advances in Fluid Mechanics*, 36:143–156.

Hogg, A. J. (2007). Two-dimensional granular slumps down slopes. *Physics of Fluids*, 19(9):9.

Iverson, R. M. (1997). The physics of debris flows. *Rev. Geophys.*, 35(3):245–296.

Jean, M. (1999). The non-smooth contact dynamics method. *Computer Methods in Applied Mechanics and Engineering*, 177(3-4):235–257.

Kerswell, R. (2005). Dam break with Coulomb friction: A model for granular slumping? *Physics of Fluids*, 17:057101.

Lacaze, L. and Kerswell, R. R. (2009). Axisymmetric Granular Collapse: A Transient 3D Flow Test of Viscoplasticity. *Physical Review Letters*, 102(10):108305.

Lajeunesse, E., Mangeney-Castelnau, A., and Vilotte, J. P. (2004). Spreading of a granular mass on a horizontal plane. *Physics of Fluids*, 16(7):2371.

Lajeunesse, E., Monnier, J. B., and Homsy, G. M. (2005). Granular slumping on a horizontal surface. *Physics of Fluids*, 17(10).

Larrieu, E., Staron, L., and Hinch, E. J. (2006). Raining into shallow water as a description of the collapse of a column of grains. *Journal of Fluid Mechanics*, 554:259–270.

Lo, C. Y., Bolton, M., and Cheng, Y. P. (2009). Discrete element simulation of granular column collapse. In *AIP Conf. Proc. Powders and Grains 2009*, volume 1145 of *6th International Conference on Micromechanics of Granular Media, Powders and Grains 2009*, pages 627–630.

Lube, G., Huppert, H. E., Sparks, R. S. J., and Freundt, A. (2005). Collapses of two-dimensional granular columns. *Physical Review E - Statistical, Nonlinear, and Soft Matter Physics*, 72(4):1–10.

Mitchell, J. K. and Soga, K. (2005). *Fundamentals of soil behavior*. John Wiley & Sons.

Moreau, J. J. (1993). New computation methods in granular dynamics. In Thornton, C., editor, *Powders and Grains*, page 227. A. A. Balkema.

Mutabaruka, P. (2013). *Modelisation numerique des milieux granulaires immerges : initiation et propagation des avalanches dans un fluide*. Phd thesis, University of Montpellier 2.

Radjai, F. and Dubois, F. (2011). *Discrete-element modeling of granular materials*. ISTE Wiley, London; Hoboken, N.J.

Radjai, F. and Richefeu, V. (2009). Contact dynamics as a nonsmooth discrete element method. *Mechanics of Materials*, 41(6):715–728.

Radjai, F., Schafer, J., Dipple, S., and Wolf, D. (1997). Collective Friction of an Array of Particles: A Crucial Test for Numerical Algorithms. *Journal de Physique I*, 7(9):1053–1070.

Rondon, L., Pouliquen, O., and Aussillous, P. (2011). Granular collapse in a fluid: Role of the initial volume fraction. *Physics of Fluids*, 23(7):073301–073301–7.

Rycroft, C. H., Orpe, A. V., and Kudrolli, A. (2009). Physical test of a particle simulation model in a sheared granular system. *Physical Review E*, 80(3):031305.

Schaefer, D. G. (1990). Instability and ill-posedness in the deformation of granular materials. *International Journal for Numerical and Analytical Methods in Geomechanics*, 14(4):253–278.

Staron, L. and Hinch, E. J. (2005). Study of the collapse of granular columns using two-dimensional discrete-grain simulation. *Journal of Fluid Mechanics*, 545:1–27.

Staron, L. and Hinch, E. J. (2007). The spreading of a granular mass: Role of grain properties and initial conditions. *Granular Matter*, 9(3-4):205–217.

Staron, L., Radjai, F., and Vilotte, J. P. (2005). Multi-scale analysis of the stress state in a granular slope in transition to failure. *The European physical journal. E, Soft matter*, 18(3):311–20.

Staron, L., Radjai, F., and Vilotte, J.-P. (2006). Granular micro-structure and avalanche precursors. *Journal of Statistical Mechanics: Theory and Experiment*, 2006(07):P07014–P07014.

Topin, V., Monerie, Y., Perales, F., and Radjaï, F. (2012). Collapse Dynamics and Runout of Dense Granular Materials in a Fluid. *Physical Review Letters*, 109(18):188001.

Utili, S., Zhao, T., and Houlsby, G. (2014). 3D DEM investigation of granular column collapse: Evaluation of debris motion and its destructive power. *Engineering Geology*.

Warnett, J. M., Denissenko, P., Thomas, P. J., Kiraci, E., and Williams, M. A. (2013). Scalings of axisymmetric granular column collapse. *Granular Matter*, 16(1):115–124.

Zenit, R. (2005). Computer simulations of the collapse of a granular column. *Physics of Fluids*, 17(Compendex):031703–1–031703–4.